Creation and Characterization of Ceramic/Polymer Bi-Continuous Composite Material for Hot-Bitumen Pipeline Coating

by

Sean Preston Wagner

A thesis submitted in partial fulfillment of the requirements for the degree of

Master of Science

in

Materials Engineering

Department of Chemical and Materials Engineering
University of Alberta

Abstract

Current composite materials base their capabilities from the dispersion of discrete reinforcing materials throughout a matrix. This method places too much reliance on the surface bond between matrix and reinforcing phase. By employing two continuous, interpenetrating materials, it is theorized that each material will be able to act as a bulk material and enjoy the benefits of reinforcement via the bond with the other material, creating a material that responds favourably to situations requiring hardness and elasticity by utilizing the properties of each comprising material selectively.

Acknowledgements

I would like to thank the following people for their help over the last few years:

Dr. Weixing Chen for his aid and support throughout this entire degree

Dr. Anastasia Elias for training me and allowing me to use her DMA

Dr. Dongyang Li for giving me access to his slurry pot and his student Bin Yu for teaching me how to use it

Dr. Gary Fisher and the Alberta Innovates-Technology Futures (AITF) for performing the very important hardness tests

Dr. Hao Zhang, Dr. Jingli Luo and Dr. Leijun Li, for providing the final vetting of my work as my defence committee

And last, all my friends who hopefully don't think I am dead due to not talking to them while I was writing.

Table of Contents

List of Tables

List of Figures

List of Equations

Chapter 1 Introduction

Bitumen is becoming more and more common as a source material for many petrochemical products found today. However due to the environment from which it is obtained and the trouble with transporting it safely with minimal risk to the environment, improved materials are required to protect the ecosphere from the toxic chemicals present in bitumen [1]. Not only can bitumen contain corrosive chemicals, but also it is regularly loaded with abrasive particles and dissolved reactive gases. As a final point, the high molecular weights of a large fraction of compounds that comprise bitumen prevent it from being able to flow easily at room temperature. Therefore volumes must be maintained at elevated temperatures during transport, whether in tanks or through pipes. In order to engineer a material that can withstand all of these demanding requirements, one must look to unorthodox areas of materials design, away from homogeneous materials such as the usual abrasion resistant steels or hard-faced coatings. Many standard composite materials have very impressive moduli or maximum strengths; however they lack the capability to hold together under wear and abrasion. Cermets as a subclass of composite materials hold promise, but the metal based composites fall victim to the same corrosion problems that plague normal abrasion resistant metals. The idea of a Cermet with the metallic phase replaced with a polymer material neatly sidesteps this problem of corrosion, providing that the ceramic portion of the material is not susceptible to reduction or oxidation while surrounded by the fluid environment.

By finding a way to fabricate a continuously inter-penetrated composite material constructed equally of ceramic materials and polymeric filling, it should be possible to not only to combine the high strength and wear resistance of the ceramic material with the elasticity and energy absorption capabilities of the polymer. With this goal in mind this thesis attempts to document the endeavor to create a Bi-Continuous Composite (BCC) material for the purposes of acting as a protective coating material for hot-bitumen pipelines and other transport containers.

This document is separated into several chapters covering information of similar topics. Chapter 2 explains the reasons for the investigations into this new type of material and gives the necessary background theories to understand how the material should behave given certain circumstances and reasoning for why the materials comprising the samples was chosen. Chapter 3 details the processes required to fabricate samples of the desired material to ensure consistent quality and controlled variability to determine through characterization testing which composition is most suited for any possible job placement. Chapter 4 details the results of these tests and how the various properties of the material can reinforce or subtract from desired capabilities under various tested circumstances, especially how an uncontrolled microstructure can be both a benefit for ease of processing but hold hidden methods of failure that need to be addressed. Chapter 5 contains all the conclusions of the research and details the ultimate verdict on the possibilities of the desired material.

Chapter 2 Literature Review

2.1 Introduction

This literature review covers: the basics of how composite materials are created and the benefits of using them over more standard materials, what the new class of materials known as Bi-Continuous Composites consists of and basic information on how they are created, and the reasons why they are thought to be a viable candidate for wear resistant coatings and the choices of materials to maximize the possibility of that outcome. With a thorough understanding of these foundational subjects, the material can be designed with all the known variables of the desired job and how to counteract them with the least amount of difficulty.

2.2 Current state of affairs

2.2.1 Types of coatings

Currently there exist two major focuses for internal diameter pipeline coatings: to prevent corrosion, or to prevent wear, abrasion and erosion. Designing a coating primarily for either of these problems individually yields deficiencies when exposed to the other. To prevent corrosion, a smooth continuous barrier layer must be established between the metal wall of the pipe and the fluid being transported. This barrier must be thick enough to prevent any possible voltage from being applied to the metal and also lack any method for the fluid to contact the pipe wall. The best materials for maintain this form of barrier are high density, high molecular weight polymers such as polyurethane [2], polyethylene [3], or more recently, multi-layer fusion bonded epoxy coatings of varying layer compositions [4],[5]. While modern polymers can provide excellent ablative erosion resistance, the coatings are eventually rendered thin enough to require either retouching or rotation of the pipe section. Also, to ensure a long enough life span of the coating to provide economic viability, the coating is applied in thicknesses that reduce the diameter of the pipe by up to 5 cm [2], which reduces the effective volume of a large diameter pipe (e.g. 30” interior diameter) by 13%. [2]

Alternatively, when designing a coating to protect primarily against abrasion and erosion, a thin layer of high density ceramic or refractory metal alloys are found to be very effective. Applied through a variety of methods such as plasma coating, high velocity arc spraying, or laser sintering, the coatings are comprised of materials containing high quantities

of extremely hard materials such as Hard Chrome, Tungsten Carbide, Chromium Oxide or Carbide, or Aluminum Oxide[6]. One problem with these types of coatings is inherent in their application methods. As these materials are incredibly hard and abrasion resistant thanks to the strength of the interatomic bonds, they are also appropriately temperature resistant, meaning that they cannot be pre-melted and applied in an even, non-porous method. Current standard procedures involve spraying semi-molten beads of material through a nozzle and having them sinter to the pipe wall and each other on impact [7]. Figure 1 shows a schematic for how Plasma Spraying is used to apply a hard-faced coating.

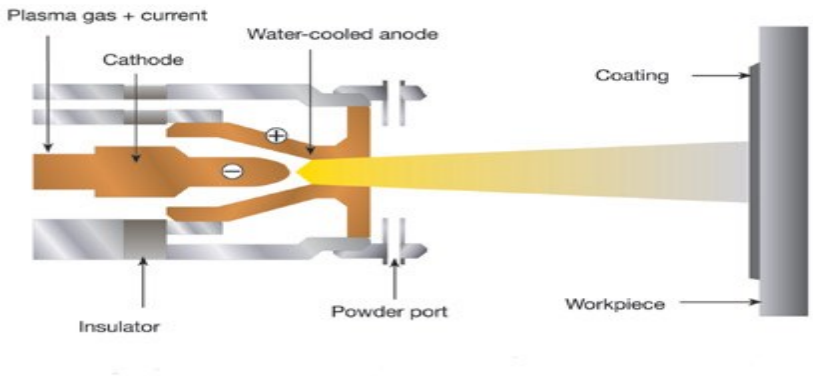

Figure 1 Plasma Spraying process[1]

The problem inherent in attempting to create a continuous layer from a feed of discrete particles is one of porosity. In order to ensure an even coating thickness, the impinging material cannot be too hot or it might run and form irregularly thick and thin areas, but by using a lower sintering temperature, the probability of voids remaining in the final layer is increased. Voids and porosity in a hard-faced coating leads to the main downfall of these classes of interior lining, corrosion disbondment. Pores or voids work to decrease the effective thickness of the coating in a specific area, which could make it possible for any electric charges to effect a reaction in the reactive steel of the pipe wall possibly through charge separation as shown in Figure 2, possibly allow oxygen to sneak through the barrier and react with the pipe wall , or even allow molecules of water to make contact with the pipe wall, which can either cause the formation of rust or, depending on the temperature difference between the fluid being transported and the environment outside of the pipe, freeze and physically separate the coating from the pipe wall via mechanical forces due to the

[1] Used under Fair Use from High Power Media, courtesy of Sulzer Metco.

increase in volume during the phase change (cold wall disbondment) [8]. Note that these problems are not limited only to hard-faced coatings, but polymer based coatings as well. Only by ensuring that the coatings are as defect free as possible can these effects be mitigated.

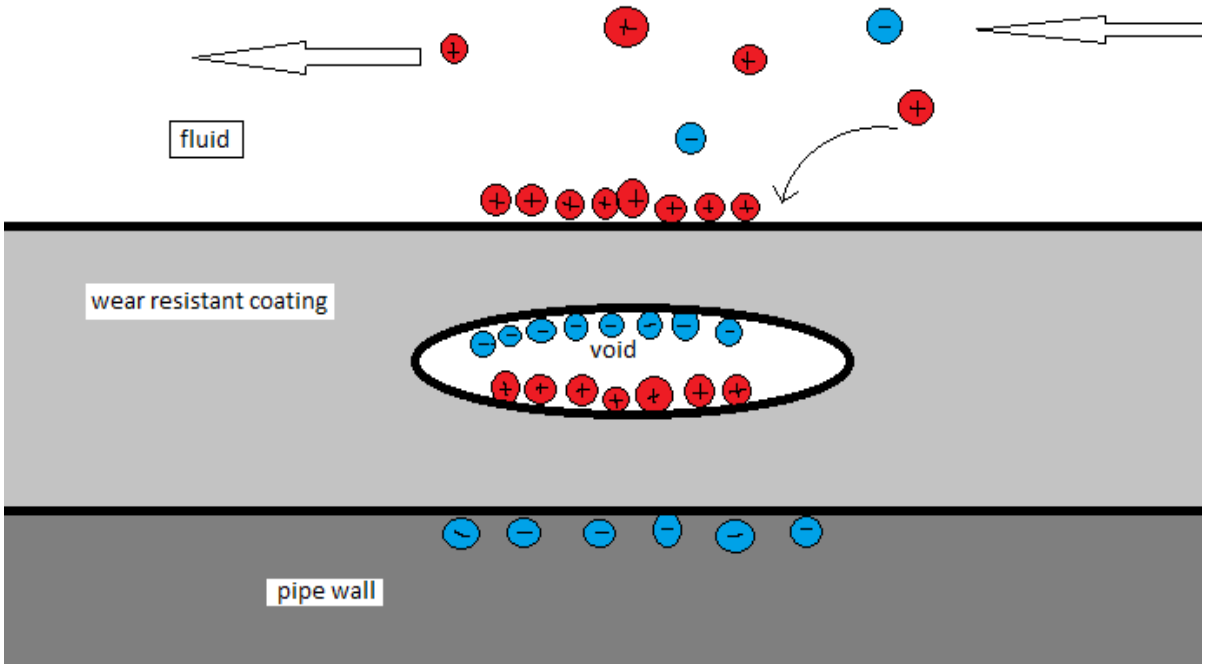

Figure 2. Charge separation mechanism for pipeline corrosion due to void in coating

In particular scenarios, such as hot bitumen pipelines from the Alberta Oilsands, both corrosion and Erosion are extremely vigorous and must be protected against equally. As such a new type of coating material is required that can handle both extremes equally efficiently. As such a change from a coating comprised of a single uniform material to a composite capable of utilizing the capabilities of multiple specialized materials simultaneously is a desirable path to investigate.

2.3 Composite material overview

2.3.1 Theory of properties mixing

Composites are derived from mixing two or more dissimilar materials from the different major groupings of materials, namely ceramics, polymers, and metals. The purpose

of this mixing is to tune the properties of the final product to precisely fit the application, rather than design a part around the capabilities of the materials. The majority of the research on composite materials is based around reinforcing a base material, called the matrix, by adding small portions of other materials in varying form factors to improve certain aspects of the matrix's properties without impacting any other properties in a significantly negative way.

Common applications of composite materials are in structural or electronic situations. For example; reducing the mass of a strut or brace while maintaining bending or tensile strength, allows planes and automobiles to have improved fuel savings, workable lifetime, or passenger capacity. Electronic composites represent a fairly recent addition to the field, showing possible use in creating flexible electronics[9], bio-implantable sensors and other devices that could not function properly in the desired application on a standard silicon substrate[10]. Standard silicon based electronics do not have the required amount of flexibility or encounter problems with the chemical atmosphere and therefore are impractical for these applications.

Which properties are altered depends on the properties, dimensions and aspect ratios of the reinforcing materials. Particles, flakes, fibers, and laminates are a few forms that can be used to give differing types of reinforcement to the base material. Each type of reinforcement gives its own benefits and drawbacks, and as such is used in differing fields and situations. Some types of composites are more universal in their applications than others, such as glass fiber reinforced polymer (GFRP) and carbon fiber reinforced polymers (CFRP). This prevalence is due to combinations of ease of use, cost, and benefit of the dispersed material per unit mass.

The method of predicting the properties of a majority of mixtures for composite materials is known as the Rules of Mixtures[11]. This rule states that the properties of a two-phase composite are theoretically determined and bounded by upper and lower limits defined by Equations 1 and 2 respectively.

$$E_c(u) = E_m V_m + E_r V_r$$

Equation 1. Upper limit of Rule of Mixtures for properties of composite materials

$$E_c(l) = \frac{E_m E_r}{V_m E_r + V_r E_m}$$

Equation 2 Lower limit of Rule of Mixtures for properties fo composite materials

Where E is the tensile, bending, shear or compressive modulus of the particular material, V stand for the volume fraction of the specific material and m denoting the matrix, r the reinforcing phase and c the final composite. By knowing these boundaries and comparing them against the known properties of the material the composite is to replace, it is possible to improve upon the standard material in as many ways as possible, without requiring as much trial and error.

2.3.2 Fibre composites

Fibre composites are very common for circumstances that require enhanced tensile strength or flexibility[12], [13]. The long, thin aspect ratio of the fibres allows for the composite to stretch and flex along the fibre much more effectively than without or even in a perpendicular direction. This anisotropy of the properties of a fibre reinforced composite allows for a further separation of differing classes of fibre reinforced composites. Aligned fibres allow for unsurpassed strengthening along the direction of the fibres. Since all the fibres are able to stretch and flex in the same direction, the amount of force that can be transferred to the fibres from the matrix is maximized. However this material is actually weaker than the matrix when stressed in a direction other than that of the aligned fibres. This is due to the lack of surface area along the direction of the stress between the fibre and the matrix. Without enough surface area, there is not enough bond strength to maintain the adhesion between the matrix and the fibre, causing shear disbondment and failure in the composite.

The amount of strengthening capable of being effected upon the matrix is dependent upon the length of the fibres. Below a critical length l_c, the fibres are unable to support the maximum amount of stress that material theoretically can. This maximum stress is called the σ_f^* and provides a delineating line to define terms to help distinguish types of fibre composites from one another. According to Equation 3 there is a direct relationship between the l_c and the σ_f^*

$$l_c = \frac{\sigma_f^* d}{2\tau_c}$$

Equation 3 Critical length of fibre reinforcement

When the fibres $l < l_c$ they are described as discontinuous, and lack the ability to fully accommodate the transfer of forces from the matrix into themselves. When the fibres are $l \geq l_c$, they are described as continuous and are able to withstand the maximum amount of force transferred from the matrix as defined by the τ_c term, which represents the shear strength of the bond between the fibres and the matrix. This strengthening mechanism using continuous fibres only works at maximum effectiveness when the fibres are aligned along the same axis [11]. If the continuous fibres are allowed to become randomly aligned, interactions between fibres can prevent proper bonding between fibre and matrix. This reduces the force transferring capabilities and thus reduces the local strength of the composite, making the entire piece more prone to failure.

Randomly aligned fibres are useful in certain situations however; aligned fibres can only improve the strength of materials in the direction of alignment, or in a plane if fibres are aligned at offset angles to groups of fibres. With randomly aligned fibres, a bulk material can gain strength in multiple directions, removing the anisotropy of the strengthening mechanism. While the increase in capabilities for randomly aligned is not as great as for aligned fibres, the benefit of having isotropic behaviour in a composite material can outweigh the loss of strengthening efficiency. This is particularly important in settings where the material can be expected to withstand tensile, bending or rotational forces coming from any direction.

2.3.3 Particulate composites

Contrary to how fiber reinforcement works, particulate reinforcement is primarily used to improve compressive strength or wear resistance. This is because of how the particles affect the surrounding matrix and respond to stresses compared to fibers. Particulate reinforcement is isotropic due to the near spherical aspect ratios of these materials. Thus while in tension the particles act similar to discontinuous fibers; the particles do not have

enough surface area along the direction of strain to fully transmit the stresses while in compression they do not buckle or warp as fibre reinforcements are prone to do. This allows the surface of the particle and the matrix surrounding it to remain in near static positions relative to each other. This is important as it prevents any slippage or shear along the surface of the particle until the forces applied to the material reach levels capable of ripping the matrix from the particle.

How a particulate reinforced composite material behaves is similar to a properly age-hardened metal alloy. In age hardening, ceramic phase precipitates are encouraged to form in a metal matrix, but only to a certain size. A properly sized precipitate will be large enough to prevent a dislocation from cutting through the particle, but small enough to maintain a coherent boundary between the particle and the matrix. By maintaining a coherent boundary, the particle exerts a stress upon the surrounding matrix, increasing the amount of energy it takes for a flaw or dislocation to move through the surrounding area. In a composite material, particulate reinforcement work in a similar way, by creating localized areas of stress surrounding them to prevent flaws from moving through the matrix. This is done either by bonding the particles tightly to the matrix material and creating a stressed coherent boundary, or by allowing polymer chains to wrap around and bond to the particle, interfering with the motion of other chains when an applied stress attempts to force movement of the molecules against each other.

The general rule for composite materials is, the stronger the bond between the matrix and the dispersed material, the larger the effect of the reinforcement upon the matrix. This bond increases the volume of the matrix material that exhibits the improved properties. Therefore by increasing the volume fraction of the reinforcing material the properties of the composite material gets closer to that of the reinforcing material[11]. If enough of the dispersed material is added, it is possible for the zones of effect of each particle to overlap with one or more of the neighbouring particles, creating a network of altered matrix throughout the material. Once a continuous network has been established within the matrix, the material properties of the dispersed phase begin to take a more prominent role in how the material behaves. Thermal and electrical properties are especially sensitive to the formation

of networks within a matrix. With networks, interesting properties come to the forefront of the material and it is these properties that this investigation is most interested in.

2.4 Bi-continuous composite materials

2.4.1 Description

A bi-continuous coating is a type of composite material where two phases of approximately equal volume are made to intertwine in a continuous and random orientation such that there is no straight, long distance, continuous sections of interface. Achieving this type of material requires that one phase be infiltrated into the other phase while in a liquid state. Thus for the remainder of this report, the matrix will be defined as the first phase to be created and then infiltrated. The intention of creating a bi-continuous coating is because of the large surface area available for bonding between the two continuous phases[14]. With normal reinforcement materials being comprised of small particulates of various form factors, even with high surface area to volume ratios, the total surface area per particle is extremely small, resulting in concurrently small values of strain required to break the bond between the matrix and the dispersed material. With bi-continuous materials, ideally, each phase is a single piece giving a much larger bonding area between the two materials requiring equally large total strains to cause disbondment. An added benefit is that if the phases are properly interpenetrated there should be very few long lines of continuous contact between the phases, limiting the amount of strain possible between the phases in a single direction before a change in direction prevents the material from moving further out of place. In order to create this type of material a porous matrix must first be created to give the second phase a framework with which to bond with.

2.4.2 Porous ceramics

Ceramics are statistically unlikely to ever be completely non-porous, barring reactions with metals and intermetallic bulk materials. Controlling the degree of porosity is done primarily through careful control of thermal conditions during sintering of a loose or pressed powder precursor. During sintering, particles of a material are heated to a point below their melting temperature, but high enough to encourage diffusion of atoms or

molecules between particles that contact each other. Particle size is also important in determining the kind of porosity that the final matrix will have. Larger initial particle sizes will give coarse structures with lower surface area per unit mass of material, while smaller particles will give very high surface area, fine structures.

While total porosity is determined by sintering time and temperature, the initial powder used is paramount in determining the average length of the pores inside the material. Larger powders will give long distances between branches in the pores where smaller powders will connect much more frequently. Which option is more optimal is determined by the desired end goal for the material in question, but it is important to take the viscosity and surface tension of the desired reinforcing material into account. The smaller the final pores in the material are enforces that both of these properties be lower in keeping with the pore diameter so that the reinforcing material is capable of actually penetrating the pores completely. If the viscosity or surface tension is too high, the liquid may not infiltrate through the ceramic even with a vacuum on the other side of the liquid surface.

Incomplete infiltration of a porous ceramic can be very detrimental to the stability and efficacy of the final material. With no reinforcement from the infiltrated phase, the matrix is free to flex and deflect into the void area and will likely fracture if placed under enough load. This fracture removes the reinforcing effect of the matrix material on the infiltrated material due to the new gap between sections of the matrix material being unable to transfer forces. Thus the forces are transferred to the infiltrated material, which begins to flex and removes that reinforcement upon the next closest section of matrix material. This catastrophic type of failure is a risk of using bi-continuous composites, as homogeneous types of materials such as ceramics and metals do not risk this due to continuous bonds of equal strength reaching through the material. In bi-continuous composites, the interface between the two materials is simultaneously and advantage and a disadvantage of the material. If the interface is broken, the two materials revert to behaving as two independent, fragile foams of their respective materials rather than one solid composite.

Catastrophic failure in BCCs with non-infiltrated areas is a concern, as it almost unavoidable in large sample groups. This is because the sintering process for porous materials has a non-zero chance of areas being unable to be infiltrated even under vacuum. For example, several particles will sinter together completely and create an enclosed bubble, or seal off a larger volume of the matrix network.

Porous ceramics have a benefit: reactive gases can be used during sintering to good effect, allowing technical ceramics to be created from a base material. Nitrides, complex oxides, and carbides are all possible final forms of any initial material, assuming that conditions, such as pressure, temperature, and atmospheric composition, or properly controlled during sintering. The porous nature of the material allows the gases to penetrate and react within the sample, allowing much faster reaction of material than a solid sample, due to smaller diffusion distances required across a spur than through a bulk material. Also, any transport of oxygen or nitrogen from the base material is improved because of these smaller diffusion distances.

2.5 Materials selection outline

2.5.1 Ceramic

In the type of BCC under investigation here, the primary framework is provided by the ceramic phase and as such care must be taken in choosing the composition. Chromium carbide is a common base material for hard-faced coatings, and is often combined with metals such as Tungsten, or Nickel for specific applications. For the purposes of creating an erosion resistant BCC, Cr_7C_3 is desired for the combination of properties it offers. The ceramic offers a range of hardness values from ~1340 kg/mm^2[15] – 1830 kg/mm^2[16], possibly due to having a hexagonally close packed crystal structure, and lacking the isotropic coordination of a standard cubic or FCC structure, testing from differing directions of the crystal could return differing values. The ceramic also has a moderate fracture toughness of 5.5 MPa$\sqrt{m}$ [16] which is necessary given the high likelihood of the need for pieces of ceramic to withstand multiple impacts without breaking even if flawed or cracked.

Chromium carbide is also known for strong resistance to corrosion due to the tight bonds with the carbon atoms and the natural formation of a passivizing oxide layer should any oxidation take place. In the environment of a hot bitumen pipeline this corrosion resistance is necessary to allow for the BCC to have even a moderate chance of surviving.

A final factor in the choice of Chromium carbide is the ability to apply a type of solution strengthening to the ceramic through the addition of cobalt in quantities of 23 wt%. Due in part to the near identical atomic radius and similar stable oxidation states, cobalt has a capability to replace chromium in the lattice of chromium carbide causing the formation of a metal amalgam ceramic $M(Cr\text{-}Co)_7C_3$ where the chromium and cobalt atoms are almost completely interchangeable in the lattice. This solutionizing of the metal portion of the ceramic provides a very noticeable increase in the hardness of the resulting material. Due to the samples being prepared as porous ceramics, direct measurements of hardness do not provide the same values as bulk measurements which were previously stated. Dong et.al provides a method and chart, shown in Figure 3, for determining the hardness increase of the chromium by comparing the measured hardness against the theoretical hardness of a pure chromium carbide sample using the Minimum Solid Area (MSA) model[17].

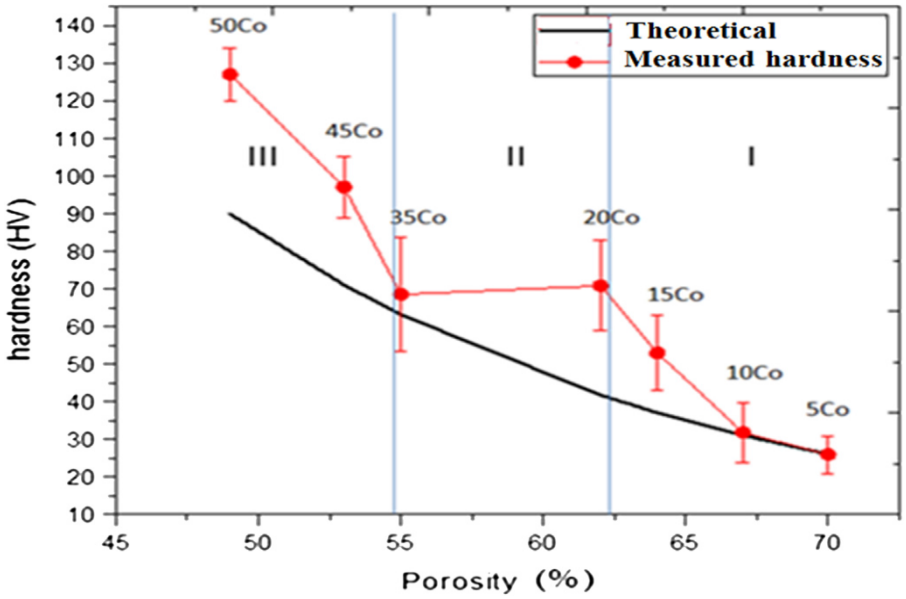

Figure 3. Comparison of porous material hardness, theoretical vs. experimental[2]

[2] Used with permission of Dr. Weixing Chen

At 23 wt.% cobalt the ceramic gives a Vickers Hardness in the low 70's, where according to theory, the hardness of pure chromium carbide for the given porosity should be approximately 46 HV. This increase in hardness comes at a modest price of a 5% increase in mass due to the slight difference in densities between chromium and cobalt. This is deemed an acceptable trade for the gain in capability these numbers suggest.

2.5.2 Polymer

Currently the standard materials for polymer based coatings within abrasive environments are either polyurethane based or a mixture of epoxies and polyolefins [2], [4], [5], [8], [18]. Starting from that information, a binary bisphenol-A based epoxy was chosen (West Systems 105 epoxy with 205 Hardener, Shore D hardness: 83, [19]). The resulting composite was created by placing the empty porous ceramic in an aluminum cup with a perforated bottom, and secured in the throat of a vacuum flask, then having the mixed epoxy poured over the ceramic and thus hopefully pulling it through into the pores of the ceramic. The aluminum cup design is shown in Figure 4.

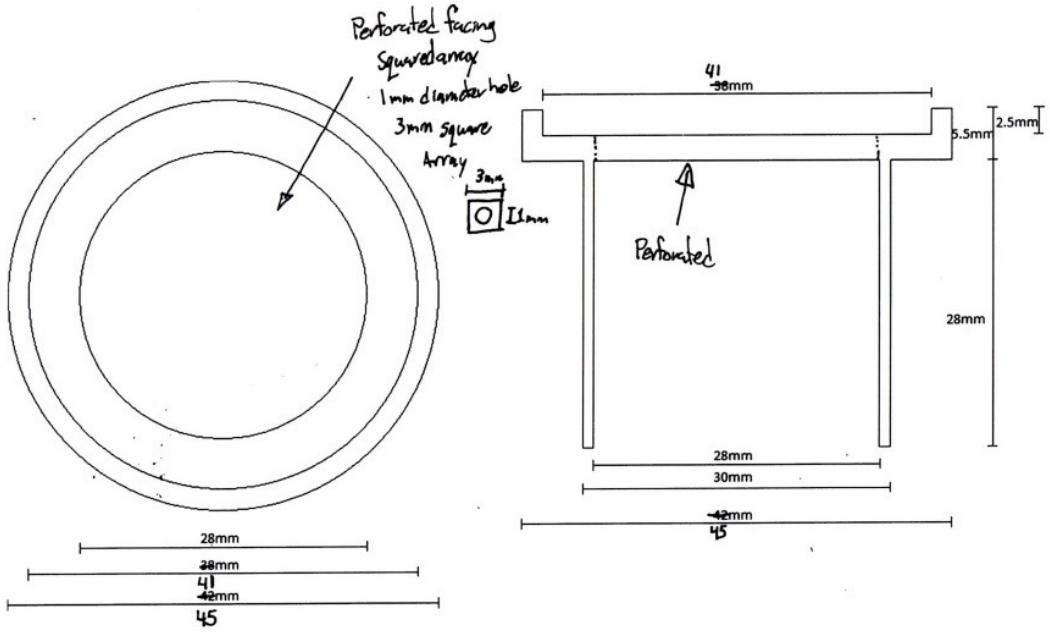

Figure 4. Vacuum flask adaptor for epoxy infiltration

The composite was found to be quite hard for a material comprised of more than 50% polymer by volume, with a Shore D hardness rating of 88 at room temperature, without addition of CNT's. Unfortunately, given that the desired environment for this material in at elevated temperatures inside hot bitumen pipelines, the epoxy runs into a problem. With a glass transition temperature of 61°C, the epoxy runs the risk of becoming plastically deformable under small loads and losing any wear resistance that it may have offered to the composite. According to DMA testing done by Souza and Reis, while the addition of filler materials or reinforcing fibres can shift the temperature of the glass transition up or down, ;the outcome of passing through that temperature is the same. The elastic modulus of the material decreases dramatically, between 80-95% as shown in the paper, and the storage modulus increases to a maximum at the T_g, but then returns to levels equal to the glassy form of the epoxy [20]. With these changes, unless there is a drastic increase in the elasticity of the material, the bisphenol-A epoxy becomes gummy and easily deformed in a plastic manner. A material that is easily plastically deformed is exceedingly good at absorbing and dispersing energy from an impact, once. After the material is deformed the first time it will not deform again until impacted with more energy, and as part of a bi-continuous composite, this behavior can be quite detrimental. When the polymer in the composite is deformed, it must be either detached from the ceramic spur, or deform the spur; placing it under stress lowering the energy required in an impact to fracture the spur.

Understanding this material flaw for the desired environment, a change in polymers is required to remove this possibility. A polymer that has a very low glass transition temperature yet can still retain elasticity after impacts. Siloxane elastomers fulfill both of these requirements and were investigated as components of bi-continuous composites.

2.6 Proposed research and objectives

This research is designed to begin investigation as to the suitability of chaotically ordered BCC materials as possible wear resistant coatings for extreme environment use, namely hot bitumen pipelines. For the preliminary investigation, the samples will be tested under STP conditions to determine which are most suitable to be considered for future work.

The samples will be tested for wear resistance, hardness, energy absorption and bending modulus. Since the ceramics are sintered in a chaotic manner, there is no ability to have the ceramic supported completely by itself. The final product can thus be modeled as an interconnected series of cantilevers composing an openly porous structure.

By measuring the hardness we can have a qualitative idea of how interconnected the samples ceramic phases are as more heavily interconnected samples will support themselves better and give higher hardness's. By measuring the bending modulus and Tan Delta, a prediction of which ones will resist impacts at various angles can be theorized by relating the energy absorption of the tan deltas with the stiffness of the bending moduli. With the relative numbers between samples prepared identically, a conclusive outcome should be possible. With the chaotic structure of the materials in question it is highly unlikely that a single composition will be able to stand out as the best for all situations. Most likely there will be two or more compositions competing for further study or co-existing by performing noticeably better under changing circumstances.

The wear resistance tests will be simplified to attempt to cover two worst case scenarios for protective materials. By testing at different impingement angles it is hoped that two major uses of abrasive resistant materials may be simulated. The lower impingement angle will be used to test impact resistance in a straight pipe from a higher than normal angle, simulating turbulent flow which could cause particles to abrade the coating from non-glancing angles. The higher impingement angle will be used to test the material for use in small chambers or pipeline elbows where flow direction can be erratic but rarely low angle.

Chapter 3: Synthesis of bi-continuous ceramic-polymer composites

3.1 Introduction

This chapter is devoted to detailing the process for creating and standardizing the BCC samples for use in all tests, beginning with the powder composition and mixing through carburization and infiltration. A firm understanding of how each sample is created and the differences between each group is important. Materials selection was based upon a mixture of prior works done by colleagues, trial and error, and general knowledge of possible strengthening mechanisms in composite materials fields. By incorporating all of these materials and processes together, it is hoped that if a new and valuable material is not made apparent that at least this exploration into a new class of composites will provide a stepping stone for further and more guided future research. By initially exploring the known facts and properties of the composing materials, an understanding of how they were chosen and the reasons why is hopefully developed. Finally, an exploration of the processing steps and methods for creating the final product are explored for the purpose of finding possible failure methods in the hopes of discovering how to avoid them in current or future endeavours.

3.2 Pre-Processing Theory

3.2.1 Carburization reactions

3.2.1.1 Ceramic oxide reduction via carburization

Carburization is the process of creating carbide ceramics from a ceramic or metallic base material by adding carbon directly into a metal, or by displacing elements from a ceramic system and reconstituting in a new configuration, such as oxygen or nitrogen being replaced by carbon via a designed chemical potential gradient. Creating this gradient requires a source of carbon and an atmospheric composition that ensures that replacing any elements currently not bonded with carbon remains energetically favourable at the desired carburization temperature.

To provide a proper environment for carburization to happen requires that the atmosphere contain a carbon source such as methane, ethane or other similar carbon bearing molecules. To create a carbon potential in the environment, the molecules need to be broken down from their initial state to provide active sites on the carbon and free molecules to bind

to the oxygen that is released from the ceramic[21]. In order to ensure full carburization, the process should happen simultaneously with the sintering of the initial powders, in order to prevent large areas of the ceramic from sintering closed and preventing access of the feed gas to the interior of the material. This balance requires a feed gas with a large enough carbon potential at sintering temperature[16]. The gas must have a specific amount of carbon to maintain the correct microstructure throughout the material by matching the carburization rate to the rate of diffusion of carbon into the material. However at temperatures above 1200 Celsius, the cracking of methane proceeds faster than the carbon can diffuse into the material and forms a blocking layer of pure carbon preventing reduction reactions from proceeding [22].

3.2.1.2 Analysis of Cr-Co-C phase diagram

Through the use of carburization outlined in the previous subsection, an initial mixture of Chromium Oxide (Cr_2O_3) and pure cobalt (Co) powder is carburized to create a ceramic material contained within the Cr-Co-C ternary system. The Cr-Co-C ternary system has several intermetallic carbide phases corresponding to the standard chromium carbides of Cr_3C_2, Cr_7C_3, and $Cr_{23}C_6$. Due to the close atomic size of chromium and cobalt, the structure of the molecular unit stays the same, the chromium atoms in the standard carbide can be replaced with cobalt or stay as chromium. This possible alternative composition is denoted by M(Cr,Co). Figure 5, shows the known phase states for a section of the Cr-Co-C ternary system at 800 Celsius [23].

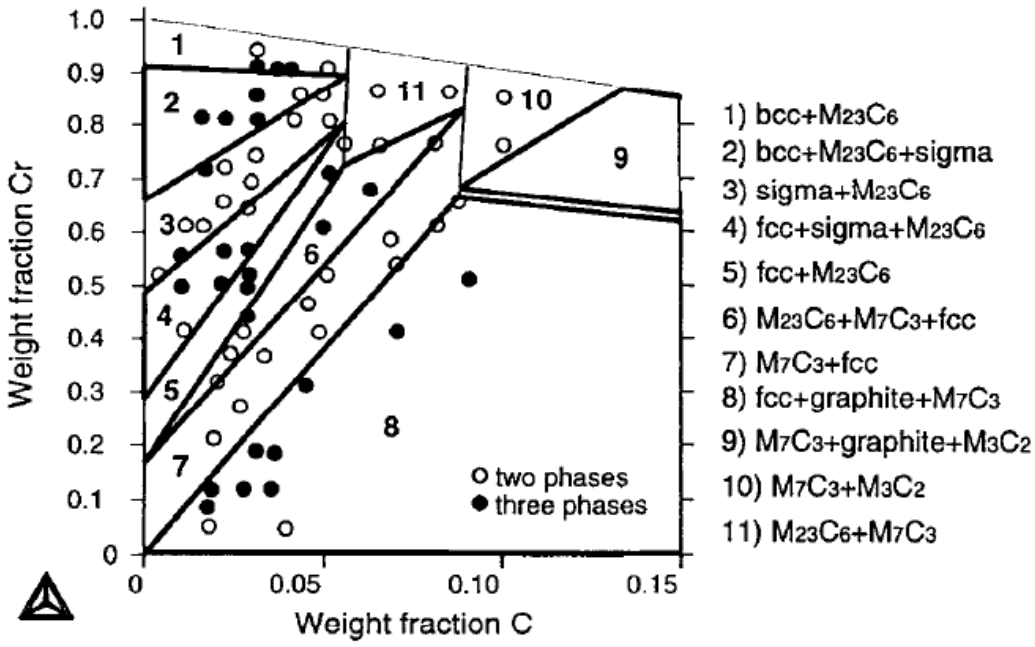

Figure 5. Phase diagram of Cr-Co-C ternary system at 800 Celsius[3]

A problem occurs during high temperature sintering, above 800 Celsius, none of the ceramic phases exist by themselves in the Cr-Co-C system. The result is an intermixing of metallic fcc or bcc Cr-Co-C with the desired ceramic carbide phase and possibly an unwanted graphite phase that does not have the same unit cell dimensions as the metallic or intermetallic phases in the Cr-Co-C system. Care must be taken to prevent the growth of a graphite phase as the mismatch in atomic lattice cause internal stresses that prevent proper amalgamation of the ceramic phases and reduces the strength of the material to near that of uncompressed graphite. This is due to the fact that unlike the metallic fcc and bcc phases, which exist at high temperatures due to the increase in the solubility of the system, the graphite does not revert to the desired metal carbide upon cooling. Figure 6 shows the difference in how a properly prepared sample streaks vs. a sample with a significant graphite concentration.

[3] Used under Fair Use from "A Thermodynamic Evaluation of the Co-Cr and the C-Co-Cr Systems" by A. Kusoffsky and B. Jansson[23]

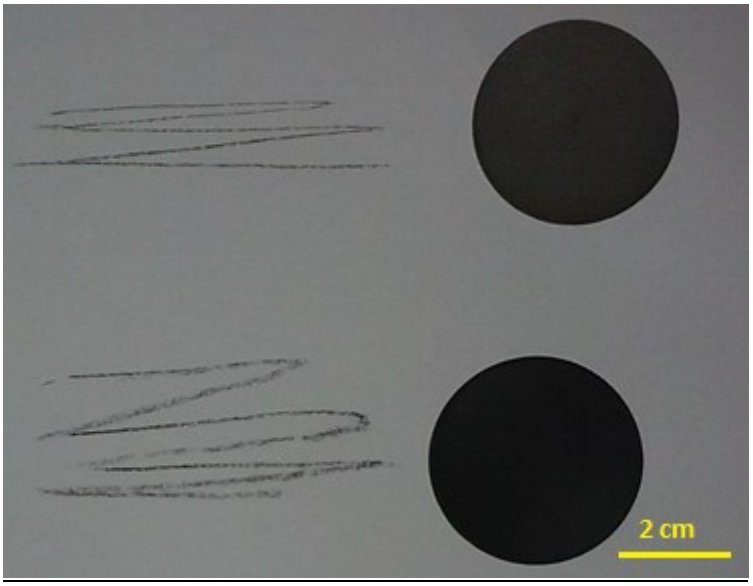

Figure 6. Streak test between porous M7C3 and porous M7C3+Graphite

The bottom sample is the one which contains excess carbon in the form of graphite. The streak from the top sample has an even thickness and consistency that widens as the edge is ground flat. The bottom sample changes between a thin dense line to a wide smudged line with a change in direction and is noticeably darker which indicates the increased carbon concentration.

3.2.2 Siloxzane polymers

3.2.2.1 Molecular chemistry

Most polymers have a backbone consisting of carbon atoms linked to each other through a variety of bond types or possibly intermediate atoms. An alternate atomic backbone is possible for artificial polymers based on silicon, known as Polydimethylsiloxane [11] (PDMS). These polymers have several interesting materials properties that can be taken advantage of due to the atomic features of these molecules. Where the backbone of a simple hydrocarbon is a single chain of carbon bonded via a sp1 bond, PDMS uses silicon-oxygen bonds. Compared to the sp1 C-C bond, the bond angle between the O-Si-O is 34% larger [24], which allows more rotational freedom for the atoms on either side of the silicon atom. Greater rotational flexibility allows for greater molecular freedom by preventing long chain polymers from entangling and locking, creating a more flexible, stretchable material.

3.2.2.2 Elastomers

Elastomers are a specific class of materials with extremely high strain values in their elastic regime. Elastic strain values up to 400% are possible with the proper siloxane mixture. The ability to return to the initial state with no damage from such strains allows these materials to fill niche applications with impact focus and repeated large displacements. A secondary benefit of the molecular make-up, is that most siloxane polymers are permeable to gases due to the large spaces between molecular chains due to the presence of the alternating Si-O atoms in the main polymer chain providing a larger free volume in the material than similar carbon based polymers [25].Silicon atoms have a larger radius than carbon atoms in standard polymers, creating larger gaps between neighbouring molecules. This, combined with the less rigid bonds of the silicon-oxygen system compared to carbon bonding, allow polymer chains to flex and slide past each other much easier than carbon chains.

This flexibility of siloxane polymers has a disadvantage. While the elasticity allows the material to suffer extremes of compression and extension with essentially no lasting damage, when subjected to a shear stress, siloxane polymers have a distinct tendency to separate and tear[24]. Care must therefore be taken when using these polymers as allowing any shear stress to be effected upon the material could cause fail under otherwise normal conditions and loadings. To mitigate this, a change in how the polymer bonds to itself is required. The low secondary bonding capability of the siloxane base is the primary reason for failure under shearing; therefore increasing the number of primary bonds between molecules, in the form of crosslinking between monomers and polymer chains, the shear strength of the material can be increased. This increase in shear stress resistance comes at the expense of elasticity, as the more crosslinking in the polymer, the less the molecules are able to flex and slide past each other, reducing the total internal mobility and therefore decreasing the inherent elasticity.

3.2.2.3 Thermal degradation pathways

Polymeric materials lack the thermal stability of metals or ceramics due to the relative weakness of their interatomic bonds. Siloxane polymers such as PDMS can normally only survive up until temperatures reach slightly over 200 Celsius, with full degradation at approximately 340 Celsius[26]. When these straight chain polymers degrade, the typical pathway is into a cyclic molecule composed of either tri- or tetrasiloxane rings. Degradation of molecular structures is a reaction to thermal energy that is extremely common among polymeric materials. The change in aspect ratio between the initial state and the degraded state causes enough stress to break the bonds between molecules in the material, therefore compromising the stability and structure of the material.

There are two methods to increase the thermal stability of a polymer. The first is to increase the degree of crosslinking between molecules, thus reducing the possible number of vibrational modes for the molecules and increasing the amount of thermal energy that must be absorbed before degradation occurs. This method is what differentiates the two primary classes of polymers; thermoplasts and thermosets. Thermoplasts are normally considered lightly cross-linked, and thus are capable of stretching and flowing around each other when heated, allowing the material to plastically deform and warp to varying degrees. Thermosets are highly cross-linked and much more thermally stable. They do not tend to exhibit a melting point or any kind of phase change or creep until the temperature reaches the level where the polymer begins to degrade completely. The second method for increasing thermal stability of a polymer is to create the final polymer out of individually more stable monomers. As such, by creating a siloxane based polymer out of the normal degradation products, such as a cyclotetrasiloxane, increases the thermal stability of the polymer[26]. By having the polymer comprised of the standard degraded products of the straight chain PDMS; there is no change in monomer shape from linear to cyclic. The polymer therefore maintains its arrangement and cohesion well beyond the normal degradation temperature of a siloxane polymer. This is a very desirable attribute for future investigations into this particular BCC composition as the desired use is in hot bitumen pipelines. In that kind of environment the polymer will have to withstand elevated temperatures without degrading or flowing while under stress. While the current tests will all be performed under STP conditions, if the

material performs well specialized investigations into more niche applications such as high temperature testing will be called for.

3.2.3 Carbon Nanotube Functionalization and Impregnation

3.2.3.1 Requirements of functionalization

Within the last few decades, the advent of carbon nanotubes (CNTs) has provided researchers and materials designers with a material that can be used to create composites with previously impossible mechanical properties for their mass. The ultra-high strength of CNTs in tension and shear, coupled with their nano-scale dimensions and exemplary thermal and electronic properties makes them very attractive for use in all manner of applications. These applications range from structural members for high performance cars to flexible electronic circuits[27]. One caveat about CNTs is that due to their size, each nanotube has a very small active surface area and is incredibly smooth with only weak pi-bonds available on the surface[28]. These features taken together make it incredibly difficult to bond the nanotubes to a matrix. Without a strong bond, the nanotubes are unable to effect the maximum possible strengthening of the matrix.

To increase the possibility of a strong bond forming between the nanotubes and the matrix, the addition of functional groups to the nanotube sidewalls can increase both the effective surface area of the nanotube, and give sites for the constituent molecules of the matrix to bond with greater strength. This is possible due to the primary use of highly polarized functional molecules such as amine groups, hydroxide groups or acetate groups. The use of polarized groups allows for high strength bonding between the polymer matrix and the functional group by using hydrogen bonds rather than the low energy pi-bonds inherent to the surface of the nanotubes. This method not only increases the probability of a good bond between the matrix and the fibres, but also increases the strength of that bond, and the amount of stress that the interface can withstand before failure. The result is hopefully, stronger composite materials that can better withstand the rigors of abrasive wear.

3.2.3.2 Dispersion

Dispersion is the process by which a reinforcing material is spread throughout an entire volume of a composite material[29]. This is important to composite materials as it helps maximize the available surface area for bonding. In the ideal case, every reinforcing particle or fibre is separated from each other by only enough distance that the zone of influence around the dispersed material does not interact with the zone of influence of any other fibre. If the dispersed materials are any closer, the zones of influence will interact, reducing the total volume of the matrix which experiences the strengthening of the fibres and thus reduce the total strengthening that the fibers can apply to the material.

There are several methods to properly disperse materials within a matrix, both chemical and mechanical. In chemical methods, changes in surface energy due to chemical additions to the matrix materials, or the solvents containing the matrix materials, are used to create an energy gradient promoting the reinforcing material to diffuse through the matrix material rather than agglomerating or clumping [30]–[34]. Mechanical methods involve applying a force to both the matrix and reinforcing materials in order to mix them homogeneously into a composite system. Impact or compressive methods such as ball milling or rolling procedures[32], [35] respectively can create proper dispersion if the reinforcing phase is harder than the matrix material but only if the matrix is still in the solid phase. By applying a compression force, the matrix material is plastically deformed around and between the material to be dispersed, forcing the fibres or particles apart from each other, thereby creating a proper degree of dispersion. Other mechanical methods such as sonication are used in situations where the materials to be dispersed are either mixed first into a solvent, or if the matrix material is a liquid prior to a curing or solidification stage.

If the reinforcing material is not properly dispersed, there may be clusters of the material within the matrix with facets or large areas of the fibres or particles in contact with each other instead of bonded to the matrix. If these clusters are too large, they will not be able to maintain a coherent interface with the matrix material, as well as having an unwanted dimension of motion along the contact line or surface with their neighbouring particle.

Consequently, that particular volume of the composite will be weaker than an area with a proper homogeneous dispersion of the reinforcing phase.

3.3 Procedure Documentation

3.3.1 Powder composition, mixing, and pressing

3.3.1.1 Molar ratios and pre-determined sample size

All samples were designed with the purpose of maintaining equivalent volumes and masses for the final sample disk, the initial powders had to be carefully controlled. The samples were designed to contain 22 wt% cobalt and 70 wt.% Chromium with the balance being composed of Carbon. The starting materials are 45.00g Chromium Oxide powder (Cr_2O_3, Alfa Aesar 98+% Purity, -325 mesh (~2 micrometer average particle diameter)) and 9.68g Cobalt powder (Co, Inframat Advanced Materials, Superfine grade, average particle diameter 1.5 micrometers, 99.95% purity). This batch size mixture contained enough for 6 samples massing ~8.5g of powder per piece.

3.3.1.2 Mixing methods

The powder batches were sealed in polyethylene bottles in 54 g batches with 200 g of high purity 8 mm alumina grinding media. The powder was then wetted with 15 ml of ethanol to prevent powders from becoming airborne in the container and not mixing properly. The samples were then placed in a roller mill for 10 hours to ensure a proper mix is obtained [17]. The samples were then removed and dried in the oven at 80 Celsius. Figure 7 shows the interior of the mixing bottle after drying

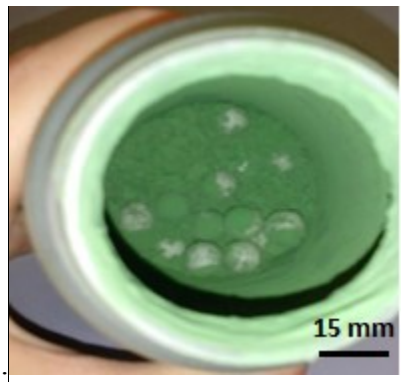

Figure 7. Mixed and dried Cr2O3-Co powder

3.3.1.3 Binding agent and sample pressing.

When the powder was dried, and removed from the bottle, it was mixed with Poly(Ethylene-Glycol) (PEG) from Aldrich (average molecular weight: 400), to create a slurry where the PEG comprises 11 wt%. The mixture was then stirred manually until the PEG coats a majority of every particle of the powder, and the closer that the mixing can come to creating a mono-dispersed powder sample the better. When the powder had been mixed with the PEG binding agent it was then placed into the Carver press in amounts equaling 9.42g. It was imperative to attempt to get the powder mixture as flat as possible before applying pressure, as the PEG would prevent the powders from flowing past each other easily and it would create non-isotropic porosity in the sample. When the powders are ready the press was sealed and 80 MPa of pressure was applied for 210 seconds and slowly released over a period of 30 seconds.

3.3.2 Sample carburization

3.3.2.1 Experimental set-up

The pressed samples were taken and set on a hemi-cylindrical ceramic platform. This was to keep the sample roughly in line with the center of the volume of the tube in the MTI GX-1600 tube furnace. The tube furnace was sealed on both ends, with the exhaust line running directly into an off-gassing flare in the fume hood. The inputs for the oven were run through a switching system to prevent mixing the gases. Two compressed gas bottles, one of argon (Praxair, 99.99% purity) and one of 2 vol% methane, with the balance being Hydrogen. Both of these bottles were set to push air at 250 kPa and the flow meters limited them to 140 mL/min for argon and 80 mL/min for the methane/hydrogen mixture.

3.3.2.2 Reaction stages

After the furnace was sealed, argon was pushed through the system to purge it of any oxygen to prevent any reactions at high temperature and to make it easier to ensure a proper reducing atmosphere. After running the purge for 1 hour, the gas was switched to the

methane mixture, and the temperature program was started. The program starts with a check on oven temperature to ensure it meets room temperature, and then ramps up to 1100 Celsius at 5 Celsius per minute. Once at full temperature, the oven holds at sintering temperature for 20 hours and then begins to cool at 5 Celsius per minute. Once the oven reaches below 200 Celsius the argon is run through the system to purge again before the oven was opened to prevent the possibility of hydrogen mixing with oxygen in unsafe quantities.

3.3.3 Polymer mixing

3.3.3.1 Molar ratios and Catalyst concentrations

The polymer phase of the bi-continuous composite is composed of a 2:1 molar ratio of 1,3,5,7-tetravinyl-1,3,5,7-tetramethylcyclotetrasiloxane (D_4^V) and 1,3,5,7-tetramethylcyclo-tetrasiloxane (D_4^H) co-polymers, which are suspended in a xylene solution, and cured with a platinum Karstadt catalyst (Platinum – Divinyltetramethyldisiloxane, 2.1%-2.4% platinum concentration), all provided from Gelest Inc. The catalyst was diluted by a ratio of 36:1 in toluene to reach a concentration of $5x10^{-4}$ g/mL, as adding the as delivered catalyst to the proper mixture of D_4^V: D_4^H results in a violent exothermic reaction capable of reaching over 900 Celsius. With the properly diluted catalyst, two main streams of infiltrated polymers are used; one containing only 30 ppm of the catalyst and one containing 120 ppm. With this spread it was meant to be able to view a wide range of materials properties and interactions with reinforcing fibres while minimizing the number of samples that are needed and not using too much of the catalyst solution.

3.3.3.2 fCNT concentrations

Acetate functionalized multi-walled carbon nanotubes, 5-7 micron length and 10-20 nanometer diameters, supplied from nanolab.com, are used as the reinforcing fibres inside the polymer matrix. Three concentrations of functionalized carbon nanotube (fCNT) solutions are prepared for each stream of catalyst concentration differentiated polymers; 0.05wt%, 0.1 wt%, and 0.15 wt%, along with a pure polymer to use as a baseline comparison. The fCNTs were first mixed with 4.8 mL of D_4^V as attempting to disperse the nanotubes within the D_4^H co-polymer resulted in the co-polymer reacting with itself when the

temperature reached over 40 Celsius. After the fCNTs were mixed with the D_4^V, the solution was sonicated in a bath sonicator for 1 hour, and then 3.4 mL of D_4^H was added and sonicated together for 20 minutes to promote proper dispersion prior to the addition of the catalyst. For the 30 ppm catalyst samples, 0.5 mL of the catalyst in toluene solution was added to the D_4^V: D_4^H solution, and for the 120 ppm samples, 2 mL was added. The solution is then sonicated again for no more than 5 minutes. Then the solution was poured into a polyethylene dish with the ceramic matrix for the final stages of curing needed to create the bi-continuous composite.

3.3.3.3 Viscosity and Dispersion relationship

The container holding the ceramic sample and the uncured polymer-fCNT composite must be sonicated continuously for 4 hours in a sonic bath. Note; if water is allowed to get into the dish, the fCNTs will preferentially migrate into the water droplet as the acetate functional groups are more attracted to the water molecules than they are to the co-polymer molecules or the xylene or toluene molecules. The sonic bath is meant to ensure that the fCNTs stay properly dispersed in the polymer and to help them penetrate as far into the porous ceramic matrix as possible. It also helps keep the co-polymers thoroughly mixed, increasing the possible number of reactions per minute in the curing reaction. By curing the polymer in-situ, it is possible to keep the fCNTs in the proper state of dispersion until the polymer reaches a high enough viscosity to prevent them from falling out of the dispersion.

3.3.4 Infiltration and Curing

3.3.4.1 Vacuum infiltration

Sonication is not the only method of ensuring that the porous ceramic is fully impregnated by the co-polymer composite solution. Immediately after the catalyst solution was added and the mixture had been poured into the dish with the porous ceramic matrix, the dish was placed in a vacuum container and pulled under a 10^{-3} torr vacuum to remove as much gas from the interior of the ceramic as possible, pulling the liquid co-polymer solution fully inside the matrix. As the sample solution warmed up, there is the possibility of vapour becoming trapped within the ceramic matrix. As such it was important to replace the sample

in the vacuum container several more times when bubbling of the solution became visible during sonication, so as to help prevent trapped vapour from preventing proper bonding between the two materials comprising the final composite.

3.3.4.2 Catalyst Solvent behaviour and process importance

By diluting the catalyst in toluene, it was hoped that the chemical similarity to the xylene that the co-polymers are dissolved in will prevent unknown side-reactions. Also by using a solvent with a higher vapour pressure (22 mm Hg @ 20 Celsius), during the vacuum infiltration it should be possible to boil off much of it preferentially, reducing the volume of the solvents in the solution and speeding up the curing rate of the polymer by increasing the co-polymer density. Increasing the co-polymer density also has the benefit of increasing the viscosity of the solution, thus helping keep the fCNTs dispersed while the final polymer composite coagulates around them.

3.3.4.3 Reaction rates and sample characteristics

The rates of reaction differ between the two catalyst concentration streams. The 120 ppm stream reaches a solid but gummy-like consistency after approximately 24 hours of curing in air, with 4 of those hours being the time spent in the sonic bath. The 30 ppm stream stays liquid over the same period of time, making repeated trips to the sonication bath important prior to the final curing step. The samples cannot however be left in the sonic bath continuously for the first 20 hours as the combination of the vibration energy and the temperature increase of the bath water will cause an accelerated curing process with a crystalline final product. This is undesirable as the inherent grain boundaries in the crystalline polymer allow for easy crack propagation throughout the composite, and the crystalline material exhibits poor resistance to thermal shock in this configuration.

Figure 8 shows several fragments from two separate samples that began to crystallize during sonication and fractured during curing. The interfaces between the grains in the polymer show up as stressed areas that lift or dimple the surface in sections.

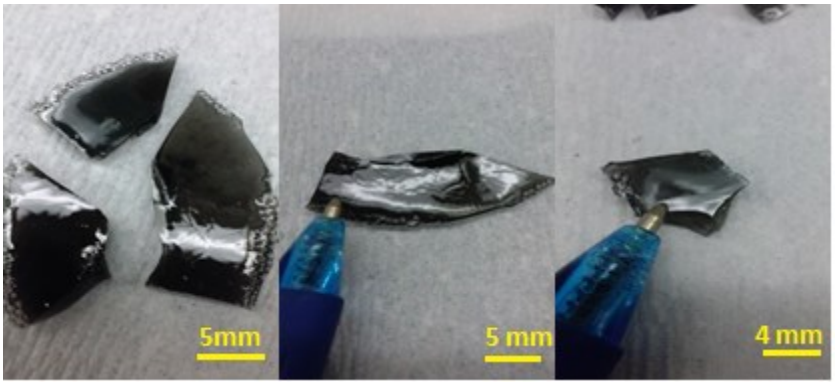

Figure 8 semi-crystalline polymer fragments

3.3.4.4 Curing and final sample behaviour

After the sample has been sonicated and allowed to cure in air overnight, check the dispersion quality of the sample and if there has been a noticeable amount of fibres falling out of the solution, then the sample needs to be run through the sonic bath again to re-disperse the reinforcing fibres. Once the dispersion is of high enough quality, the samples need to be placed in an oven at 80 Celsius for final curing over 24 hours. This stage hopefully evaporates the last of the xylene and toluene solvents from the polymer and leaves an amorphous, glass-like siloxane polymer. Figure 9 shows a selection of BCC materials still encased in polymer prior to being removed and ground to shape for wear testing.

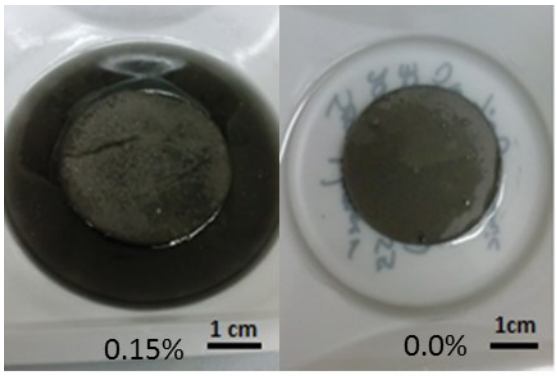

Figure 9. Infiltrated and cured BCC samples of various fCNT concentration

3.4 Results and Discussions of Synthesis

3.4.1 Ceramic phase

3.4.1.1 X-Ray Diffraction analysis

Using x-ray diffraction (XRD) it is possible to determine the atomic structure of the porous ceramic. Following from section 2.3.2 this procedure was designed to create a

material that, during sintering, consisted of the Cr-Co-C fcc phase and the intermetallic $M(Cr, Co)_7C_3$ phase as shown in Figure 5 in Section 3.2.1.2. The hope is that, during cooling, the fcc phase would convert to the intermetallic due to the lower limits of solubility of carbon in the Cr-Co-C system at lower temperature. Figure 10 is an intensity map of x-ray diffraction of a sample of produced Cr-Co-C ceramic measured against the known intensity peaks of Cr_7C_3. Note that the peaks match up in intensity for almost all visible peaks, but the predicted peaks do not match what is determined experimentally. This is due to the addition of the cobalt to the initial chromium oxide feed material, which creates an amalgam metallic phase M(Cr,Co).

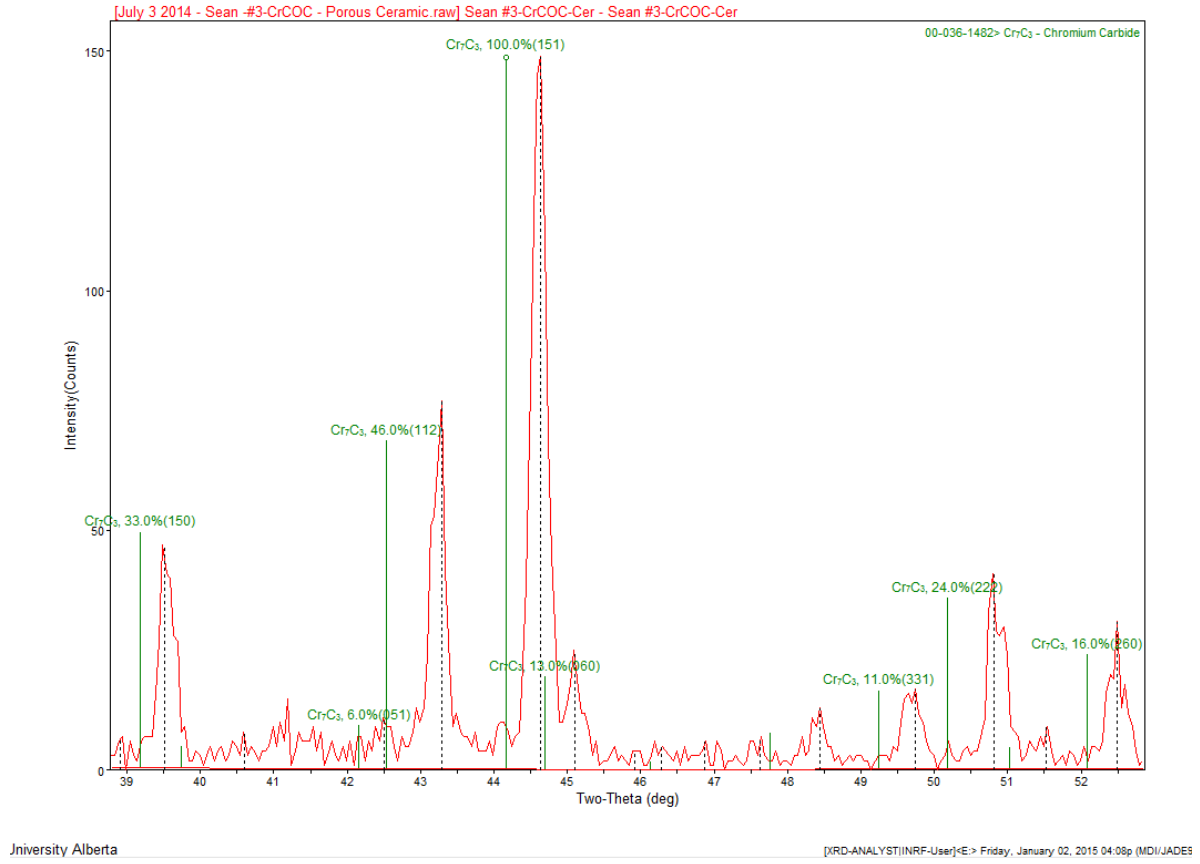

Figure 10. XRD spectra for $M(Cr\text{-}Co)_7C_3$ with listed peak locations for standard Cr_7C_3 in green

Cobalt has an atomic diameter of 125 pm while chromium is 128 pm[11]. By forming an metal carbide with the two metals acting interchangeably in the carbide, but keeping the same molecular structure in the intermetallic M_7C_3, the average inter-planar distances are

decreased. Bragg's law, shown in Equation 4, relates the angle of reflection from an atomic plane to the planar spacing, d, and the incident wavelength of light, λ[11].

$$2dsin(\theta) = n\lambda$$

Equation 4. Braggs Law

As the XRD uses a single wavelength, it is possible to determine from this figure that there has been a change in interatomic spacing d. Given that the average inter planar distances are decreased, the only way for the nλ term to remain constant is if the angle between the incident wave and detected wave is increased. This matches with Figure 10 that shows a small but significant increase in 2θ for every major peak between the measured data and the known standard data for pure Cr_7C_3, leading to the conclusion that the $M(Cr,Co)_7C_3$ is in fact the dominant composition in the sample.

3.4.1.2 SEM analysis

Relying on only XRD to add evidence to the presumed close relationship between microstructural morphologies of a pure Chromium carbide porous ceramic and $M(Cr\text{-}Co)_7C_3$ is not scientifically sound. By comparing visible microstructures of the two materials it is possible to further shore up the theory that they retain similar microstructural composition and crystal structure. Figure 11 shows porous Chromium carbide on the left and infiltrated $M(Cr\text{-}Co)_7C_3$ on the right.

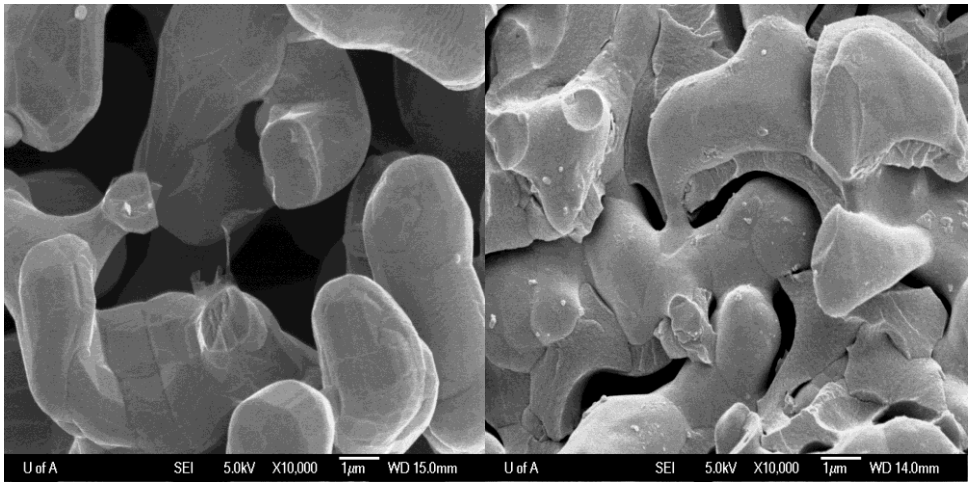

Figure 11 Microstructure Comparison between pure Chromium Carbide and $M(Cr\text{-}Co)_7C_3$

Comparing these microstructures we notice a very similar construction in the faceting of the ceramic phase, which indicates multiple crystal grains per ceramic spar, however looking at the differences between the visible fracture surfaces, there is a definite change from a rhomboid cross section, leading to the conclusion that this chromium carbide baseline picture is actually mostly ortho-rhomboid Cr_3C_2 and the hexagonal Cr_7C_3, to a more circular cross section and a more ductile appearance of the fracture..

There is also the possibility that there is a cobalt enriched phase that is not detected by XRD, as such a complication was found to be occurring by Dong et al. [17]. The occurrence of an enriched cobalt phase becomes significant only at high cobalt concentrations, above what is being pursued in this document, but should not alter the ordering of the ceramic phase substantially as pure cobalt also has a HCP crystal structure. While there would probably be a small lattice mismatch, from the images in Figure 11 it is obviously not enough to cause major structural damage. In fact the lattice mismatch is possibly the mechanism by which the surface of the ceramic struts appears smoothed and the structure is noticeably more circularized, due to the difference in lattice parameters preventing larger crystal grains from forming in any direction and preventing any long range crystal ordering.

Another effect the addition of cobalt to the material seems to have is shrinking the average dimensions of the ceramic spars. The pure chromium carbide spars are approximately rectangular with a major axis usually around 2 μm in length while the minor axis is between 1-1.5 μm. With the addition of cobalt, the ceramic struts become noticeably more circular and seem to maintain a diameter of approximately 1 μm. With the addition of the slightly smaller cobalt powder, and also possibly due to the lower melting temperature of the cobalt when compared to the Cr_2O_3 powder, it is probable that the cobalt powder begins to sinter before the chromium oxide, which could provide a flux path to promote faster diffusion of atoms between adjacent particles of oxide that have a bridge of mobile cobalt between them increasing the cross-sectional area available to transport diffusing atoms between chromium rich particles.

It is not only the ceramic phase that sees a reduction in feature scale due to the addition of cobalt, the average pore diameters also tend to shrink, by a noticeable amount by comparing the SEM pictures in Figure 11. This trend is known from the initial work on the ceramic phase by Dong et al., to be caused by the addition of cobalt[17], firstly due to the promotion of a larger number of interconnections between particles in the pre-sintered sample during the initial stages of sintering. With increasing concentrations of cobalt a pure metallic cobalt phase is formed surrounding the ceramic, increasing the spar size at the expense of porosity and pore diameter. According to Figure 12, the porosity of the ceramic drops off with increasing cobalt concentration.

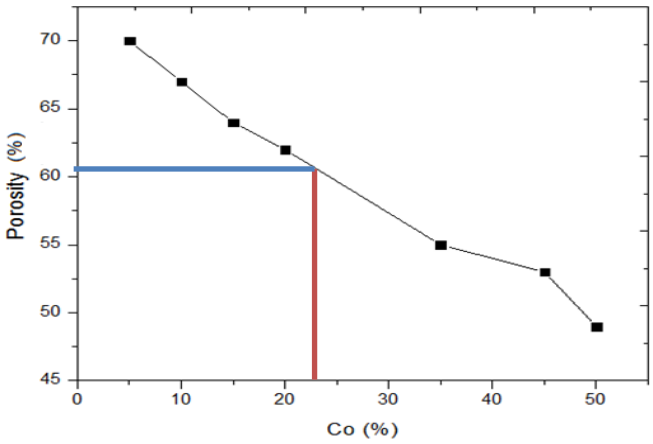

Figure 12 Porosity as a function of cobalt concentration[17][4]

The known concentration of cobalt is marked on the figure in red leading to the conclusion that the samples in this document have all approximately 60-61% porosity by volume.

3.4.2 Polymer Phase

3.4.2.1 Polymer compatibility

From Figure 6 it is notable that the polymer has trouble bonding to the surface of the ceramic. Several gaps are noticeable between the siloxane and the carbide in Figure 11, but despite them all being on the same side there, this lack of contact is not an artifact of directional wear or shear forces pulling the materials apart. Figure 13 shows a sample where an entire spar of ceramic is not bonded to the siloxane, which indicates that this is due to a

[4] Used with permission of Dr. Weixing Chen

lack of bonding between the materials during curing, and then either due to shrinkage from curing or cooling, the polymer pulls away from the ceramic.

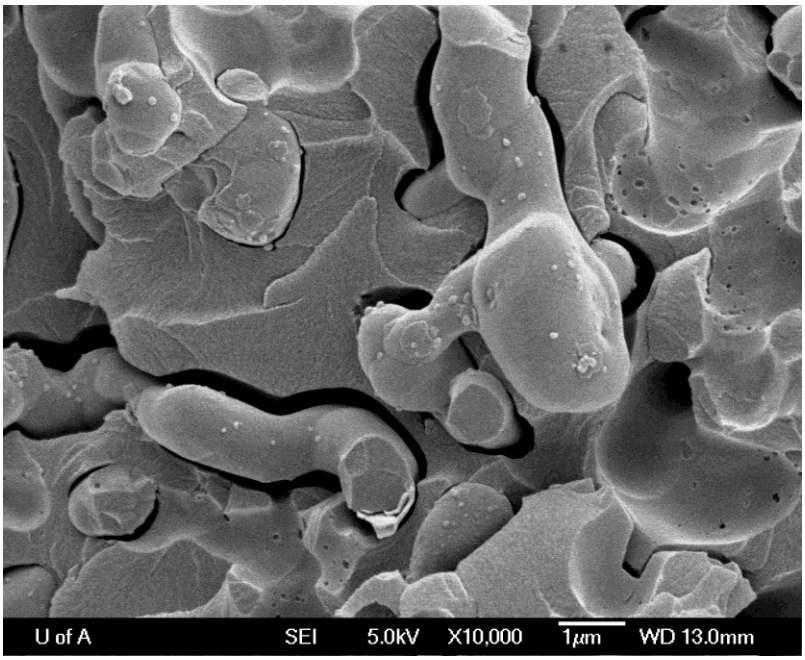

Figure 13 examples of poor bonding between siloxane filler and ceramic spars

The polymers in figures 11 and 13 are low catalyst concentrations with no impregnated fCNTs, and while they do seem to behave as glassy polymers there does seem to be noticeable striations on the fracture faces. This could indicate that the polymer has crystalline properties on a small enough scale, allowing limited amounts of intermolecular slip when under an applied stress leading to plastic deformation rather than failing while still in the elastic regime as a normal glass would.

The primary goal with creating a BCC is to have a well bonded material that can transfer any force or stress easily and efficiently from one material to the other and back, allowing each portion to handle the types of stress that it is most adept at dealing with. Compressive stresses and impacts can be handled by the ceramic phase while bending moments are countered by the polymer, unfortunately tensile stresses are difficult to deal with, as the polymer portion of the BCC cannot deform to compensate until the strain exceeds the maximum of the ceramic portion of the BCC. Luckily, BCCs have an inherent mechanism for allowing each material to apply their strongest properties in more than one type of situation. This mechanism will be expanded upon in a later section.

These theoretical capabilities for BCC's are all dependent on maintaining a bond between both materials across every available surface. Only with a near perfect bond across the entire surface of the initial framework can forces be transmitted back and forth between materials with the proper efficiency and efficacy. From Figures 11 and 13 it is obvious that the current material choices are not measuring up to that requirement.

The obvious gaps between materials are probably the result of several factors. Due to the presence of the carrier solvent xylene, which contains both co-polymers, and toluene, which is used to dilute the catalyst, the curing reaction is therefore happening simultaneously with the vaporization and attempted preferential removal of two volatile organic compounds. Having two compounds coming out of solution via a vapour phase would not normally be much of a stumbling block towards creating a uniform polymeric material. However as the siloxane in this case is intertwined in 3 dimensions with a ceramic scaffold, it is more than likely that while a volume of polymer begins to coagulate and cure inside the ceramic pores, there will be some vapour pressure preventing the newly cured polymer from being attached to a ceramic strut and bonding onto it as it cures, thus preventing the final composite from achieving maximum efficacy in transmitting forces throughout itself.

Future investigations into BCCs for this purpose might find better results in binary epoxies and other non-catalyzed, solvent-less polymers in order to prevent this from occurring. If fully bonded surfaces can be achieved between the two materials, perhaps the addition of CNTs as a reinforcing material can be a viable method to increase the capabilities of the material beyond what would normally be possible. But as the results have shown, the amount of bonding between the comprising materials is the primary strengthening mechanism for BCCs, and attempting to strengthen one material when that bond is not ensured is simply wasting time and resources.

3.4.2.2 Thermal Stability

Due to bitumen containing high volumes of large molecular weight organic materials[36] transporting it through pipelines of any sort, whether from facility to facility of from one storage tank to another, requires that it be kept hot (~433K [37]) in order to reduce the viscosity enough to make it flow at all. For this reason primarily was the Siloxane

polymer chosen, as by using a cyclosiloxane and constructing a material out of the initial decomposition products of straight chain siloxanes, the theory is that the temperatures required to break down this material will be greatly increased. Studies have shown that not only are cyclosiloxanes thermally stable until over 673K [24], but also that by performing an annealing procedure under argon at high temperatures, the last of the volatiles in the material can be removed. This procedure results in increasing the onset of thermal decomposition of the material closer to that of the constituent co-polymer molecules themselves at approximately 798K [26] and maintained their mass when heated to 300°C in an oxygenated environment.

For these reasons was the mixture of 1,3,5,7-tetravinyl-1,3,5,7-tetramethyl-cyclotetrasiloxane (D_4^V) and 1,3,5,7-tetramethylcyclo-tetrasiloxane (D_4^H) considered as a viable choice. Other known high-temperature polymers such as Poly(Ether Ether Ketone) (PEEK) are thermoplastic rather than thermosetting and as such tend to melt at high enough temperatures, 507 K for PEEK[38], which is not a viable material for use in a hot fluid environment. Other thermosetting materials that degrade at temperatures higher than the cyclosiloxane mixture, such as Polytetrafluoroethylene (PTFE aka Teflon) which starts degrading at 746 K, require the handling of extremely hazardous precursors that the laboratory space used are unable to accommodate. Polycyclosiloxanes are a good combination of strength, thermal stability and simple handling, making them an excellent choice for use in BCC materials that require exposure to high temperatures in fluid environments.

3.4.3 Bi-Continuous composite

3.4.3.1 Sample fabrication limitations

With the production methods outlined in Section 3.3, it takes approximately one week to create a single sample. Due to the size limitations of the roller mill for mixing the initial powders, the samples are created in batches large enough to create only 6 samples. The samples are labeled in the order they are created in each batch and grouped via the day that

the initial powders were mixed. Table 1 shows the full list of samples created for wear and erosion testing, and their respective masses before sintering, after sintering and after infiltration as well as the final density of the samples.

Table 1 BCC sample creation data

sample names	catalyst ppm	CNT concentration	Initial Mass	carburized mass	Infiltrated Mass	Density
090913-B2-S1	120	0.00%	9.43g	6.81g	7.43	2.86
020413-B2-S3	30	0.00%	9.43g	6.77g	7.48	2.88
090913-B1-S3	120	0.05%	9.43g	6.76g	7.86	2.76
090913-B1-S4	30	0.05%	9.42g	6.77g	6.98	2.66
090913-B1-S1	120	0.10%	9.42g	6.78g	7.73	2.99
020413-B1-S4	30	0.10%	9.43g	6.75g	7.13	2.81
090913-B1-S5	120	0.15%	9.43g	6.77g	7.65	3.03
090913-B2-S4	30	0.15%	9.44g	7.39g	8.36	2.88
090913-B2-S2	120	0.00%	9.43g	6.77g	7.73	2.85
090913-B2-S6	30	0.00%	9.43g	7.45g	6.59	2.62
151113-B1-S2	120	0.05%	9.42g	6.96g	7.60	2.89
151113-B1-S3	30	0.05%	9.42g	6.84g	7.03	2.84
151113-B1-S1	120	0.10%	9.42g	7.03g	7.95	2.86
090913-B1-S2	30	0.10%	9.42g	6.77g	7.71	2.82
151113-B1-S4	120	0.15%	9.42g	6.83g	7.63	2.97
151113-B1-S5	30	0.15%	9.42g	6.93g	7.47	2.92
151113-B1-S6	120	0.00%	9.42g	7.03g	7.34	2.75
151113-B2-S1	30	0.00%	9.42g	7.14g	7.53	2.75
151113-B2-S2	120	0.05%	9.42g	6.98g	7.37	2.77
151113-B2-S3	30	0.05%	9.42g	7.03g	7.21	2.84
151113-B2-S4	120	0.10%	9.42g	6.94g	7.43	2.75
151113-B2-S5	30	0.10%	9.42g	6.98g	7.67	3.12
151113-B2-S6	120	0.15%	9.42g	6.92g	7.72	2.81
200214-B1-S1	30	0.15%	9.42g	6.93g	6.57	2.56
200214-B1-S2	120	0.00%	9.42g	6.93g	7.07	2.84
200214-B1-S3	30	0.00%	9.42g	6.95g	7.43	2.95
200214-B1-S4	120	0.05%	9.42g	6.88g	7.19	2.87
200214-B1-S5	30	0.05%	9.42g	7.04g	7.53	2.91
200214-B1-S6	120	0.10%	9.42g	7.01g	7.02	2.85
200214-B2-S1	30	0.10%	9.42g	7.06g	7.77	2.78
200214-B2-S2	120	0.15%	9.42g	6.91g	7.32	2.85
200214-B2-S3	30	0.15%	9.42g	7.00g	6.65	2.81
200214-B2-S4	spare		9.42g	7.00g		#DIV/0!
200214-B2-S5	spare		9.42g	7.00g		#DIV/0!
200214-B2-S6	spare		9.42g	7.16g		#DIV/0!

The sample densities are calculated from the volumes of the prepped samples shown in Tables 28-35 in Appendix D.

3.4.3.2 Shear loading and Poisson's ratio

When the porous matrix is infiltrated with the reinforcing phase, so long as the surfaces are properly bonded, an interesting effect takes place. Due to the different Poisson's ratios between the two materials, any strain in any direction from either material, will cause the resulting force from the other material to act against the initial strain. A tensile strain in the matrix will cause a reduction in thickness of a spur, pulling in the surrounding reinforcing material and creating an orthogonal tensile force operating against the initial tensile strain in the matrix. This effect is only possible due to the mixing of materials with differing Poisson's ratios; as if the ratios are similar there will be no orthogonal stress to counteract the initial strain. This effect only lasts until the forces transmitting between the materials is large enough to break any bonding between the materials in question. And materials with low Poisson's ratios are more likely to suffer disbondment from the matrix material, due to the greater strain in the initial direction required to create a large enough reactive stress in the matrix material to prevent a larger increase in strain. It is this interior balance of forces between the materials that comprise the composite that makes BCCs theoretically able to withstand impressive forces in any direction.

As the reinforcing material strains, the materials on both sides of the interface or pulled further away from their initial positions resulting in a shear stress. If the shear stress exceeds the strength of the bond between the matrix and reinforcing materials, the two materials will disbond, and the material will become susceptible to catastrophic failure as the two materials will not be able to reinforce each other to their maximum capability. Luckily the strain required to do this is unlikely to be met within the confines of the composite, as the random orientation of the pores within the matrix prevent any material from moving more than a few diameters of the initial powders. Knowing this, porous ceramics can be designed to complement the reinforcing material and prevent shearing disbondment by altering the particle diameter of the initial powder such that the maximum length in any one direction is lower than the minimum strain required for shearing the interface.

3.4.3.3 Theoretical Property Evaluation

As with other composites the capability of a bi-continuous composite is predicated on the volume fraction of each material. As such the Rule of Mixtures is still an adequate method for predicting how the material will perform in any desired circumstances, but with the limiting fact that the forces applied to the material will only last until the stress becomes too much for the bond between the two materials comprising the composite. It is in this regard that bi-continuous composites differ from standard reinforced composite, as a bond failure between the matrix and the dispersed material will only effect the local area of the material as the stress will migrate to the other pieces of the dispersed material in the composite, whereas with a BCC, due to the continuous nature of both interpenetrated materials, failure of a bond reduces the strength of the whole material once that first failure begins. From this it is safe to say that a relationship, like that with fibre composites having a critical length that determines the minimum dimensions required to support the maximum stress transfer in the composite, between the shear strength required to break the bond between the matrix and infiltrated material and the maximum stress is likely to be very similar to that espoused in Equation 3. Thus by determining the energy required to shear the infiltrated material from that of the matrix, it should be possible to place limits upon the maximum strength of a BCC of any composition, and to determine the appropriate pore length and diameter to prevent any shear strain from reaching the required magnitude to cause failure. Pore diameter can be approximated visually as shown in Figure 14 and the attached Table 2. Unfortunately due to the lack of any long range order and the continuously curving nature of the porous ceramic phase the pore length cannot be as easily obtained from a two dimensional source image.

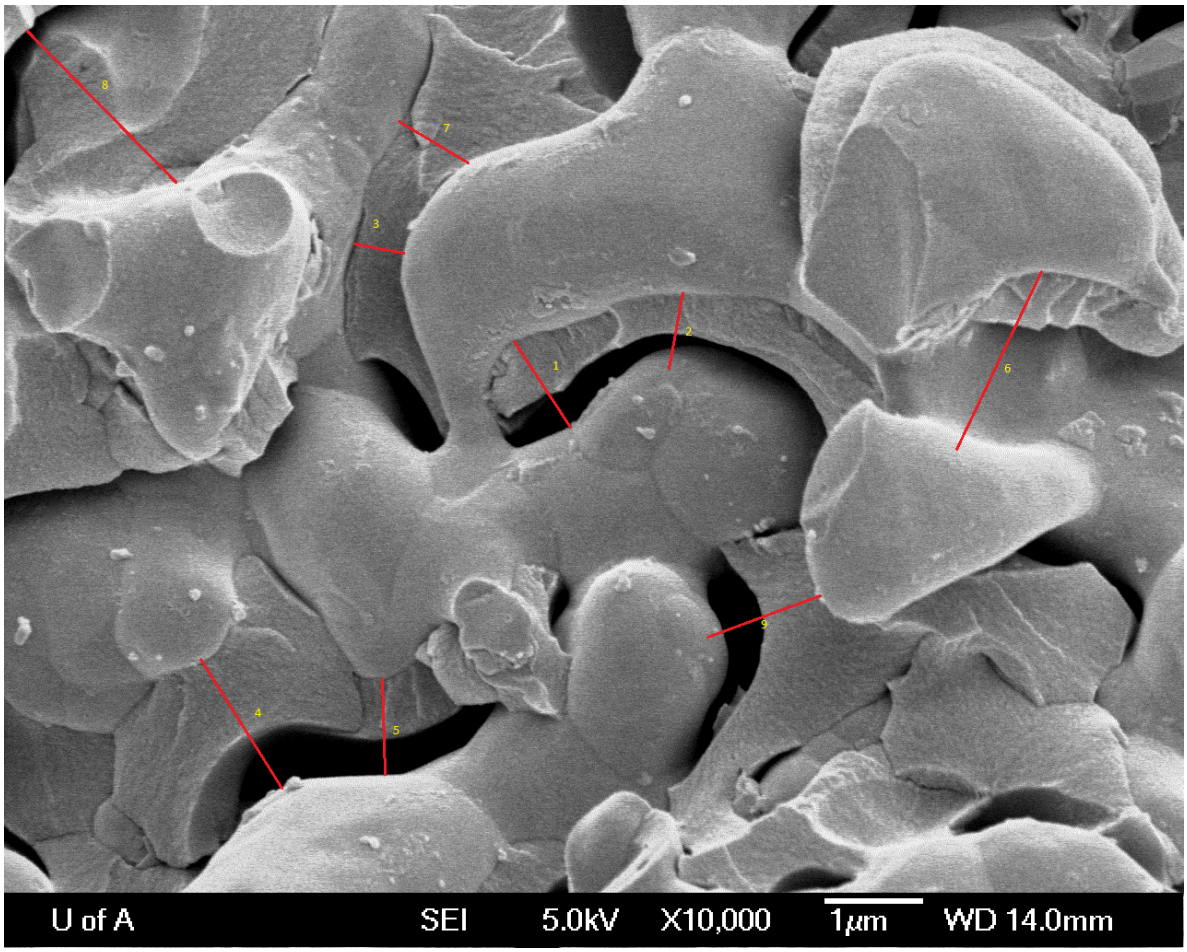

Figure 14. Approximation of pore widths.

Table 2. Determination of pixel lengths to um

line #	pixels	angle	length
1	72.226	-62.526	1.057
2	63.266	-94.357	0.99
3	83.537	-6.882	0.541
4	82.191	-44.523	1.591
5	94.192	-94.044	0.927
6	121.937	-110.589	1.895
7	121.262	-27.613	0.688
8	117.188	-44.471	2.157
9	83.397	22.357	1.256
average			1.233556
std dev			0.51427

Without a reliable value for the pore length or an accurate model of the porous ceramic to determine the available surface area of pores along an axis, it is impossible to predict the possible values of the ideal materials strength.

3.5 Conclusions of Synthesis

The process for creating a BCC can be a simple task of 3 steps, or expand to encompass multiple stages for refining each portion of the material into advanced and expensive materials. However as with all processes, inserting additional steps or processes increases the number of points of failure in the entire process, and thus requires much more energy and attention to ensure a satisfactory amount of throughput when creating the product. At which point there begins to be diminishing returns for increased effort or even a regression in cost/benefit is another academic field and beyond the scope of this document. When embarking upon fundamental research into a new field, simplification as a method of quality control cannot be overvalued. However, with the materials selected and included in this specific study, as many possible process failure outcomes were avoided if possible, or identified and catalogued if not to help determine whether pursuing this specific composition is still able to be considered worth the effort and expense.

Chapter 4: Wear and erosion evaluation of ceramic-polymer BCCs

4.1 Introduction

The intention of this chapter is to explore how the various materials alterations to the samples affect the materials in terms of hardness, bending modulus and tan delta and how these changes to fundamental properties lead to changes in wear resistance. These changes are due to the unique structure of the BCC. Relying on the standard tell-tale properties of hardness and fracture toughness could possibly lead to missing an important relationship that could yield a new path to explore about BCC materials. By exploring the unique micro and macro scale effects of a material comprised of under-constrained joints, it is hoped that this material can provide a new method for preventing wear and abrasion without resorting to thick coatings of expensive and heavy refractory ceramic materials for the purposes of exploiting the unique freedom of motion offered as a method of absorbing, reflecting and dispersing the energy of a particle impact.

4.2 Experimental

4.2.1 Wear and Erosion testing

4.2.1.1 G65 ASTM standards for testing

For testing materials for wear resistance against abrasion and erosion via sand particles, the majority of facilities use the ASTM G65 standard for testing. This standard involves mounting and allowing a rubber wheel to contact the surface of the sample while spinning and having a steady stream of sand grains poured into the contact area between wheel and sample. The pressure of the abrasion is maintained at a constant level by having the sample on a free hanging joint with a resting position located behind the wheel outer edge, causing the weight of the sample and arm to pull itself into the wheel as the sample is abraded[39].

The G65 test does not however provide quantitative measurements for abrasion resistance for all possible environments. Changes in particle size, composition, speed; aspect ratio, friability, and fluid environment all change the rate of erosion. As such, the G65 is standardized to provide a relative ranking system between materials. With a standard test time, wheel speed and grit media, it is possible to get very accurate results for ranking

multiple types of materials for wear resistance. However, since the composite is meant to survive in a tailings pipeline or slurry, and as it was not possible with available equipment to create a sample large enough to satisfy the requirements of the G65 standard, it is not an apt method for studying the failure modes of the bi-continuous composite material.

4.2.1.2 Slurry pot testing and attempted equivalence

To attempt to gain reliable data for erosion and abrasion resistance in a liquid system, a slurry pot testing rig is used. This method involves rotating samples with known available surface areas inside a mixture of water and abrasive particles. In this set of experiments, silica sand with an average diameter of 120 microns was used. The samples were spaced equidistant around a circular holder and rotated to any desired angle against the direction of rotation. In this paper, angles of 45° and 22° were tested. Samples were held in place via holders designed to expose only a defined area of the sample. For this paper, a rotation speed of 660 RPM was used on a 20 cm wide plate which acted as the sample holder frame, equating to a speed of 5.5 m/s for the specimens. The sample holders were fitted with front covering plates with an opening meant to expose exactly 6 cm^2 in a 2 cm wide by 3 cm tall rectangle. By knowing the initial mass of the sample and the density, and then comparing the final mass, it was possible to determine the approximate mass percentage and volume percentage loss of the exposed area. Figure 28 in Appendix B shows a blueprint used to fabricate the sample holder frame.

4.2.1.3 Bending modulus and tan delta

A chaotic orientation of the struts and mores comprising the ceramic frame of the BCC prevents the joints between struts from being fully supported. Thus the bending strength of the material becomes paramount as the defining value for determining the failure point of the material. By subjecting the material to bending and measuring both the force required and the energy returned after bending the various types of samples were compared to determine which sample composition was best suited to withstanding an impact from an abrasive particle without damage. Either through absorbing the energy of the impact into the internal structure, or by deflecting it away from the surface.

High energy absorption would be the preferred method for high orthogonal vector energy impingements. This would allow the energy to be shared throughout the material which would ideally prevent fractures and subsequent loss of material. For low orthogonal energy impingements, a harder material that deflects the material is more suited as it minimizes the time spent dragging along the surface by the abrasive particle, thus minimizing the chances of the particle finding a surface flaw and removing excess material from the coating.

Testing the different material compositions will give the capability to theorize which BCC samples should perform best under differing circumstances. This will be further examined in section 4.3.2.

4.3 Results

4.3.1 Wear Resistance

4.3.1.1 Outcomes and lost volumes

Samples were tested in two major batches, meant to differentiate how the material behaved while being abraded at two different angles. The first groups were tested at 45° to determine how the material handled a worst case of impact abrasion, such as in a corner piece of piping where a large volume of slurry is forced to change direction very rapidly. The second batch was tested at 22° to approximate glancing angle impacts to the best possible ability of the geometry of the sample holders, and to attempt to find equivalence with the ASTM G65 standard.

While measuring the wear resistance in terms of material lost is useful for discounting the effects of sample size and density, it lacks an objective standard to define the wear resistance of the material if subjected to different kinds of erosion or abrasion. This requires that these samples be tested against a standard material prepared and used in the same testing style in order to find some form of baseline. This is exactly how the ASTM G65 standard operates, by setting up a relative scale of material capabilities compared with each other instead of an objective absolute. Table 3 shows the results of testing samples of X60 pipeline

steel in an attempt to determine how the BCC compares as a wear resistant material against the material it is being engineered to protect.

Table 3: X60 pipeline steel slurry pot erosion results

mm^3 lost	
45° impingment	22° impingment
4.285332448	0.879514505
4.432804752	0.792845919

Figures 15 and 16 show the outcomes of 8 sets of slurry pot tests, meant to cover 2 tests of each fCNT concentration in every group of different catalyst concentration at each angle. These are compared against the average volume loss of 2 samples of X60 pipeline steel tested at the same angle of impingement. The data from which these figures are drawn can be found in Appendix A.

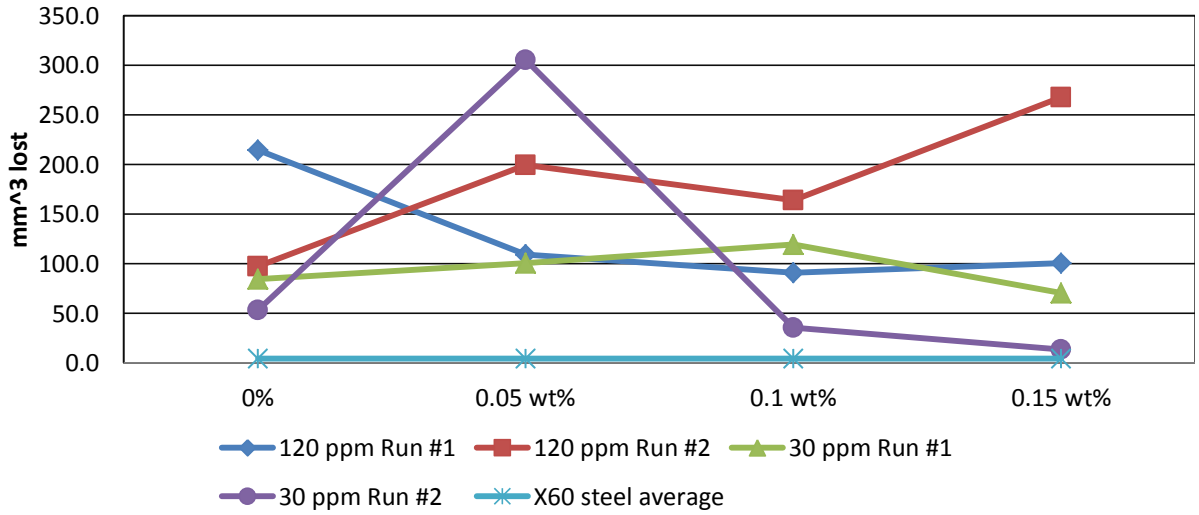

Figure 15: 45° impingement

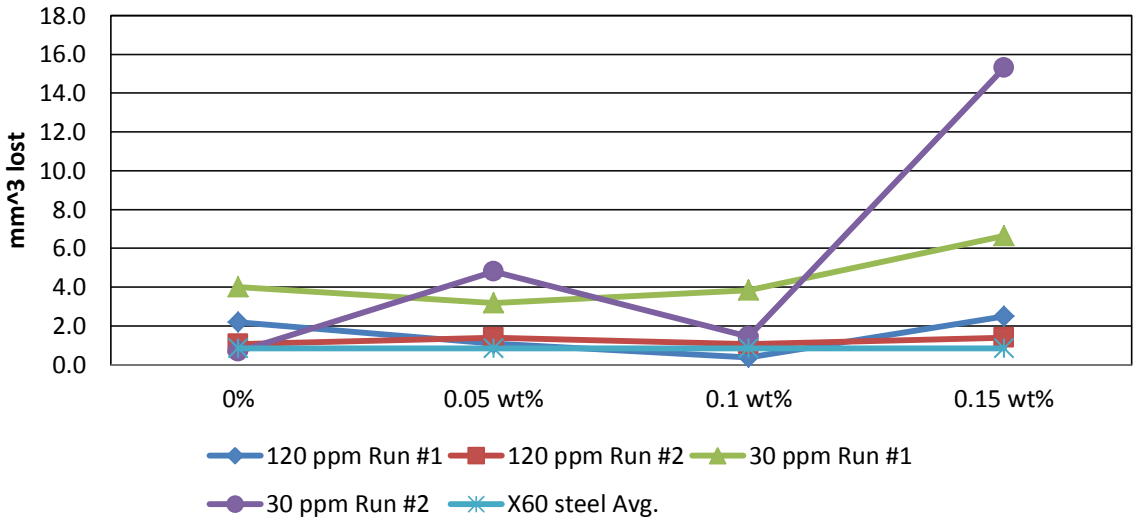

Figure 16: 22° impingement

All values are in mm^3 lost to ensure they are not based off of the density or volume of these specific samples, allowing data to be compared between multiple groups. The data from which these values are derived is shown in Table 5 of Appendix A.

Comparing the data from the BCC samples to the standard samples is difficult due to the lack of correlation among the wear resistance of BCC samples. What is noticeable, even without correlating data among the tested samples, is that there is a noticeable change in the rate of erosion between the angles of impingement for both the baseline metals and the BCC samples, and that the degree of change is not the same for the metal samples as it is for the BCC. In order to determine how to define this difference, the samples must be properly differentiated among themselves to determine if there are statistical differences between the different treatments comprising the BCC samples.

4.3.1.2 Statistical grouping comparisons

Having 16 permutations for sample creation and testing, it is important to differentiate groups from each other. Using a Single Factor ANOVA test with an alpha value of 0.05 to determine which factors create separate entities, it is shown that the addition of fCNTs to the polymer matrix does not equate to a statistically significant difference in

abrasion resistance amount for any of the catalyst concentrations or under any tested impingement angle. Tables 18 and 19 in Appendix B show the results of ANOVA testing on the 4 main groupings of tests, differentiated by catalyst concentration. The resulting P-values for each are shown below in Table 4 along with the different P-values for when the outlier in the 45°, 30 ppm test was removed.

Table 4 P-values from Single Factor ANOVA tests

	45 degrees		22 degrees	
	120 ppm	30 ppm	120 ppm	30 ppm
P-Value	0.920914	0.333492	0.342862	0.174139
no outlier	----------	0.729511	----------	----------

Comparing these values against the set alpha value of 0.05, the conclusion is that the addition of fCNTs to the polymer does not statistically affect the abrasion resistance of the resulting materials. fCNT concentration is not the only variable at work, and the difference between abrasion resistance due to catalyst concentration is also an important point. Running the same tests, shown in Appendix B, by comparing the different catalyst groups that are all tested at the same impingement angle, it is determined that there is a statistically significant difference between the 120 ppm and 30 ppm catalysts for both the 45° and 22° tests.

The average mm^3 lost for each of the catalyst concentrations is tabulated below in Figures 17 and 18. This is to determine which polymer properties appear most beneficial under abrasive conditions.

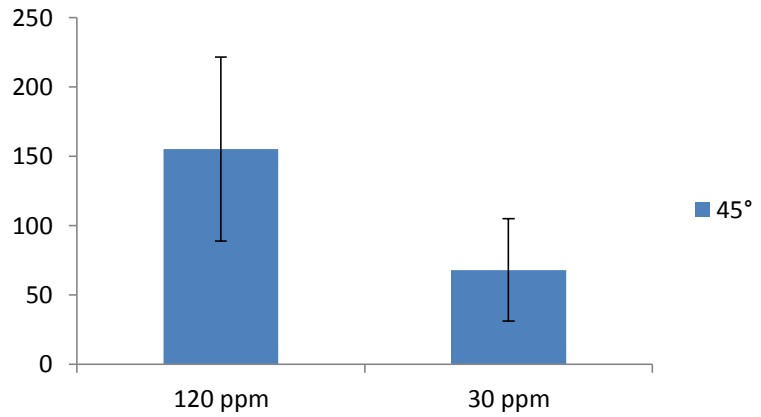

Figure 17 Average BCC Volume Losses at 45°

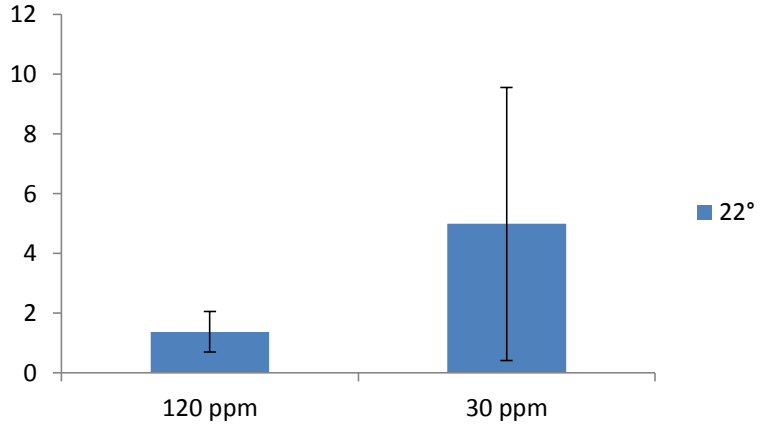

Figure 18 Average BCC Volume Losses at 22°

What is apparent is a shift in how each batch responds before and after the initial polymer facing has worn away. Under the 22 degree abrasion, the <150 μm polymer facing is worn away at a much faster rate when the polymer is soft and elastic. But when both classes of BCCs are fully stripped of their polymer facing, the softer reinforcing polymer seems to improve the wear resistance of the combined BCC. Possibly this is due to a greater damping ability of the more elastic polymer such that, even despite the desired 100% bonded surface area between the ceramic and polymer volumes, the oscillatory bending of the ceramic struts after being impacted by an abrasive particle is absorbed, dispersed and dampened by the more elastic 30 ppm polymer rather than the harder 120 ppm polymer.

4.3.1.3 Wear resistance equivalence

As this material is being designed to handle the harsh environments of tailings pipes and hot bitumen transport pipes, it is imperative that it stand up well against the materials currently used as abrasive coatings for these situations or situations similar to them. As most coatings are tested with the ASTM G65 dry abrasion standard, it would be beneficial to find a comparison between the data obtained from the slurry pot and the G65. One way of finding this comparison would be to use the small data set from testing the X60 grade pipeline steel for baseline numbers for the BCC wear resistance, and to find dry abrasion test data on for that grade or a similar grade and compare them to determine approximately how effective the BCC would be in a G65 test.

X70 grade steel was used as an initial test by Victor Jaimes MSc. to determine the reliability of a newly calibrated G65 apparatus[40]. By taking a best case scenario and assuming that X60 and X70 grade steels have essentially identical wear resistance, a conversion factor for volume lost in the slurry pot, compared to a G65 test can be determined and applied to known values for BCC erosion. From the Jaimes thesis, the volume lost from a X70 steel sample under the ASTM G65 A procedure is 268.29 mm^3[40]. To ensure that the error for the conversion is minimized, the linear wear distance must be normalized between the two testing methods, as the G65 Procedure A test runs for a linear 4309 m[39], while the slurry pot testing runs for a linear 11,550 m. Converting the X60 value to the equivalent distance for a G65 test yields a volume loss ratio of 1.626 mm^3 X60 to 268.29 mm^3 X70. Dividing the X70 volume loss by the X60 volume loss gives a conversion factor of 164.97[5]. Converting the BCC erosion data to an equivalent G65 linear abrasion distance and then applying the discovered conversion factor gives the approximate value for the volume of each sample material that would be lost if a G65 test was able to be performed on them. This data is displayed in Figure 19 and compared against the value of the volume lost by the X70 sample. The data that this figure is derived from is shown in Table 8 in Appendix A.

[5] This ratio is probably lower than if actual X60 data from a G65 test had been found, as X70 steel is harder and has higher yield strength than X60 steel. As such it is safe to assume that X60 pipeline steel would lose more volume in a G65 test, thus giving a larger conversion factor.

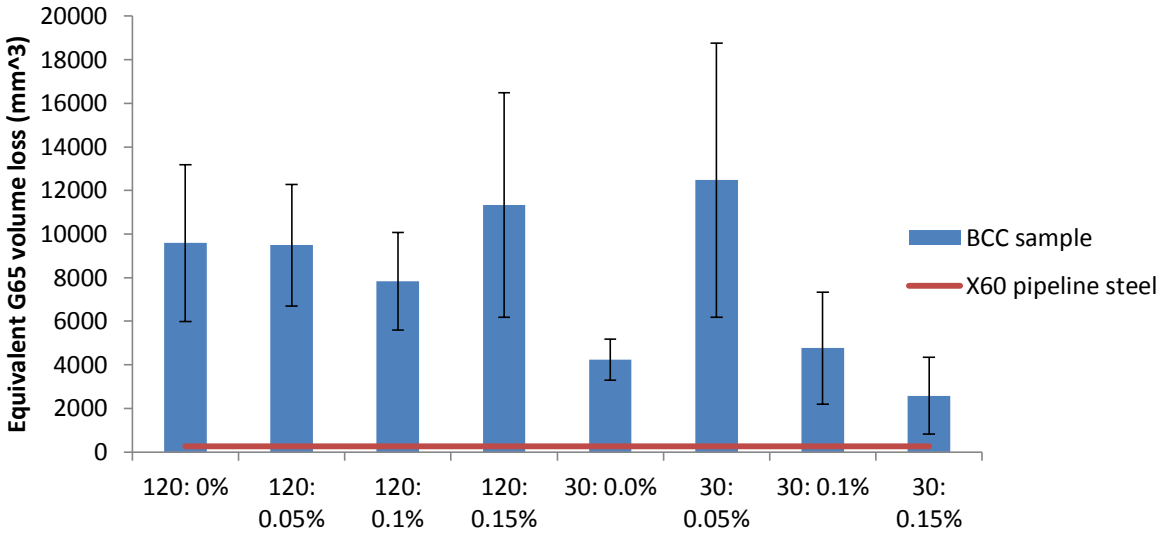

Figure 19 Equivalent volume loss to G65 tested X60 sample at 45 Degrees impingement

From this figure it is obvious that the BCC is significantly inferior to bare steel in terms of wear resistance. Even ignoring the 120 ppm: 0.15 fCNT wt% and 30 ppm: 0.05 fCNT wt% samples as outliers none of the other samples show the ability to match the wear resistance of the X60 steel. To see if this disparity in capability is constant for differing impingement angles, the data for the 22° tests is compared in the same manner. By performing the same calculations, an equivalency ratio between the slurry pot erosion and the G65 test is found to be equal to 860.01 as shown in Table 10 in Appendix A. Using this ratio the data shown in Figure 20[6] can be compiled and compared.

[6] For clarity of the figure, the 30 pm: 0.15 fCNT wt.% data point is removed as an outlier as it was more than a standard deviation above the next most eroded sample making the figure difficult to determine any fine details. The chart from which the data was drawn is shown in full in as Table 11 in Appendix A

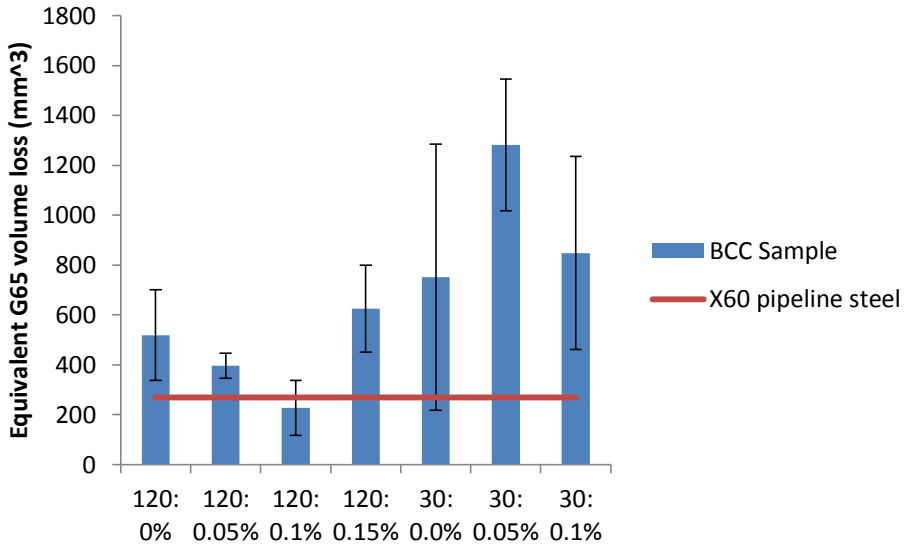

Figure 20 Equivalent volume loss to G65 tested X60 sample at 22 Degrees impingement

It is encouraging to notice that in this data set there is actually one type of sample that actually appears to improve upon the wear resistance of bare pipeline steel. There is another point of interest when comparing the two data sets against the recorded hardness of the samples. At higher impingement angles the softer, 30 ppm polymer composites exhibit better performance than the stiffer 120 ppm samples. It is not enough to improve upon the bare steel, but at low impingement angles the harder polymer composites appear to exhibit superior properties relative to the 30 ppm samples. This insinuates a possible correlation between the energy of impact and which method of preventing damage is superior. At low angles a hard faced coating can withstand the impact and maintain integrity better than a softer, more absorbing material, but above an unknown threshold, a more elastic material is better suited to absorbing and dispersing the energy into itself.

The final outcome is that while there does seem to be promise in the BCC for use as an erosion resistant coating, as shown by the single sample composition that improves upon wear resistance of bare steel, current iterations do not have the capability to perform to the necessary level for this application.

4.3.2. Storage modulus and damping

Using Dr. Anastasia Elias's Dynamic Mechanical Analysis machine (DMA) (Perkin Elmer DMA 8000), the storage modulus and Tan Delta ratio for the BCC samples were determined. By flexing the sample to a preset displacement at a set frequency and measuring the force required to bend the sample, the amount of energy that the material can absorb during bending can be determined. By propagating this data out to steady state the actual bending modulus can be found at t = ∞. Figure 21 shows this collected data[7], plot data is shown in Table 7 in Appendix A and direct recorded data is displayed in figures 30-35 in Appendix B.

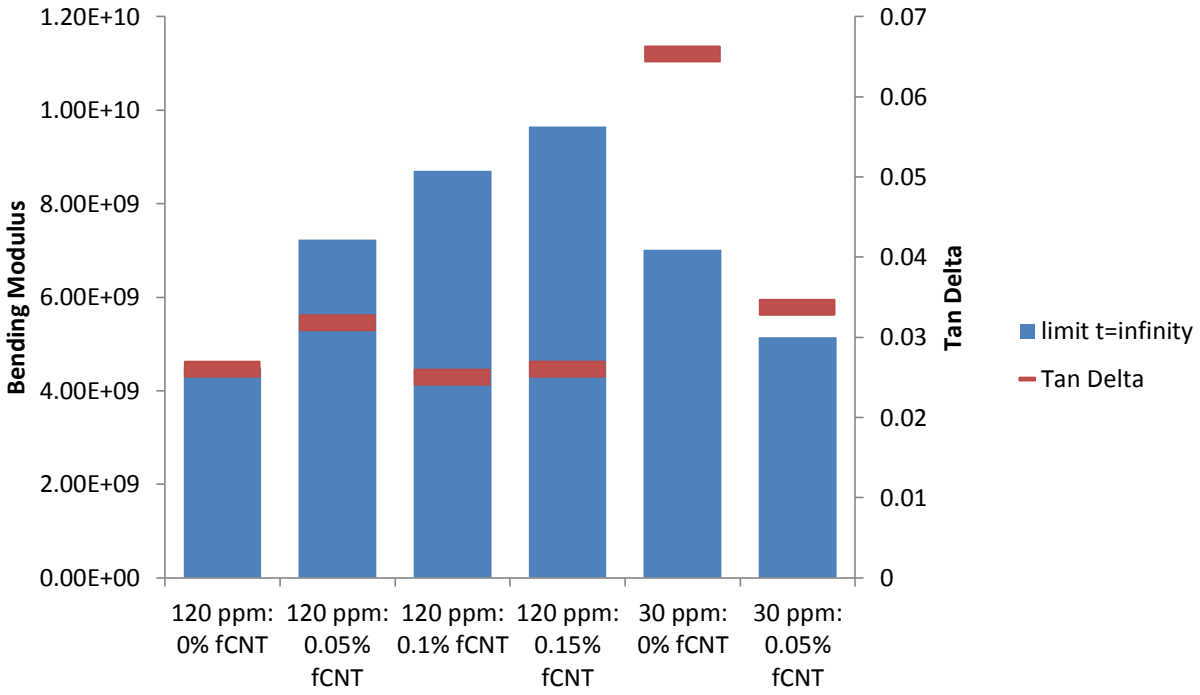

Figure 21. Bending and Storage Moduli of BCC samples

From this data we see two expected trends. The 120 ppm composites steadily increase in ability with increasing fCNT concentrations, but maintain very similar tan delta values. The 30 ppm samples on the other hand begin to weaken with the addition of fCNTs and with anything more than 0.05 wt% fCNT concentration, the polymer has lost so much stiffness

[7] There is no data available for 30 ppm samples of 0.1% or 0.15% fCNT concentration as they were broken in half by the DMA on the first oscillation.

that bending the material is essentially equal to bending the plain porous ceramic and the samples snap under the 5 N load. The tan delta for the pure 30 ppm samples however is noticeably larger than those of the 120 ppm samples, which agrees with the findings in the previous sections that the 30 ppm polymers are more capable of dissipating impact forces into the polymer phase. The lower storage modulus also explains why the 30 ppm samples did not perform as well as the 120 ppm samples when the polymer layer was still intact as the material was unable to withstand the energy of impact and proceeded to tear and be worn away faster.

4.3.3 Hardness

4.3.3.1 Statistical comparisons

Figure 22 shows the hardness of the selection of composites tested and the various fCNT polymer composites employed in creating the final BCC samples. This is to determine the effects of both fCNT concentration on the polymer phase and the addition of said polymer to the base ceramic to create the BCC.

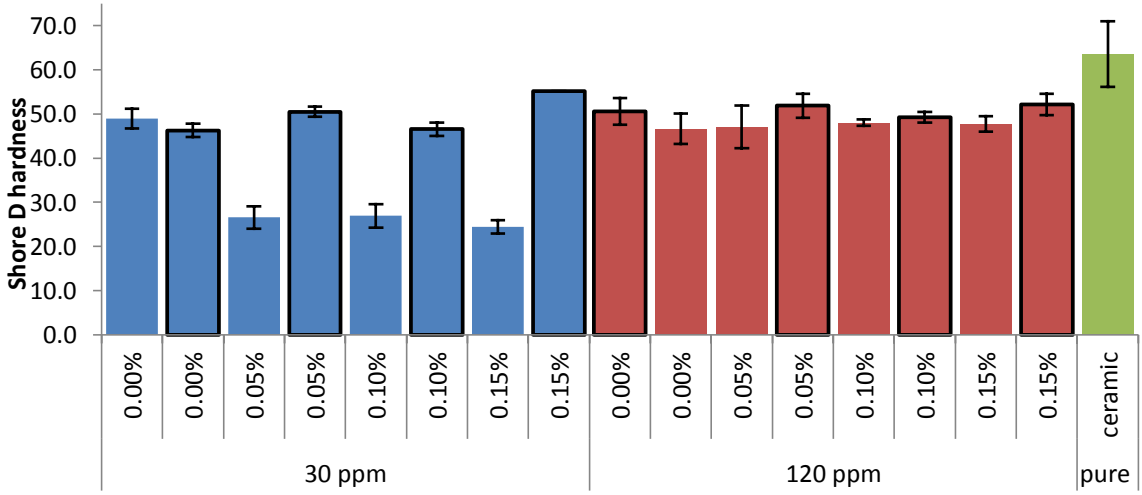

Figure 22. Shore D hardness of polymers and composites[8]

[8] Direct hardness data from Alberta Innovates Technology Futures (AITF) is displayed in Appendix B, while collected data and conversion process from Shore A to Shore D is shown in Tables 12, 13 and 14 and Figure 30 in Appendix A

In the above figure, the hardness values of the BCC samples are outlined in black with the polymers comprising them shown next to those bars without outlines. There is very little visible correlation between the hardness of the polymer and that of the composite. In fact, according to ANOVA tests (Tables 20-27 shown in Appendix C), with 95% confidence, there is a statistically significant difference between all polymers and composites for the 120 ppm samples, while only the pure 30 ppm polymer is not statistically harder or softer than the composite. This data indicates that there is an actual mixing of properties for all composite samples other than the 30 pm 0% fCNT sample, which could be comprised of the two phases completely separated from each other.

When comparing the composite materials against each other, the 120 ppm samples are not statistically different from each other, indicating that the addition of functionalized carbon nanotubes does not appreciably affect the final hardness of the material. The 30 ppm samples on the other hand are statistically dissimilar from each other, indicating a possible problem with the interactions between the various fCNT loadings in the polymer and the ceramic. Oddly, when comparing the composites across the polymer types, the 0.05% fCNT 30 ppm composite 151113-B2-S3 was statistically indistinguishable from the 120 ppm as shown in Table 27 in Appendix C. From that, it would be expected that the sample would perform similarly to the 120 ppm samples. However, sample 151113-B2-S3 is not the hardest sample in the 30 ppm group, and as such should theoretically only retain the second most amount of material during the test. Figure 16 shows that it actually retains significantly more mass than the hardest sample in the same group which is the 0.15% fCNT sample 200214-B1-S1. A reason for this could be a lack of material toughness due to the poor bonding between the ceramic and polymer phases, which was likely responsible for the failure of the same sample type under DMA testing. With only hardness to prevent wear, but with the small scale of the features, the ceramic would have steadily been removed under the impacts of the sand, taking the soft polymer phase with it.

Fundamentally, there are enough statistical differences between the composite groups to allow for realistically accurate conclusions to be drawn as to the effectiveness of varying compositions of BCC materials under the effects of abrasive environments.

4.3.3.2 Hardness and wear resistance across impingement angles

As stated in the previous section the 120 ppm BCC samples are not statistically different from each other in terms of hardness, as such by assuming that the samples are equivalent, by comparing the data that makes up Figures 19 and 20, it is easy to see that the 120 ppm samples performed noticeably better when the angle of impingement was low. This conclusion aligns well with the theory stated in Section 4.2.1.3, stating that a harder substance will perform better trying to deflect a particle with a low momentum vector normal to the surface of the material, than it will against an impinging particle at a more vertical incoming vector, as there is less ability to deform and absorb the energy of the blow.

Comparing the relationship of hardness to wear resistance of the 30 ppm BCC sample groups is more difficult, as the materials exhibit a wide enough spread in hardness that they cannot be classified as all being statistically similar. This forces any comparison between hardness and wear resistance to consider each BCC type separately. The easiest way to compare the samples is to determine the relative amounts of wear, and compare those for each impingement angle to the relative hardness of the material. By setting the value that all samples will be compared against to the highest value for each data set it should be possible to see how hardness affects how much material is removed. Figure 23 shows this compiled data but removes the 0.15% 30 ppm sample as an outlier just as in Figure 20. If the theory that softer materials are better suited to dealing with high impingement angle abrasion is correct then the 30 ppm data should show that as the samples get softer, the 45 degree samples will lose less material relative to their maximum than the 22 degrees samples

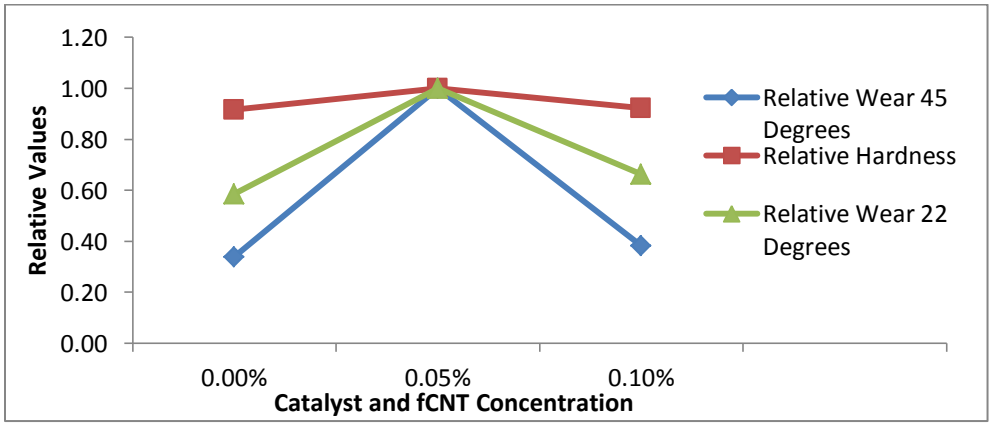

Figure 23. Comparison of relative hardness against relative wear for each impingement angle for 30 ppm

Just as predicted the softer 30 ppm samples show significant gains in wear resistance at high impingement angles with only a small reduction in hardness of the sample. Figures 19 and 20 in Section 4.3.1.3 support the idea that the softer 30 ppm material is not only superior to the 120 ppm BCC at high angle abrasion but also that significant gains can be found by reducing the hardness within reason. Thus, with further research it may be possible to design a BCC that is actually capable of outperforming a standard abrasion resistant coating.

4.4 Discussions

4.4.1 Failure Mechanisms

4.4.1.1 Ceramic failure

Despite the intrinsic hardness and wear resistance of the $M(Cr\text{-}Co)_7C_3$ system, the structure of the porous ceramic itself is a major barrier to attaining the maximum possible material strength. This is due to the fact that the material is randomly oriented in its porosity. By relying on randomly oriented spars of interconnecting ceramic, the compressive strength of the ceramic is subverted and bypassed, as the dominant failure method of a randomly oriented porous ceramic, regardless of the stress orientation, is due to bending failure[41]. This is due to junctions of the ceramic spars lacking enough points of reinforcement to fully constrain all directions of movement of the junction according to Maxwell's Criterion[42], shown in Equation 5.

$$s - m = b - 3j + 6 \geq 0$$

Equation 5. Maxwell's Criterion for defining the constraint of a joint

Equation 5 defines the required number of beams (b) and frictionless joints (j) for a 3 dimensional interconnected system to cause the number of self-stresses (s) to be greater or equal to the number of applied mechanical stresses (m) to qualify the system as fully constrained or over-constrained. By having an under-constrained join between multiple spars, there is a free direction of motion for that join, allowing a bending stress to be applied to the spars that comprise the junction. If the ceramic portion of a BCC was instead constructed to be properly constrained at each junction or over-constrained, any applied forces would be transferred into the rest of the material through compressive phonons in the material

structure. By returning the method of force transfer through the material to a compression based method rather than a bending stress, the maximum strength of the ceramic would be available to the final material.

Given the size of the ceramic spars and the diameter of the pores between them, the impact of a 250 μm silica particle can be assumed to be affecting both materials comprising the BCC in equal measure. If the conditions for a properly constrained and rigid microstructure were able to be met in this material, the force of the impact would be dispersed through every connecting strut deep into the material and dispersed in the dampening polymer phase. Instead, the force races through the ceramic phase preferentially at the speed of sound and when it finds a spar that is not supported enough, it can shatter the connection between the material on either side of the strut. Continued exposure to impacts equivalent to that will continue to erode connections between the ceramic and the polymer, and break the remaining spars connecting the volume of ceramic to the bulk. When the last connecting strut connecting the volume in question to the bulk material breaks, the remaining force of the impact and the force of all subsequent impacts onto the interface between the polymer and the now loose section of ceramic.

Once there is a disconnected section of ceramic, the repeated impacts of the impinging particles causes repeated stress upon the interface between the components of the BCC, with the capability of slowly removing the bond between the materials, causing rapid deterioration in the local wear resistance of the material. Figure 23 shows areas of a worn sample that are likely the result of this form of erosion, where one area has worn away faster than the surrounding area, forming a “pocket” in the exposed face of the sample.

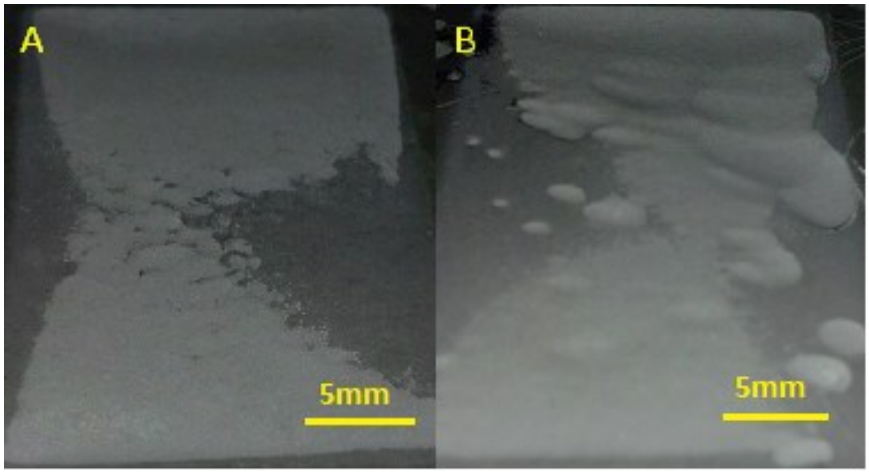

Figure 24 dimpling of erosion area due to disconnection of underlying ceramic structure: A) 120 ppm, 0% fCNT B) 120 ppm, 0.05% fCNT

The dimpling pictured can be fairly subtle or quite severe depending on the underlying structure of the ceramic. Unfortunately there is currently no way to predict which samples in a batch will have this flaw. The possibility of any sample of this material exhibiting this failure mechanism is fairly small, these are the only two samples that have visible signs of dimpling out of 32 tested in the slurry pot, but the formation of these dimples exposes more surface area per linear length to any abrasive media and thus creates an area that will be worn away preferentially if used as a wear resistant material coating.

4.4.1.2 Polymer failure

The polymer is cured specifically to have an amorphous structure, meant to prevent slip systems within the polymer, such as would appear with a crystalline microstructure, with the intention of increasing the elastic modulus of the polymer, preventing plastic deformation during abrasion. By preventing plastic deformation, the polymer isn't worn away from the interface with the ceramic a little at a time from the surface, but instead requires enough force to break the interface from the initial bond strength. However there are also the possibilities of asperities within the siloxane polymer, where stresses could concentrate and fracture the material. Pictures of fractured polymer sections such as in Figure 24, show small shards of polymer kept next to the main body of material through small electrostatic forces.

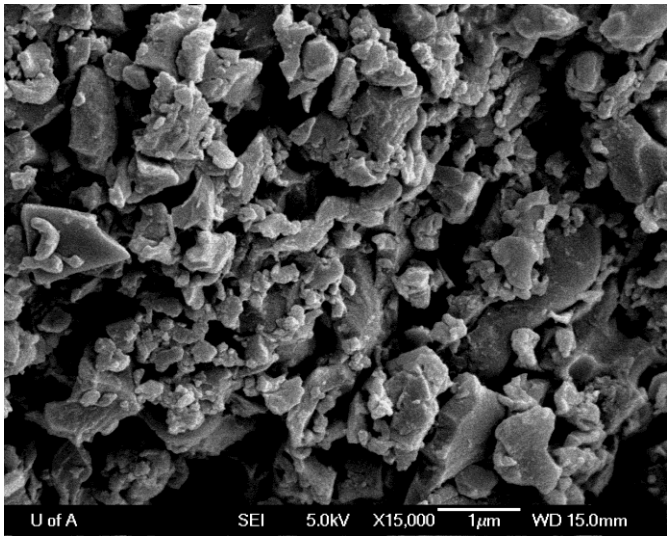

Figure 25 Polymer fracture and cling

This possibility of applied stresses promoting interior fractures would contribute to the rapid wear of the composite material under abrasive testing. If this theory is correct, we would expect to see a definitive pattern of wear in a polymer facing, proceeding in one direction along the direction the abrasive material travels across the sample. Figure 25 shows the characteristic scallops of the polymer having been "scooped" out by each impinging particle, the resulting siloxane shards that are left behind, and a comparison against the initial state of the polymer prior to abrasion.

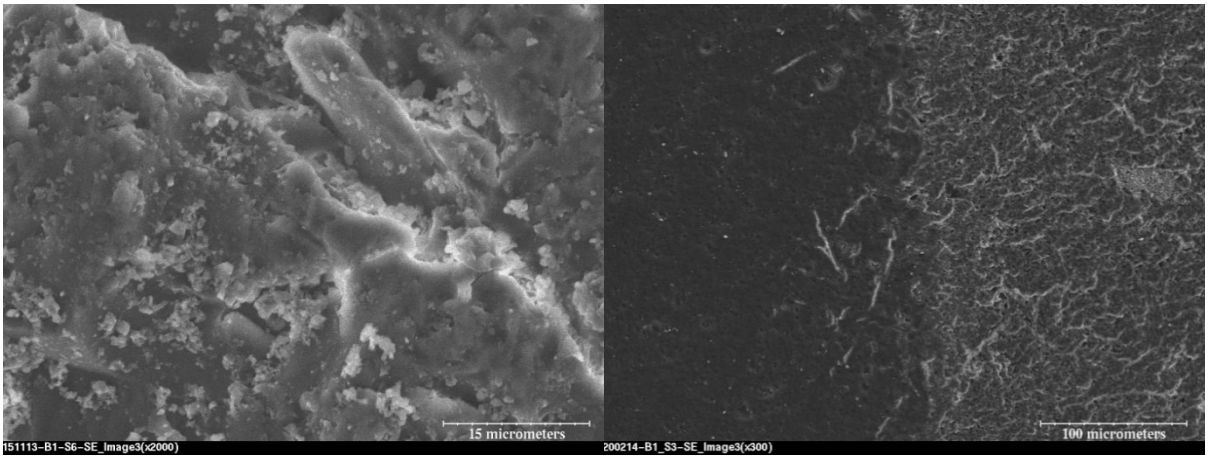

Figure 26 Aftermath of polymer erosion and comparison between abraded section and original surface

The process by which these scallops and shards are formed is illustrated in Figure 26, assuming that an abrasive grain hits the surface of the sample with enough force to shear off a volume.

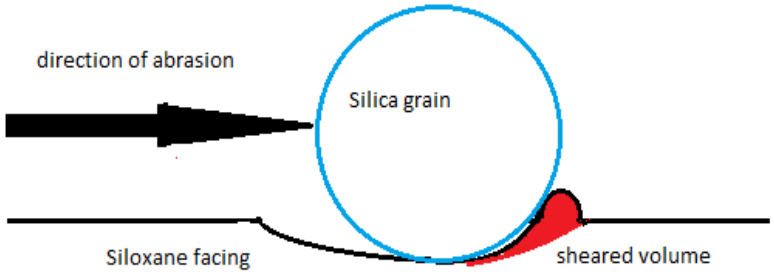

Figure 27 Polymer wear mechanism through shearing

The sheared volume is not perfect of course, and each sheared volume can be broken along several lines which populates the eroded surface with bits of polymer. Due to the amount of impregnated reinforcing fCNTs in the polymer, there is a difference in the amount of energy required to shear the polymer. Because of this, there is visible differentiation in the final appearance of the eroded polymer. Figure 27 shows polymer erosion of 4 different fCNT and catalyst concentration combinations comprising the test samples.

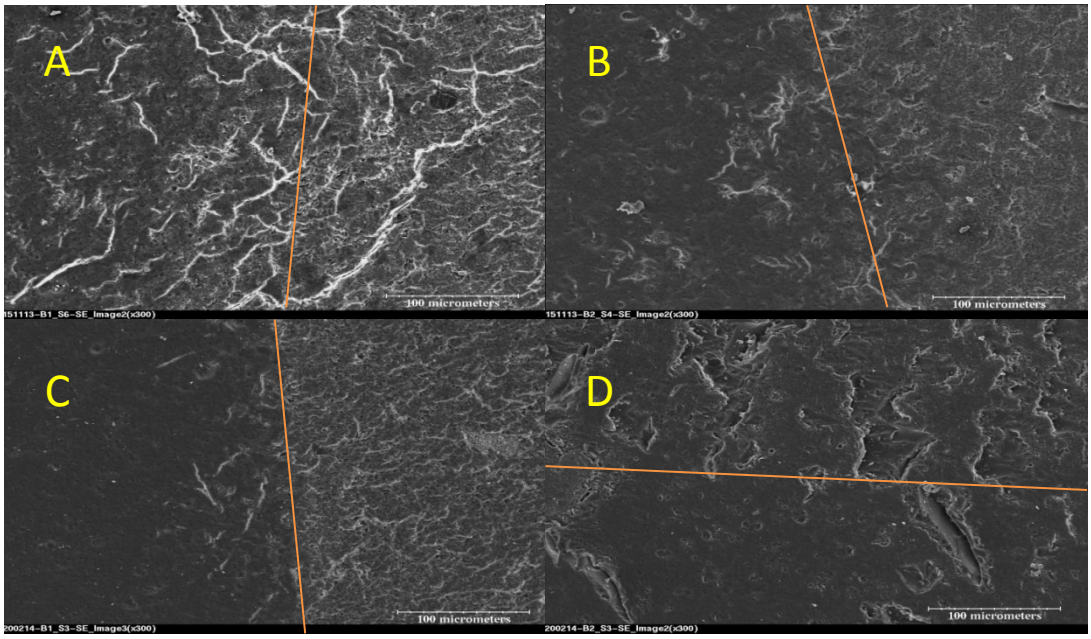

Figure 28 Comparison between wear outcomes with differing catalyst and fCNT compositions in the 22° erosion tests: A) 120 ppm catalyst, 0 wt.% fCNT B) 120 ppm catalyst, 0.1 wt.% fCNT C) 30 ppm catalyst, 0 wt.% fCNT D) 30 ppm catalyst, 0.15 wt.%

While the addition of carbon nanotubes made no statistically significant difference in the total wear resistance of any group of samples at any impingement angle, that does not mean that they made no difference in how the polymer reacts to the abrasive media. Comparing sections A and B of Figure 27 shows that the addition of fCNTs to the polymer reduced not only the amount of wear on the face of the material, but also inhibited transport of shear forces across the boundary of exposure, delineated by the thin orange line. To be able to reduce the damage incurred on an area outside of direct influence indicates that the addition of the fCNTs, instead of hardening the polymer, in fact increased the elasticity, allowing the polymer to stretch farther than normal before tearing or fracturing.

A problem occurs when this alteration is applied towards the already softer 30 ppm polymer. With the addition of the fCNTs the polymer actually softens. Sometimes enough that the stretching induced in the non-exposed area is enough to tear open large sections of the polymer. One reason for this could be steric interference from both the fCNT and the functional groups attached to it. In a normal chained polymer material, the acetate groups on the surface of the CNT would end up surrounded and wrapped by polymer chains before bonding with a chain farther away from the CNT, but with a networked polymer comprised

of ring molecules, the acetate group simply takes up volume that the polymer could have used to network itself and thus reduces the strength of the network. If the polymer network is already less interconnected than it could be, as in the case with the 30 ppm samples, this amount of interference can noticeably decrease the tear strength of the polymer.

4.4.2 Limitations: Sources of error during experimentation

4.4.2.1 Oven and Sintering

During the middle of sample production for testing, the lab was forced to move locations, and during this move, the thermocouple on the MTI furnace that was used was broken. A new thermocouple was procured for the oven but due to a lack of capabilities in the university, a proper on site calibration could not be obtained for the thermo couple. Due to this, reliance on the stated company calibration was required. While the company calibration was stated to be equivalent to ±1.4°C [43] there was no way to verify that claim. The experiments were forced to proceed due to limitations on the available time remaining to craft enough samples for the desired number of test runs. If the thermocouple was not in fact accurate in situ, there would be no way of correcting the discrepancy without requiring the use of weeks of trial and error.

The oven could also not be used to sinter multiple samples simultaneously, as with only one heating zone, the area available for use was not as wide as two samples and the temperature gradient across the samples was enough to cause severe warping of the samples during the procedure.

4.4.2.2 Polymer Curing

All polymer curing happened under atmospheric conditions in the lab for the first 24 hours prior to spending 24 hours in the drying oven at 80°C. When dealing with polymer curing, humidity can be a serious factor in the length of cure required, and as there was no way to control the humidity in the lab there was no way to isolate for this variable during experimentation. As such, some samples may have not been cured enough prior to putting them in the drying oven for the final curing step.

Another source of error would be the sonication step. The sonicator was not able to maintain a temperature for the bath, this resulted in the temperature of the bath needing to be started out much colder than required in order to ensure that the bath did not get too warm during the fCNT dispersion stage. Once the water bath began to exceed 45°C, the curing reaction began to speed up noticeably and over 50°C would proceed to completion in under 1 hour. The final outcome of this rapid curing during sonication was a crystalline form of the polymer that broke under mild stress and sometimes the stress of cooling was enough to crack not only the polymer phase but also the BCC itself.

4.4.2.3 Slurry Pot

Errors from the slurry pot are related to the fundamental limitations of the construction of the sample holders. Due to the fact that there is a face plate covering the front of the sample, ostensibly to only expose a controlled amount of area to the abrasive environment of the slurry, there are inconsistencies with how the sample is eroded relative to the leading edge and the trailing edge. The leading edge of the samples is partially occluded by the faceplate and thus there is a small "shadow" where the faceplate prevents any abrasive material from touching the exposed surface. The reduction in impacts in this area creates a definite slope in the final erosion profile of the sample face, leading towards the trailing edge of the sample face.

At the trailing edge, another non-isotropic outcome is shown. Due to the fact that the sample is abrading faster than the facing of the sample holder, the sample starts to undercut the faceplate, thus losing material that is not meant to be exposed to the abrasive environment of the slurry pot. This erosion spreads almost equivalently from the point where the sample touches the trailing edge of the opening in the faceplate in a hemispherical fashion. Figure 28 shows a diagram of how the volume is etched away over time. With the leading edge of the sample wearing only slightly and at an initial angle similar to the impingement angle of the sand, and the trailing edge is preferentially worn away as the sand exposes more of the sample beneath the cover plate.

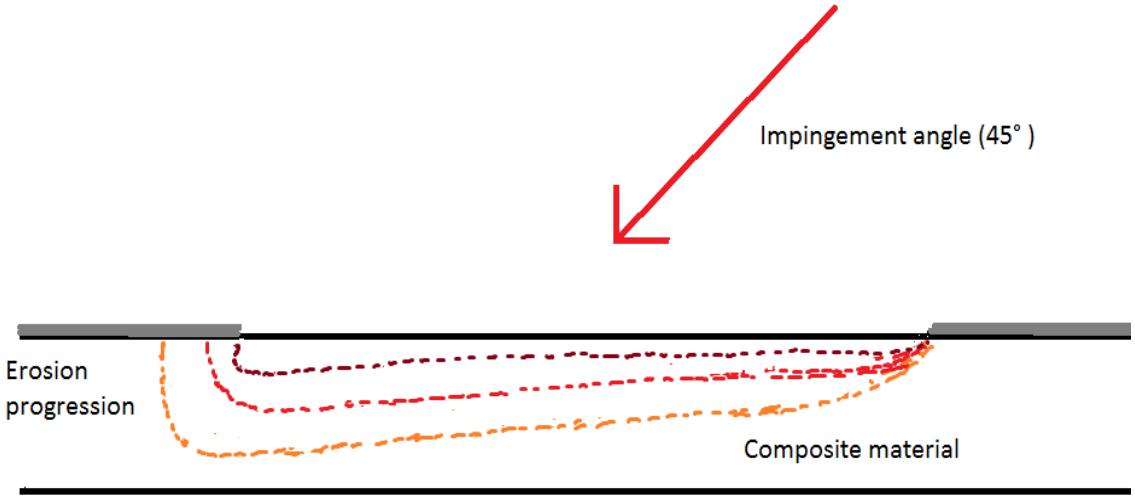

Figure 29 Time lapse of BCC material erosion in slurry pot

This is very similar to how lithographic etching occurs, as a covering layer is placed on the surface and a chemical etchant is used to remove a volume of the exposed underlying material, but as the etchant behaves in an isotropic manner, semicircular cross sections are also removed from underneath the covering layer.

4.5 Conclusions

By comparing the samples that exhibit the best wear resistance and their associated hardness, bending modulus and tan delta, it becomes possible to determine which samples are worth looking into for future work and possible reasons why. Due to the chaotic nature of the porous ceramic base material, relying only on material hardness is insufficient for this new class of materials to be useful as wear resistant coatings. The material of choice may start off with a hard material but it must also exhibit particular characteristics for the desired type of wear and abrasion that it is expected to undergo. For high angle contacts that have a large energy vector perpendicular to the surface, a high tan delta and a high bending modulus is important to prevent flex in the material from exceeding the strain required to break any possible struts where stress may concentrate and to also disperse the impact energy throughout the material as efficiently as possible. For a low angle contact a low bending modulus and low tan delta allows the material to not only flex under the impact to reduce dragging forces between the particle but also to rebound and push the particle off of the surface to minimize the time of contact, reducing the available time for the particle to

damage the surface. By mixing these properties with a high hardness base material to prevent as much scratching as possible it should be possible to develop targeted coatings for targeted applications in hostile, abrasive environments.

Chapter 5: Future work and summary of conclusions

BCC's exhibit properties that make them attractive for several possible applications, not just as a protective coating for other materials, but also as base materials themselves for structural purposes. Theoretically, by mixing specific ceramics or metals with polymers it should be possible to create a ceramic or metal based BCC with properties tuned for any specific job. For a situation where high compressive strength is required at a low weight cost, say when building a support piling for a super-tall skyscraper, an advanced technical ceramic such as pure tungsten carbide (WC) or boron carbide (B_4C), which are either too heavy or too expensive, or both, to use as a bulk material, can be sintered into a porous structure and infiltrated with a stiff thermosetting polymer to maintain the high compressive loading that the ceramics are capable of, while also giving the material a less catastrophic failure profile, allowing any cracks or flaws a chance to make themselves known before the entire piece becomes compromised.

Despite the use of a ceramic material known for fracture toughness and hardness, and a polymer designed for high temperature tolerance and tunable elasticity, the current composition and construction of a BCC material comprised of these materials is not capable of withstanding the rigors of production and application in any high temperature abrasive fluid environment. With more investigation into the causes of poor bonding between these materials and a more precisely designed framework on which to base the material, a viable BCC can be completed and marketed as not only a wear resistant material for a variety of abrasive fluids, but one that can also ignore most corrosive environments. Using the data in this document it is hoped that any future investigations can avoid the many dead-ends and pitfalls of attempting to combined these dissimilar materials into a functional whole.

References

[1] J. A. Wess, L. D. Olsen, and M. H. Sweeney, “Concise International Chemical Assessment Document 59 ASPHALT (BITUMEN),” 2005.

[2] R. A. Carter, “Progress in Pipe Wear Protection - EMJ,” *Engineering and Mining Journal*, 2014. [Online]. Available: http://www.e-mj.com/features/3737-progress-in-pipe-wear-protection.html#.VCciMfldWCl. [Accessed: 27-Sep-2014].

[3] Insitumain, “INSITUMAIN SYSTEM FOR WATER APPLICATIONS,” 2013. [Online]. Available: http://www.insituform.com/Water-Rehabilitation/InsituMain/~/media/Corporate/Files/Insituform/InsituMain Brochure.ashx. [Accessed: 13-Dec-2014].

[4] United States of America Department of Defense Division 33 - Utilities, *Unified Facilities Guide Specifications: Liquid Fuels Pipeline Coating Systems*, vol. 80, no. February 2010. Bibliogov, 2014, pp. 1–20.

[5] Pipelines International, “Inside and out: benefits of pipeline coating — Pipelines International — The international pipeline magazine.” [Online]. Available: http://pipelinesinternational.com/news/inside_and_out_benefits_of_pipeline_coating/053589/. [Accessed: 27-Sep-2014].

[6] TST Engineered Coating Solutions, “Wear Resistant Coatings, Tungsten Carbide and Ceramic Coatings| Thermal Spray Technologies Inc.” [Online]. Available: http://www.tstcoatings.com/wear_resistant_coatings.html. [Accessed: 28-Sep-2014].

[7] S. Kuroda, J. Kawakita, M. Watanabe, and H. Katanoda, “Warm spraying—a novel coating process based on high-velocity impact of solid particles,” *Sci. Technol. Adv. Mater.*, vol. 9, no. 3, p. 033002, Jul. 2008.

[8] J. R. Kosek, J. N. DuPont, and a. R. Marder, “Effect of Porosity on Resistance of Epoxy Coatings to Cold-Wall Blistering,” *Corrosion*, vol. 51, no. 11, pp. 861–871, Nov. 1995.

[9] Y. Pan, L. Li, S. H. Chan, and J. Zhao, “Correlation between dispersion state and electrical conductivity of MWCNTs/PP composites prepared by melt blending,” *Compos. Part A Appl. Sci. Manuf.*, vol. 41, no. 3, pp. 419–426, Mar. 2010.

[10] I. H. Paik, N. S. Goo, Y. C. Jung, and J. W. Cho, “Development and application of conducting shape memory polyurethane actuators,” *Smart Mater. Struct.*, vol. 15, no. 5, pp. 1476–1482, Oct. 2006.

[11] W. D. J. Callister and D. G. Rethwisch, *Materials Science and Engineering: An Introduction, 94-95*, 8th Editio. John Wiley & Sons Inc., 1997.

[12] J. N. Coleman, M. Cadek, R. Blake, V. Nicolosi, K. P. Ryan, C. Belton, a. Fonseca, J. B. Nagy, Y. K. Gun’ko, and W. J. Blau, “High Performance Nanotube-Reinforced Plastics: Understanding

the Mechanism of Strength Increase," *Adv. Funct. Mater.*, vol. 14, no. 8, pp. 791–798, Aug. 2004.

[13] G. Gorrasi, R. Di Lieto, G. Patimo, S. De Pasquale, and A. Sorrentino, "Structure–property relationships on uniaxially oriented carbon nanotube/polyethylene composites," *Polymer (Guildf).*, vol. 52, no. 4, pp. 1124–1132, Feb. 2011.

[14] Y. Xia, E. I. Saavedra Flores, H. X. Peng, and M. I. Friswell, "Estimating Mechanical Properties of Bi-continuous Two-Phase Composites for Optimised Multi-Functionality," vol. 7978, pp. 797808–797808–7, Mar. 2011.

[15] R. Chattopadhyay, *Surface Wear: Analysis, Treatment, and Prevention*. Materials Park, OH: ASM International, 2001, p. 307.

[16] T. Xing, X. Cui, W. Chen, and R. Yang, "Synthesis of porous chromium carbides by carburization," *Mater. Chem. Phys.*, vol. 128, no. 1–2, pp. 181–186, Jul. 2011.

[17] Z. Dong and W. Chen, "Synthesis and hardness evaluation of porous M(Cr, Co)7C3–Co composites," *Mater. Sci. Eng. A*, vol. 576, pp. 52–60, Aug. 2013.

[18] Insituform, "ID Coatings (Internal Diameter Coatings)," 2014. [Online]. Available: http://www.insituform.com/Energy-Mining/Coatings/ID-Coating.aspx. [Accessed: 27-Sep-2014].

[19] G. B. Inc., "Technical Data Sheet 105 system 105 Epoxy/205 Hardener," Bay City, MI, USA, 2013.

[20] J. P. Souza and J. M. Reis, "Thermal behavior of DGEBA (Diglycidyl Ether of Bisphenol A) adhesives and its influence on the strength of joints," *Appl. Adhes. Sci.*, vol. 1, no. 1, p. 6, 2013.

[21] O. Karabelchtchikova, "Fundamentals of Mass Transfer in Gas Carburizing by," no. November, 2007.

[22] O. Ostrovski and G. Zhang, "Reduction and carburization of metal oxides by methane-containing gas," *AIChE J.*, vol. 52, no. 1, pp. 300–310, Jan. 2006.

[23] A. Kusoffsky and B. Jansson, "A Thermodynamic Evaluation of the Co-Cr and the C-Co-Cr Systems," *Calphad*, vol. 21, no. 3, pp. 321–333, 1998.

[24] P. Zheng and T. J. McCarthy, "Rediscovering silicones: molecularly smooth, low surface energy, unfilled, UV/vis-transparent, extremely cross-linked, thermally stable, hard, elastic PDMS.," *Langmuir*, vol. 26, no. 24, pp. 18585–90, Dec. 2010.

[25] S. U. a. Redondo, E. Radovanovic, I. L. Torriani, and I. V. P. Yoshida, "Polycyclic silicone membranes. Synthesis, characterization and permeability evaluation," *Polymer (Guildf).*, vol. 42, no. 4, pp. 1319–1327, Feb. 2001.

[26] M. J. Michalczyk, W. E. Farneth, and A. J. Vega, “Stabilization, High-temperature Glasses, Cross-linked Siloxanes,” vol. 5, no. 12, pp. 1687–1689, 1993.

[27] Z. Spitalsky, D. Tasis, K. Papagelis, and C. Galiotis, “Carbon nanotube–polymer composites: Chemistry, processing, mechanical and electrical properties,” *Prog. Polym. Sci.*, vol. 35, no. 3, pp. 357–401, Mar. 2010.

[28] Z. Chen, X. J. Dai, K. Magniez, P. R. Lamb, D. Rubin de Celis Leal, B. L. Fox, and X. Wang, “Improving the mechanical properties of epoxy using multiwalled carbon nanotubes functionalized by a novel plasma treatment,” *Compos. Part A Appl. Sci. Manuf.*, vol. 45, pp. 145–152, Feb. 2013.

[29] P.-C. Ma, N. a. Siddiqui, G. Marom, and J.-K. Kim, “Dispersion and functionalization of carbon nanotubes for polymer-based nanocomposites: A review,” *Compos. Part A Appl. Sci. Manuf.*, vol. 41, no. 10, pp. 1345–1367, Oct. 2010.

[30] S. Dumonteil, A. Demortier, S. Detriche, C. Raes, A. Fonseca, M. Rühle, and J. B. Nagy, “Dispersion of carbon nanotubes using organic solvents.,” *J. Nanosci. Nanotechnol.*, vol. 6, no. 5, pp. 1315–1318, 2006.

[31] C.-X. Liu and J.-W. Choi, “Improved Dispersion of Carbon Nanotubes in Polymers at High Concentrations,” *Nanomaterials*, vol. 2, no. 4, pp. 329–347, Oct. 2012.

[32] S. Pegel, P. Pötschke, G. Petzold, I. Alig, S. M. Dudkin, and D. Lellinger, “Dispersion, agglomeration, and network formation of multiwalled carbon nanotubes in polycarbonate melts,” *Polymer (Guildf).*, vol. 49, no. 4, pp. 974–984, Feb. 2008.

[33] E. E. Tkalya, M. Ghislandi, G. de With, and C. E. Koning, “The use of surfactants for dispersing carbon nanotubes and graphene to make conductive nanocomposites,” *Curr. Opin. Colloid Interface Sci.*, vol. 17, no. 4, pp. 225–232, Aug. 2012.

[34] S. Zhao, Z. Song, J. Cui, C. Li, and Y. Yan, “Improving dispersion and integration of single-walled carbon nanotubes in epoxy composites by using a reactive noncovalent dispersant,” *J. Polym. Sci. Part A Polym. Chem.*, vol. 50, no. 21, pp. 4548–4556, Nov. 2012.

[35] V. Tishkova, G. Bonnet, F. Pont, B. Gautier, P. H. Cadaux, P. Puech, and W. S. Bacsa, “Uniform dispersion of nanotubes in thermoplastic polymer through thermal annealing,” *Carbon N. Y.*, vol. 53, pp. 399–402, Mar. 2013.

[36] J. Read and D. Whiteoak, *The Shell Bitumen Handbook*. Thomas Telford, 2003, p. 460.

[37] “Emerson Process Management - News - Emersons Smart Wireless network assures bitumen pipeline stays hot during ship unloading at Terminals Pty Ltd in Australia.” [Online]. Available: http://www2.emersonprocess.com/en-us/news/pr/pages/811-geelong.aspx. [Accessed: 01-Aug-2014].

[38] C. L. Beyler and M. M. Hirschler, “Thermal Decomposition of Polymers,” in *SFPE handbook of fire protection engineering*, 2nd ed., Quincy (Mass), 1995, pp. 110–131.

[39] “Standard Test Method for Measuring Abrasion Using the Dry Sand / Rubber Wheel,” West Conshohocken, PA, USA, 2014.

[40] V. Jaimes, “Abrasive Wear Assessment of X-70 Steel and Polyurethane Coupons on a Modified Dry/Sand Rubber Wheel Apparatus,” University of Alberta, 2013.

[41] X. Zheng, H. Lee, T. H. Weisgraber, M. Shusteff, J. DeOtte, E. B. Duoss, J. D. Kuntz, M. M. Biener, Q. Ge, J. A. Jackson, S. O. Kucheyev, N. X. Fang, and C. M. Spadaccini, “Ultralight, Ultrastiff Mechanical Metamaterials,” *Science (80-.).*, vol. 344, no. 6190, pp. 1373–1377, 2014.

[42] V. S. Deshpande, M. F. Ashby, and N. a. Fleck, “Foam topology: bending versus stretching dominated architectures,” *Acta Mater.*, vol. 49, no. 6, pp. 1035–1040, Apr. 2001.

[43] “Thermal Couple B type (Pt-Rh to Pt-Rh) 9" Length with ceramic sheath (Up to 1700C).” [Online]. Available: http://www.mtixtl.com/thermalcouple-EQ-TC-B-GSL-16.aspx. [Accessed: 30-Jul-2014].

Appendix A

Table 5: Volume lost to Abrasion in Slurry Pot[9]

	mm^3 lost							
	45° impingment				22° impingment			
	120ppm		30 ppm		120ppm		30 ppm	
[fCNT]	Run#1	Run#2	Run#1	Run#2	Run#1	Run#2	Run#1	Run#2
0%	214.3261	97.31942	84.20599	53.45252	2.182616	1.05488	4.002106	0.677169
0.05 wt%	108.8859	199.4026	100.3767	304.9657	1.082469	1.394705	3.169383	4.815411
0.1 wt%	91.01273	163.6653	119.0755	35.74796	0.363128	1.051592	3.849897	1.437974
0.15 wt%	100.2833	267.8235	70.71694	13.31243	2.493307	1.403506	6.645827	15.31737

Table 6 Average volume eroded

	45°		22°	
	120 ppm	30 ppm	120 ppm	30 ppm
average	155.3398	68.12687	1.378275	4.989392
std Dev	66.3716	36.89945	0.678285	4.570631

[9] One note, run #2 of the 30 ppm, 45 degree test was locked in the testing room for 80 minutes rather than the normal 35 minutes as there was no auto-shut down feature on the testing apparatus. The values shown in Table 1 are normalized to 35 minutes as best as possible, but it should be noted that these values may not be as accurate as wished. The actual recorded values for mm^3 lost are recorded in Table 16 in Appendix B. Also in all following data derivations from this table, the 0.05wt% 30 ppm data point in run #2 of the 45 degree test, marked in red, is discarded as an outlier.

Table 7 Storage Moduli and Tan Delta of BCC samples

	catalyst	fCNT	storage modulus (Pa)	limit t→infinity	Tan Delta
020413-b2-s5	120 ppm	0%	3.83E+09	4.50E+09	0.026
151113-b2-s2	120ppm	0.05%	6.82E+09	7.23E+09	0.0318
151113-b2-s4	120 ppm	0.10%	8.01E+09	8.70E+09	0.025
151113-b2-s6	120 ppm	0.15%	9.17E+09	9.65E+09	0.026
200214-b1-s3	30 ppm	0%	6.06E+09	7.02E+09	0.0653
200214-b1-s5	30 ppm	0.05%	4.97E+09	5.15E+09	0.0337

Table 8 45 Degree Wear volume conversions and equivalences

BCC # @ 45 Degrees	sample composition	original volume lost (mm^3)	G65 distance wear volume (mm^3)	converted G65 Equivalence
090913-B2-S1	120, 0%	214.3260801	79.96048354	13191.24549
090913-B1-S3	120, 0.05%	108.8858636	40.62299045	6701.658319
090913-B1-S1	120, 0.1%	91.0127299	33.95490595	5601.610699
090913-B1-S5	120, 0.15%	100.2832952	37.41355589	6172.191296
020413-B2-S3	120, 0%	97.31941788	36.30779655	5989.771903
090913-B1-S4	120, 0.05%	199.4025731	74.39284177	12272.74018
020413-B1-S4	120, 0.1%	163.6653054	61.06003037	10073.19885
090913-B2-S4	120, 0.15%	267.8234679	99.9192165	16483.87874
090913-B2-S6	30, 0.0%	53.45251865	19.94199323	3289.871655
151113-B1-S3	30, 0.05%	304.9656805	113.7761828	18769.89099
090913-B1-S2	30, 0.1%	35.74795705	13.33679938	2200.199235
151113-B1-S5	30, 0.15%	13.31243443	4.966584999	819.3477464
090913-B2-S2	30, 0.0%	84.20598729	31.41545564	5182.672356
151113-B1-S2	30, 0.05%	100.3767097	37.44840683	6177.940728
151113-B1-S1	30, 0.1%	119.0755323	44.42453823	7328.807478
151113-B1-S4	30, 0.15%	70.7169425	26.38298108	4352.454674

Table 9 Plotted data for 45 Degree wear test equivalence

45 Degree samples				
comp.	Run #1	Run #2	Average	Std. Dev.
120: 0%	13191.24549	5989.771903	9590.508699	3600.736795
120: 0.05%	6701.658319	12272.74018	9487.199247	2785.540928
120: 0.1%	5601.610699	10073.19885	7837.404772	2235.794073
120: 0.15%	6172.191296	16483.87874	11328.03502	5155.843721
30: 0.0%	3289.871655	5182.672356	4236.272005	946.4003505
30: 0.05%	18769.89099	6177.940728	12473.91586	6295.975129
30: 0.1%	2200.199235	7328.807478	4764.503356	2564.304122
30: 0.15%	819.3477464	4352.454674	2585.90121	1766.553464
X60 pipeline steel	268.29			

Table 10 22 Degree Wear volume conversions and equivalence

BCC # @ 22 Degrees	sample composition	original volume lost (mm^3)	G65 distance wear volume	converted G65 Equivalence
151113-B1-S6	120: 0%	2.1826159	0.81428738	700.2964307
151113-B2-S2	120: 0.05%	1.0824695	0.403846238	347.3123694
151113-B2-S4	120: 0.1%	0.3631279	0.135475273	116.510279
151113-B2-S6	120: 0.15%	2.4933071	0.930199646	799.9823013
200214-B1-S2	120: 0%	1.0548797	0.393553093	338.4601471
200214-B1-S4	120: 0.05%	1.3947052	0.520334739	447.4938085
200214-B1-S6	120: 0.1%	1.0515922	0.392326606	337.4053543
200214-B2-S2	120: 0.15%	1.4035064	0.523618256	450.3176698
151113-B2-S1	30: 0.0%	4.0021055	1.493100102	1284.083111
151113-B2-S3	30: 0.05%	3.1693831	1.182429163	1016.902562
151113-B2-S5	30: 0.1%	3.8498970	1.436314354	1235.246721
200214-B1-S1	30: 0.15%	6.6458270	2.479416123	2132.326135
200214-B1-S3	30: 0.0%	0.6771691	0.252637339	217.2709924
200214-B1-S5	30: 0.05%	4.8154109	1.796526983	1545.033688
200214-B2-S1	30: 0.1%	1.4379735	0.536477206	461.3765142
200214-B2-S3	30: 0.15%	15.3173732	5.714584839	4914.608116

Table 11 Plotted Data for 22 Degree wear test equivalence

22 Degree samples				
comp.	Run #1	Run #2	Average	Std. Dev.
120: 0%	700.2964307	338.4601471	519.3782889	180.9181418
120: 0.05%	347.3123694	447.4938085	397.4030889	50.09071956
120: 0.1%	116.510279	337.4053543	226.9578166	110.4475376
120: 0.15%	799.9823013	450.3176698	625.1499855	174.8323158
30: 0.0%	1284.083111	217.2709924	750.6770516	533.4060593
30: 0.05%	1016.902562	1545.033688	1280.968125	264.0655633
30: 0.1%	1235.246721	461.3765142	848.3116174	386.9351033
30: 0.15%	2132.326135	4914.608116	3523.467126	1391.140991
X60 pipeline steel	268.29			

Table 12 Shore A Hardness Measurements from AITF

Sample Types				AITF Hardness Measurements (Shore A)						
Sample ID	[Catalyst]	[fCNT]	composition	#1	#2	#3	#4	#5	Average	Std. Dev.
-	30 ppm	0%	polymer	94	98	97	95	97	96.2	1.47
151113-B2	30 ppm	0%	composite	93	96	95	94	94	94.4	1.02
-	30 ppm	0.05%	polymer	74	75	77	82	75	76.6	2.87
151113-B2	30 ppm	0.05%	composite	98	97	96	97	98	97.2	0.75
-	30 ppm	0.10%	polymer	74	81	73	80	77	77	3.16
151113-B2	30 ppm	0.10%	composite	95	94	93	96	95	94.6	1.02
-	30 ppm	0.15%	polymer	75	71	77	73	74	74	2.00
200214-B1	30 ppm	0.15%	composite	>100	>100	>100	100	>100	100	0.00
200214-B1	120 ppm	0%	composite	96	99	94	98	99	97.2	1.94
	120 ppm	0%	polymer	94	91	94	96	98	94.6	2.33
	120 ppm	0.05%	polymer	95	91	92	96	100	94.8	3.19
200214-B1	120 ppm	0.05%	composite	99	99	96	96	100	98	1.67
	120 ppm	0.10%	polymer	95	96	96	96	95	95.6	0.49
200214-B1	120 ppm	0.10%	composite	97	95	97	96	97	96.4	0.80
	120 ppm	0.15%	polymer	97	96	94	94	96	95.4	1.20
200214-B2	120 ppm	0.15%	composite	99	97	100	99	96	98.2	1.47

Table 13 Conversion table from Shore A to Shore D

Shore D	58	46	39	33	29	25	22	19	16	14	12	10	8	7	6	N/A	N/A	N/A	N/A	N/A
Shore A	100	95	90	85	80	75	70	65	60	55	50	45	40	35	30	25	20	15	10	5

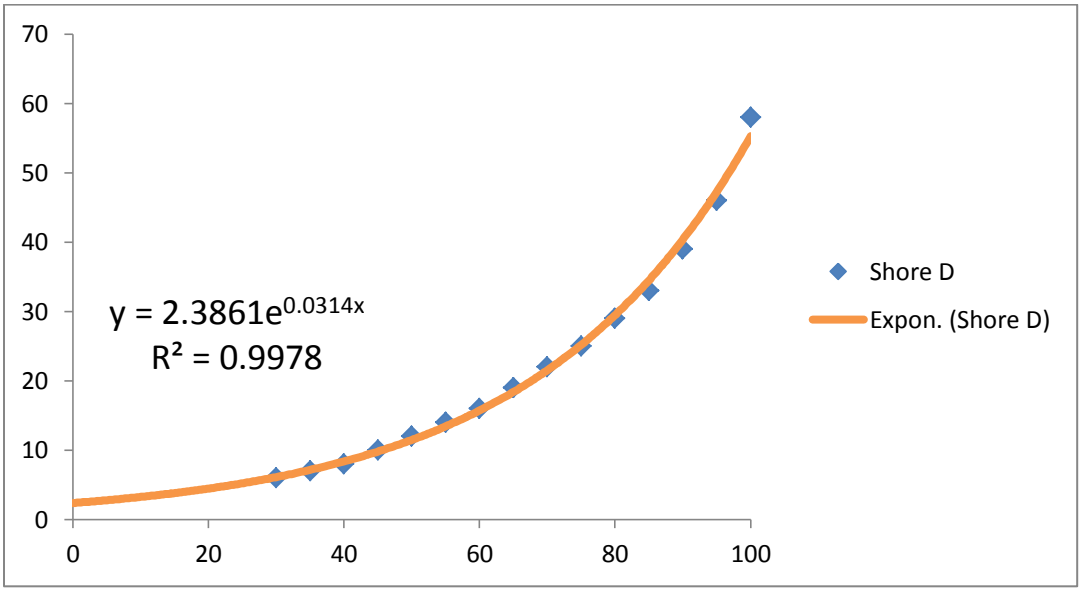

Figure 30 Shore A to Shore D conversion chart and equation

Table 14. Converted Shore D Hardness

Sample Types					Converted Hardness Measurements (Shore D)								
Sample ID		[Catalyst]	[fCNT]	composition	#1	#2	#3	#4	#5	#6	#7	Average	Std. Dev.
-	020413-B2-S6	0	0.00%	porous ceramic	62	50	72	59	64	64	74	63.6	7.4
ML-14-426-01	-	30 ppm	0.00%	polymer	45.7	51.8	50.2	47.1	50.2			49.0	2.2
ML-14-426-02	151113-B2-S1	30 ppm	0.00%	composite	44.3	48.6	47.1	45.7	45.7			46.3	1.5
ML-14-426-03	-	30 ppm	0.05%	polymer	24.4	25.1	26.8	31.3	25.1			26.6	2.5
ML-14-426-04	151113-B2-S3	30 ppm	0.05%	composite	51.8	50.2	48.6	50.2	51.8			50.5	1.2
ML-14-426-05	-	30 ppm	0.10%	polymer	24.4	30.4	23.6	29.4	26.8			26.9	2.7
ML-14-426-06	151113-B2-S5	30 ppm	0.10%	composite	47.1	45.7	44.3	48.6	47.1			46.6	1.5
ML-14-426-07	-	30 ppm	0.15%	polymer	25.1	22.2	26.8	23.6	24.4			24.4	1.5
ML-14-426-08	200214-B1-S1	30 ppm	0.15%	composite	>55.1	>55.1	>55.1	55.1	>55.1			55.1	0.0
ML-14-426-09	200214-B1-S2	120 ppm	0.00%	composite	48.6	53.4	45.7	51.8	53.4			50.6	3.0
ML-14-426-10		120 ppm	0.00%	polymer	45.7	41.6	45.7	48.6	51.8			46.7	3.4
ML-14-426-11		120 ppm	0.05%	polymer	47.1	41.6	42.9	48.6	55.1			47.1	4.8
ML-14-426-12	200214-B1-S4	120 ppm	0.05%	composite	53.4	53.4	48.6	48.6	55.1			51.8	2.7
ML-14-426-13		120 ppm	0.10%	polymer	47.1	48.6	48.6	48.6	47.1			48.0	0.7
ML-14-426-14	200214-B1-S6	120 ppm	0.10%	composite	50.2	47.1	50.2	48.6	50.2			49.3	1.2
ML-14-426-15		120 ppm	0.15%	polymer	50.2	48.6	45.7	45.7	48.6			47.7	1.8
ML-14-426-16	200214-B2-S2	120 ppm	0.15%	composite	53.4	50.2	55.1	53.4	48.6			52.2	2.4

Appendix B

Table 15 sample dimensions and test parameters for DMA

Frequency	1 Hz					
Displacement	0.05 mm					
Sample ID	020413-B2-S5	151113-B2-S2	151113-B2-S4	151113-B2-S6	200214-B1-S3	200214-B1-S5
Length (mm)	12.4	12.4	12.4	12.4	12.4	12.4
Width (mm)	6.02	5.38	5.45	5.48	5.63	5.59
Thickness (mm)	3.03	2.19	2.36	2.35	2.24	2.27
Diameter (mm)						
Clamp Mass (g)	4.205	4.205	4.205	4.205	4.205	4.205
Geom. Const.	4.39167E-05	1.4819E-05	1.87861E-05	1.86504E-05	1.65942E-05	1.71472E-05
Strain Factor	29.55905307	21.3644641	23.02289282	22.92533819	21.85223725	22.14490114

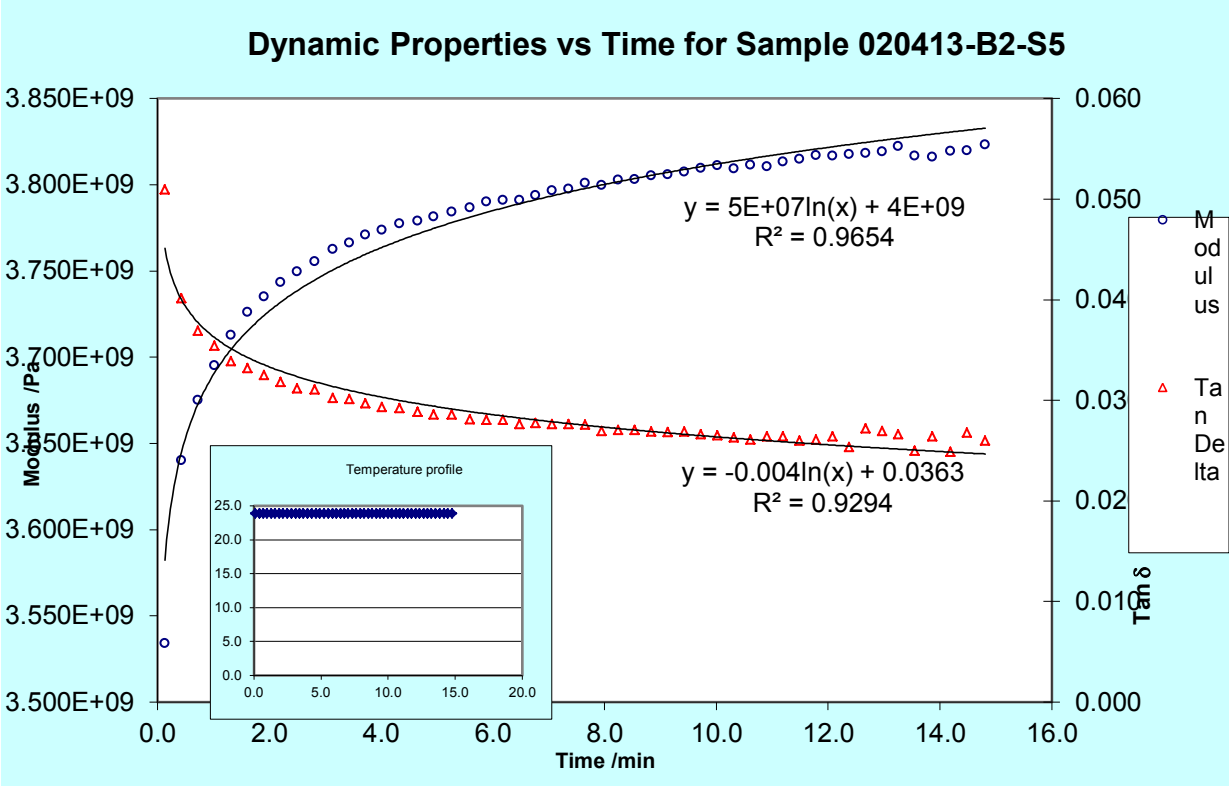

Figure 31 DMA plot for 120 ppm 0% fCNT

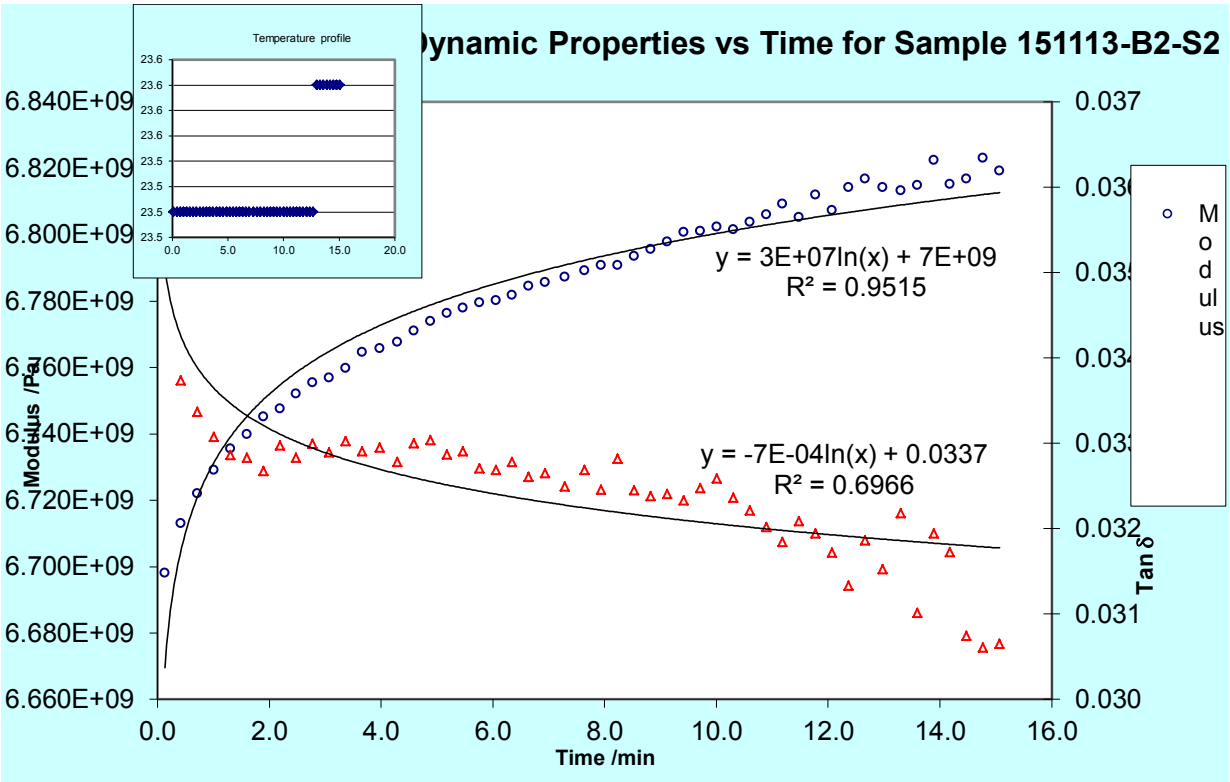

Figure 32 DMA plot for 120 ppm 0.05% fCNT

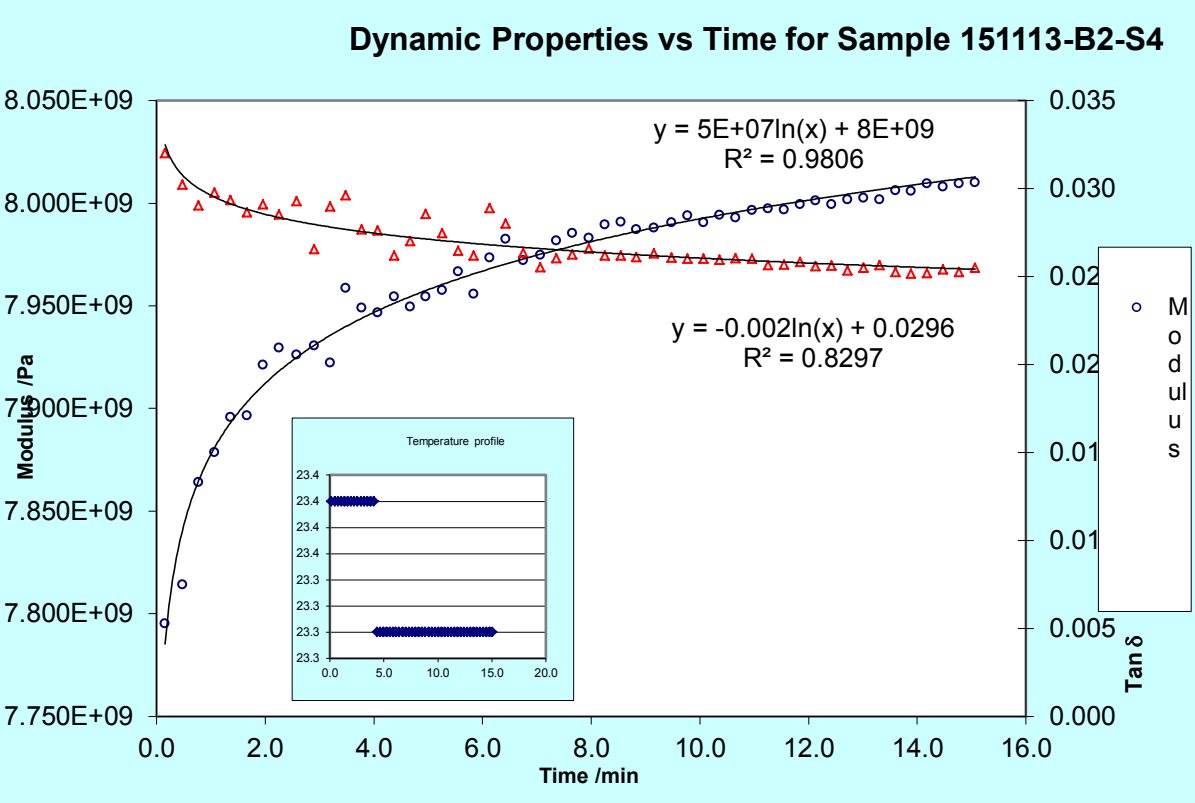

Figure 33 DMA plot for 120 ppm 0.1% fCNT

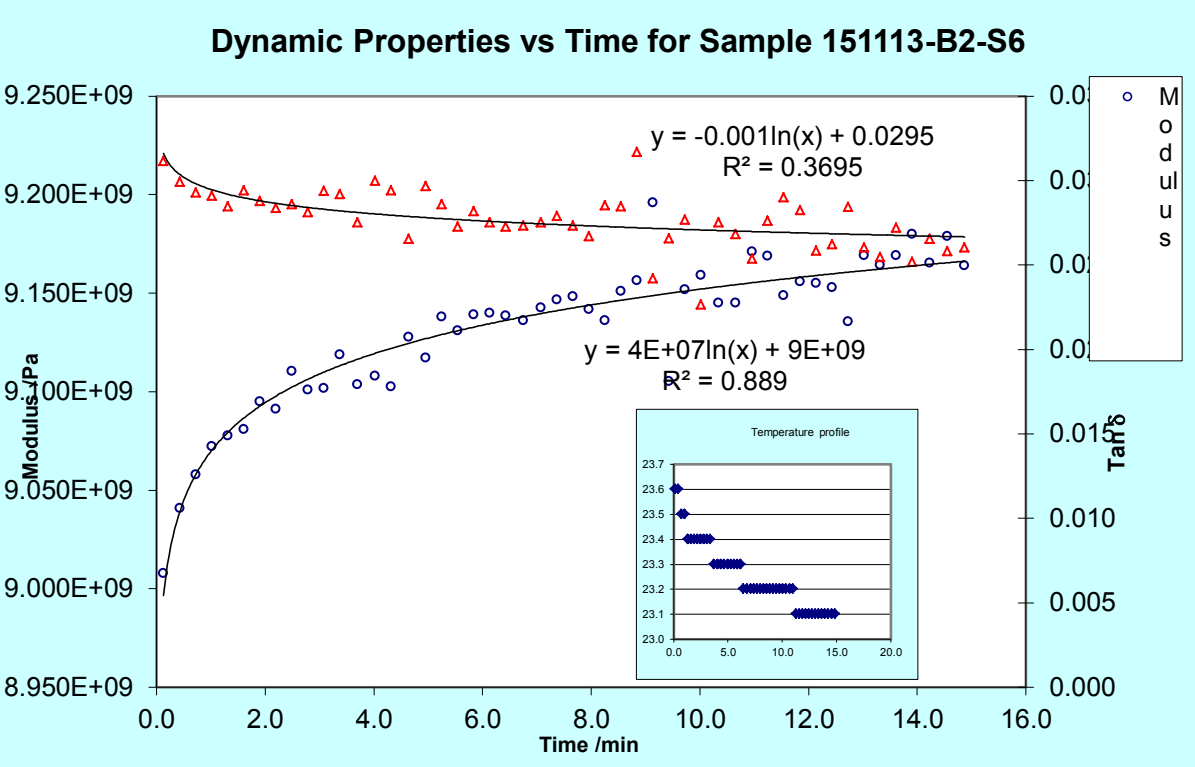

Figure 34 DMA plot for 120 ppm 0.15% fCNT

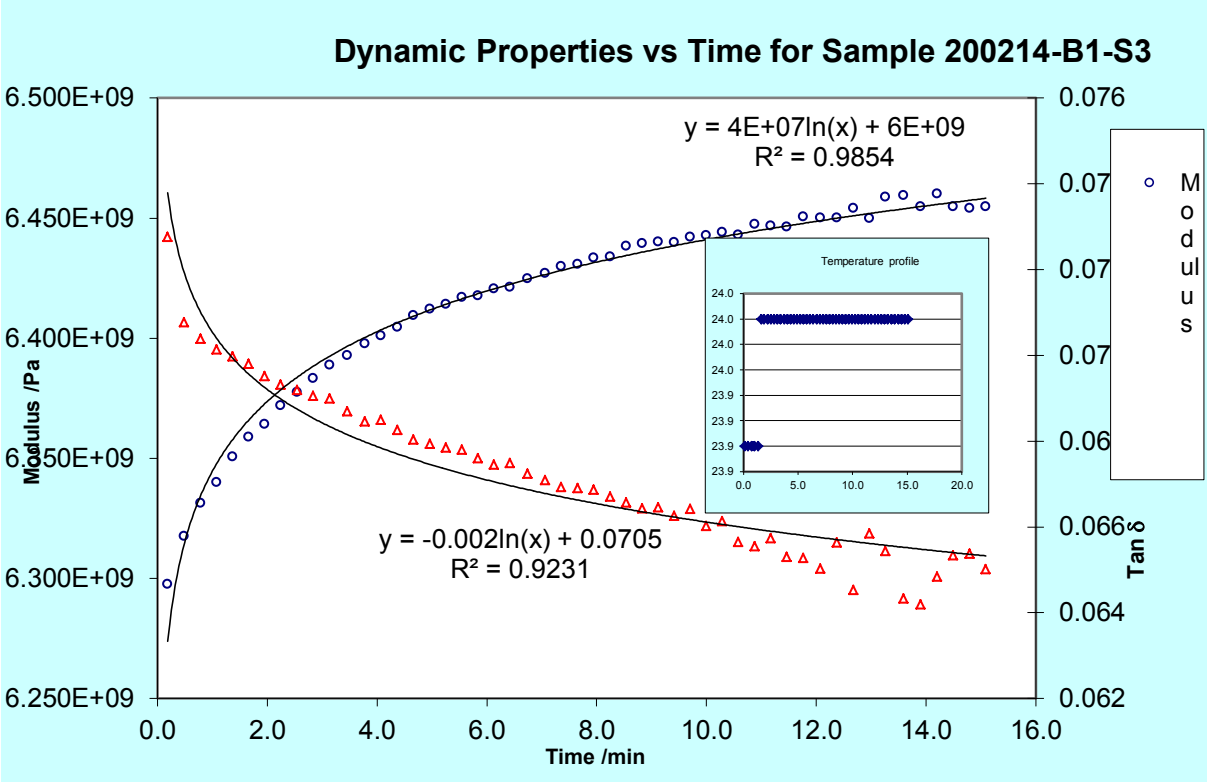

Figure 35 DMA plot for 30 ppm 0% fCNT

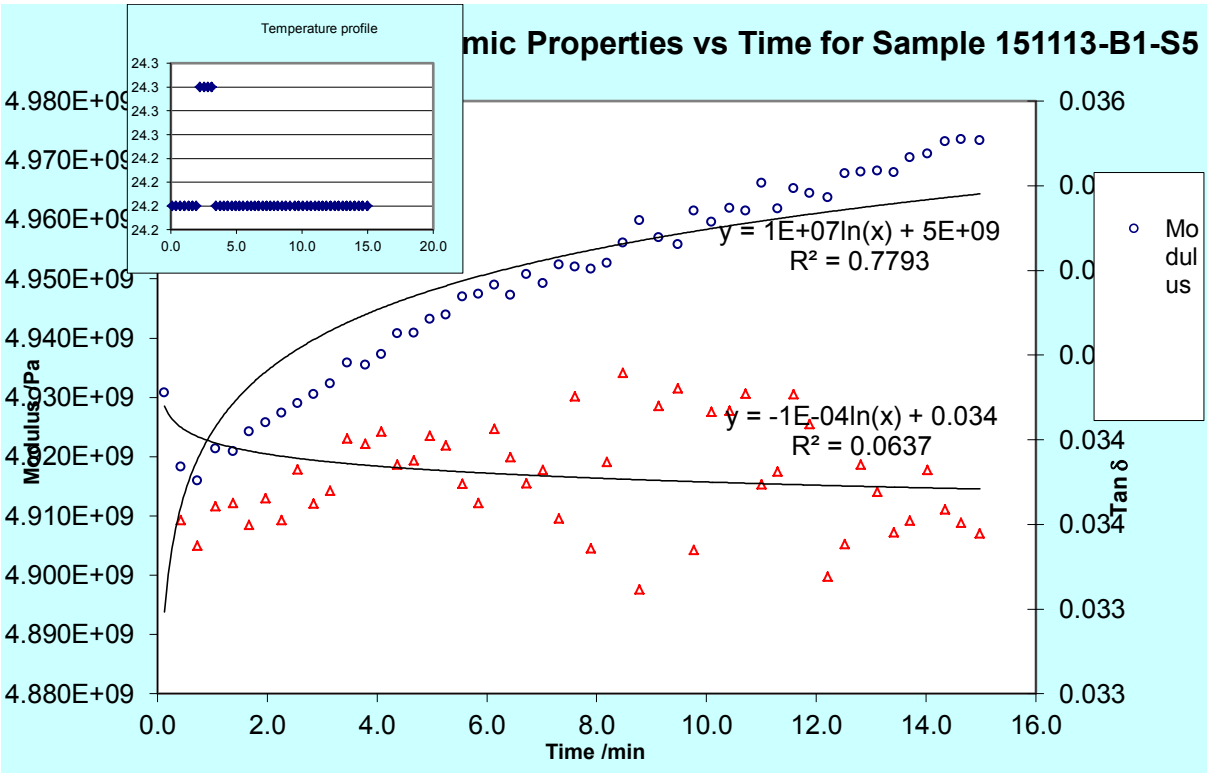

Figure 36 DMA plot for 30 ppm 0.05% fCNT

Table 16 initial data recording for sample mass loss after slurry pot testing

sample #	initial mass (g)	final mass (g)	sample thickness (mm)	density (g/cm^3)	initial mass of exposed area	final mass of exposed area	mass % lost	vol% lost	mm^3 lost
090913-B2-S1	7.43	6.78	2.286	3.033	4.160	3.510	15.626	0.156	214.326
090913-B1-S3	7.86	7.56	2.616	2.755	4.325	4.025	6.937	0.069	108.886
090913-B1-S1	7.73	7.47	2.374	2.857	4.069	3.809	6.390	0.064	91.013
090913-B1-S5	7.65	7.35	2.346	2.992	4.211	3.911	7.124	0.071	100.283
020413-B2-S3	7.48	7.2	2.37	2.877	4.091	3.811	6.844	0.068	97.319
090913-B1-S4	6.98	6.45	2.362	2.658	3.767	3.237	14.070	0.141	199.403
020413-B1-S4	7.13	6.67	2.28	2.811	3.845	3.385	11.964	0.120	163.665
090913-B2-S4	8.36	7.59	2.572	2.875	4.437	3.667	17.355	0.174	267.823
090913-B2-S6	6.59	6.27	2.416	2.620	3.798	3.478	8.428	0.084	122.177
151113-B1-S3	7.03	5.05	2.284	2.840	3.891	1.912	50.866	0.509	697.064
090913-B1-S2	7.71	7.48	2.448	2.818	4.139	3.909	5.563	0.056	81.710
151113-B1-S5	7.47	7.38	2.354	2.916	4.118	4.029	2.154	0.022	30.428
090913-B2-S2	7.73	7.49	2.46	2.850	4.207	3.967	5.705	0.057	84.206
151113-B1-S2	7.6	7.31	2.406	2.889	4.171	3.881	6.953	0.070	100.377
151113-B1-S1	7.95	7.61	2.486	2.855	4.259	3.919	7.983	0.080	119.076
151113-B1-S4	7.63	7.42	2.34	2.970	4.169	3.959	5.037	0.050	70.717
151113-B1-S6	7.34	7.334	2.38	2.749	3.926	3.920	0.153	0.002	2.183
151113-B2-S2	7.37	7.367	2.386	2.771	3.968	3.965	0.076	0.001	1.082
151113-B2-S4	7.43	7.429	2.448	2.754	4.045	4.044	0.025	0.000	0.363
151113-B2-S6	7.72	7.713	2.45	2.808	4.127	4.120	0.170	0.002	2.493
151113-B2-S1	7.53	7.519	2.442	2.749	4.027	4.016	0.273	0.003	4.002
151113-B2-S3	7.21	7.201	2.262	2.840	3.854	3.845	0.234	0.002	3.169
151113-B2-S5	7.67	7.658	2.408	3.117	4.503	4.491	0.266	0.003	3.850
200214-B1-S1	6.57	6.553	2.17	2.558	3.331	3.314	0.510	0.005	6.646
200214-B1-S2	7.07	7.067	2.266	2.844	3.867	3.864	0.078	0.001	1.055
200214-B1-S4	7.19	7.186	2.28	2.868	3.923	3.919	0.102	0.001	1.395
200214-B1-S6	7.02	7.017	2.274	2.853	3.892	3.889	0.077	0.001	1.052
200214-B2-S2	7.32	7.316	2.318	2.850	3.964	3.960	0.101	0.001	1.404
200214-B1-S3	7.43	7.428	2.25	2.953	3.987	3.985	0.050	0.001	0.677
200214-B1-S5	7.53	7.516	2.304	2.907	4.019	4.005	0.348	0.003	4.815
200214-B2-S1	7.77	7.766	2.498	2.782	4.169	4.165	0.096	0.001	1.438
200214-B2-S3	6.65	6.607	2.118	2.807	3.567	3.524	1.205	0.012	15.317
X60 #1	17.9246	17.8901	2	8.051	9.661	9.626	0.357	0.004	4.285
X60 #2	17.9734	17.9663	2	8.073	9.687	9.680	0.073	0.001	0.880
X60 #3	17.931	17.8953	2	8.054	9.664	9.629	0.369	0.004	4.433
X60 #4	17.9724	17.966	2	8.072	9.687	9.680	0.066	0.001	0.793

Table 17 Legend for Table 15

colour	fCNT wt%
	0%
	0.05%
	0.10%
	0.15%

Table 18 ANOVA: Single factor tests for 45 Degree samples

Anova: Single Factor						
45-120ppm ANOVA						
SUMMARY						
Groups	*Count*	*Sum*	*Average*	*Variance*		
0.00%	2	311.65	155.82	6845.279		
0.05%	2	308.29	154.14	4096.637		
0.10%	2	254.68	127.34	2639.198		
0.15%	2	368.11	184.05	14034.85		
ANOVA						
Source of Variation	*SS*	*df*	*MS*	*F*	*P-value*	*F crit*
Between Groups	3220.35	3	1073.45	0.155483	0.920914	6.591382
Within Groups	27615.97	4	6903.99			
Total	30836.32	7				
45 30ppm with outlier						
SUMMARY						
Groups	*Count*	*Sum*	*Average*	*Variance*		
0.00%	2	137.66	68.83	472.8879		
0.05%	2	405.34	202.67	20928.32		
0.10%	2	154.82	77.41	3471.742		
0.15%	2	84.03	42.01	1647.639		
ANOVA						
Source of Variation	*SS*	*df*	*MS*	*F*	*P-value*	*F crit*
Between Groups	30729.87	3	10243.29	1.544956	0.333492	6.591382
Within Groups	26520.59	4	6630.15			
Total	57250.46	7				
45 30ppm no outlier						
SUMMARY						
Groups	*Count*	*Sum*	*Average*	*Variance*		
0.00%	2	137.66	68.82925	472.8879		
0.05%	1	100.38	100.3767	#DIV/0!		
0.10%	2	154.82	77.41174	3471.742		
0.15%	2	84.03	42.01469	1647.639		
ANOVA						
Source of Variation	*SS*	*df*	*MS*	*F*	*P-value*	*F crit*
Between Groups	2577.149	3	859.0496	0.460841	0.729511	9.276628
Within Groups	5592.269	3	1864.09			
Total	8169.418	6				

Table 19 ANOVA: Single factor tests for 22 Degree samples

22-120ppm ANOVA						
SUMMARY						
Groups	*Count*	*Sum*	*Average*	*Variance*		
0	2	3.24	1.62	0.64		
0.05 wt%	2	2.48	1.24	0.05		
0.1 wt%	2	1.41	0.71	0.24		
0.15 wt%	2	3.90	1.95	0.59		
ANOVA						
Source of Variation	*SS*	*df*	*MS*	*F*	*P-value*	*F crit*
Between Groups	1.71	3	0.57	1.500	0.342862	6.591382
Within Groups	1.52	4	0.38			
Total	3.22	7				
22-30ppm ANOVA						
SUMMARY						
Groups	*Count*	*Sum*	*Average*	*Variance*		
0	2	4.68	2.34	5.53		
0.05 wt%	2	7.98	3.99	1.35		
0.1 wt%	2	5.29	2.64	2.91		
0.15 wt%	2	21.96	10.98	37.60		
ANOVA						
Source of Variation	*SS*	*df*	*MS*	*F*	*P-value*	*F crit*
Between Groups	98.85	3	32.95	2.781	0.174139	6.591382
Within Groups	47.39	4	11.85			
Total	146.23	7				

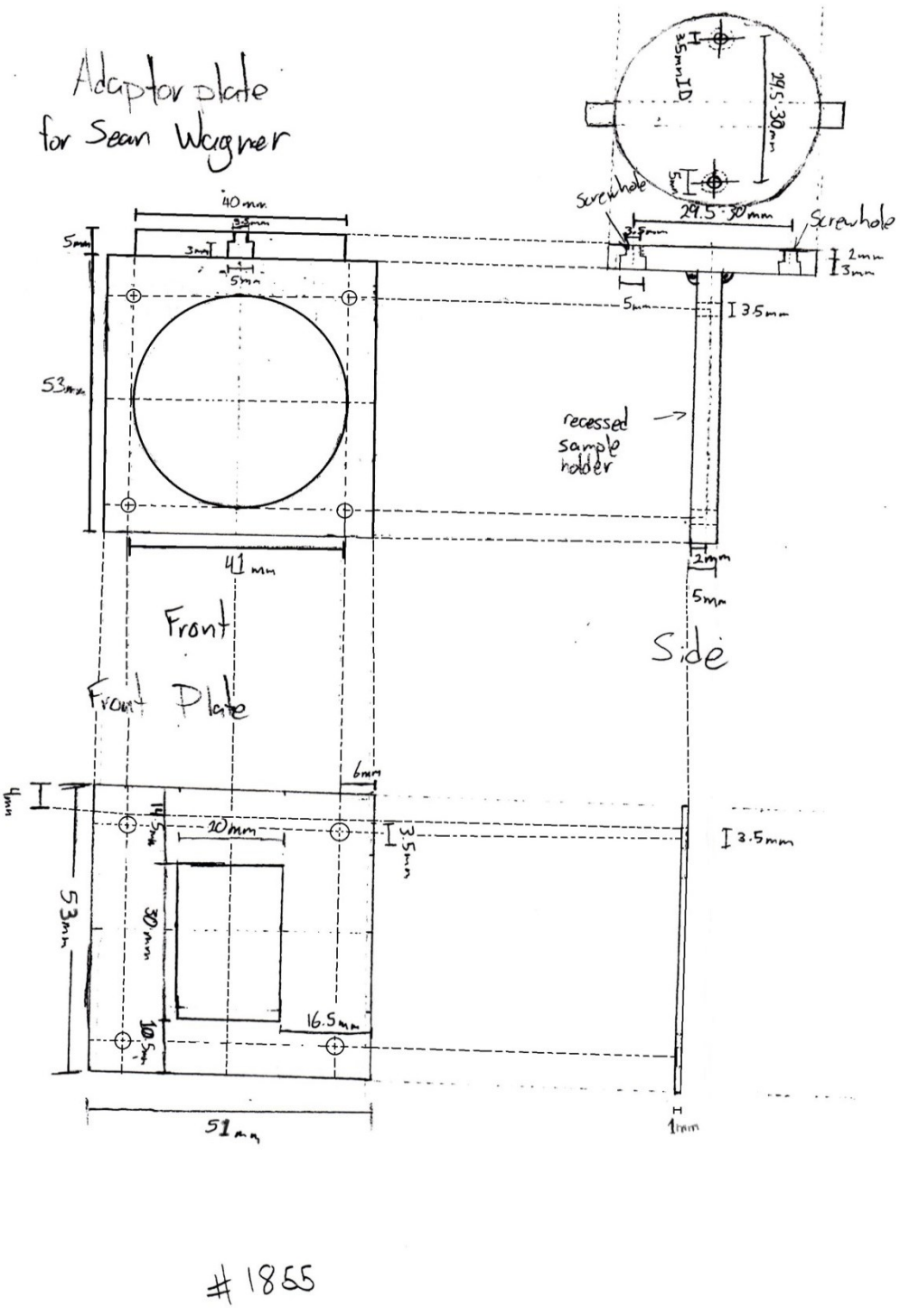

Figure 37. Blueprint for adaptor plate and front cover.

Appendix C

Table 20. 120 ppm polymer statistical grouping

Anova: Single Factor						
120 ppm polymer						
SUMMARY						
Groups	*Count*	*Sum*	*Average*	*Variance*		
ML-14-426-10	5	233.274	46.6548	14.50518		
ML-14-426-11	5	235.3067	47.06134	28.81852		
ML-14-426-13	5	240.1002	48.02003	0.67769		
ML-14-426-15	5	238.738	47.74761	4.026688		
ANOVA						
Source of Variation	*SS*	*df*	*MS*	*F*	*P-value*	*F crit*
Between Groups	5.859576	3	1.953192	0.162671	0.919918	3.238872
Within Groups	192.1123	16	12.00702			
Total	197.9719	19				

Table 21. 120 ppm BCC statistical grouping

Anova: Single Factor						
120 ppm composite						
SUMMARY						
Groups	*Count*	*Sum*	*Average*	*Variance*		
ML-14-426-09	5	252.9035	50.5807	11.40631		
ML-14-426-12	5	259.2186	51.84372	9.137729		
ML-14-426-14	5	246.2559	49.25119	1.872715		
ML-14-426-16	5	260.7695	52.15391	7.119877		
ANOVA						
Source of Variation	*SS*	*df*	*MS*	*F*	*P-value*	*F crit*
Between Groups	26.35128	3	8.783759	1.189541	0.345164	3.238872
Within Groups	118.1465	16	7.384159			
Total	144.4978	19				

Table 22. 120 ppm polymer-BCC statistical comparison

Anova: Single Factor						
120 ppm						
SUMMARY						
Groups	*Count*	*Sum*	*Average*	*Variance*		
120 ppm polymer	20	947.4189	47.37095	10.41957		
120 ppm composite	20	1019.148	50.95738	7.605148		
ANOVA						
Source of Variation	*SS*	*df*	*MS*	*F*	*P-value*	*F crit*
Between Groups	128.6251	1	128.6251	14.27208	0.000543	4.098172
Within Groups	342.4697	38	9.01236			
Total	471.0948	39				

Table 23. 30 ppm polymer statistical grouping

Anova: Single Factor

30ppm polymer

SUMMARY

Groups	*Count*	*Sum*	*Average*	*Variance*
ML-14-426-01	5	244.8968	48.97937	6.2795
ML-14-426-03	5	132.7589	26.55179	7.893588
ML-14-426-05	5	134.5346	26.90692	8.88211
ML-14-426-07	5	122.0791	24.41583	2.938184

ANOVA

Source of Variation	*SS*	*df*	*MS*	*F*	*P-value*	*F crit*
Between Groups	2005.563	3	668.5211	102.8756	1.14E-10	3.238872
Within Groups	103.9735	16	6.498345			
Total	2109.537	19				

Anova: Single Factor

30 ppm polymer no outlier (empty polymer)

SUMMARY

Groups	*Count*	*Sum*	*Average*	*Variance*
ML-14-426-03	5	132.7589	26.55179	7.893588
ML-14-426-05	5	134.5346	26.90692	8.88211
ML-14-426-07	5	122.0791	24.41583	2.938184

ANOVA

Source of Variation	*SS*	*df*	*MS*	*F*	*P-value*	*F crit*
Between Groups	18.15664	2	9.078318	1.381512	0.288427	3.885294
Within Groups	78.85552	12	6.571294			
Total	97.01216	14				

Table 24. 30 ppm BCC statistical grouping

Anova: Single Factor

30 ppm composite

SUMMARY

Groups	*Count*	*Sum*	*Average*	*Variance*
ML-14-426-02	5	231.3131	46.26262	2.766767
ML-14-426-04	5	252.5107	50.50213	1.745882
ML-14-426-06	5	232.7696	46.55393	2.753442
ML-14-426-08	5	275.5281	55.10563	0.000158

ANOVA

Source of Variation	*SS*	*df*	*MS*	*F*	*P-value*	*F crit*
Between Groups	257.7113	3	85.90376	47.28919	3.55E-08	3.238872
Within Groups	29.06499	16	1.816562			
Total	286.7763	19				

Anova: Single Factor

30 ppm composite no outlier (0.15% fCNT)

SUMMARY

Groups	*Count*	*Sum*	*Average*	*Variance*
ML-14-426-02	5	231.3131	46.26262	2.766767
ML-14-426-04	5	252.5107	50.50213	1.745882
ML-14-426-06	5	232.7696	46.55393	2.753442

ANOVA

Source of Variation	*SS*	*df*	*MS*	*F*	*P-value*	*F crit*
Between Groups	56.07765	2	28.03882	11.57658	0.001582	3.885294
Within Groups	29.06436	12	2.42203			
Total	85.14201	14				

Table 25. 30ppm and 120 ppm polymer comparison

Anova: Single Factor						
polymer comp.						
SUMMARY						
Groups	*Count*	*Sum*	*Average*	*Variance*		
30ppm polymer	15	389.3727	25.95818	6.92944		
120 ppm polymer	20	947.4189	47.37095	10.41957		
ANOVA						
Source of Variation	*SS*	*df*	*MS*	*F*	*P-value*	*F crit*
Between Groups	3930.057	1	3930.057	439.6573	1.2E-20	4.139252
Within Groups	294.984	33	8.93891			
Total	4225.041	34				

Table 26. comparison of individual 30 ppm polymers and equivalent BCC samples

Anova: Single Factor						
30 ppm 0.0% fCNT						
SUMMARY						
Groups	*Count*	*Sum*	*Average*	*Variance*		
ML-14-426-01	5	244.8968	48.97937	6.2795		
ML-14-426-02	5	231.3131	46.26262	2.766767		
ANOVA						
Source of Variation	*SS*	*df*	*MS*	*F*	*P-value*	*F crit*
Between Groups	18.45172	1	18.45172	4.079412	0.078088226	5.317655
Within Groups	36.18507	8	4.523133			
Total	54.63679	9				
Anova: Single Factor						
30 ppm 0.05% fCNT						
SUMMARY						
Groups	*Count*	*Sum*	*Average*	*Variance*		
ML-14-426-03	5	132.7589	26.55179	7.893588		
ML-14-426-04	5	252.5107	50.50213	1.745882		
ANOVA						
Source of Variation	*SS*	*df*	*MS*	*F*	*P-value*	*F crit*
Between Groups	1434.047	1	1434.047	297.5365	1.29887E-07	5.317655
Within Groups	38.55788	8	4.819735			
Total	1472.605	9				
Anova: Single Factor						
30 ppm 0.1% fCNT						
SUMMARY						
Groups	*Count*	*Sum*	*Average*	*Variance*		
ML-14-426-05	5	134.5346	26.90692	8.88211		
ML-14-426-06	5	232.7696	46.55393	2.753442		
ANOVA						
Source of Variation	*SS*	*df*	*MS*	*F*	*P-value*	*F crit*
Between Groups	965.0128	1	965.0128	165.8732	1.24865E-06	5.317655
Within Groups	46.5422	8	5.817776			
Total	1011.555	9				
Anova: Single Factor						
30 ppm 0.15% fCNT						
SUMMARY						
Groups	*Count*	*Sum*	*Average*	*Variance*		
ML-14-426-07	5	122.0791	24.41583	2.938184		
ML-14-426-08	5	275.5281	55.10563	0.000158		
ANOVA						
Source of Variation	*SS*	*df*	*MS*	*F*	*P-value*	*F crit*
Between Groups	2354.66	1	2354.66	1602.713	1.66729E-10	5.317655
Within Groups	11.75337	8	1.469171			
Total	2366.413	9				

Table 27. statistical comparison between 30 ppm BCC samples and 120 ppm BCC sample group

Anova: Single Factor

0.0% fCNT

SUMMARY

Groups	*Count*	*Sum*	*Average*	*Variance*
ML-14-426	5	231.3131	46.26262	2.766767
120 ppm c	20	1019.148	50.95738	7.605148

ANOVA

ce of Varic	*SS*	*df*	*MS*	*F*	*P-value*	*F crit*
Between (	88.16296	1	88.16296	13.03474	0.001472	4.279344
Within Gr	155.5649	23	6.76369			
Total	243.7278	24				

Anova: Single Factor

0.05% fCNT

SUMMARY

Groups	*Count*	*Sum*	*Average*	*Variance*
ML-14-426	5	252.5107	50.50213	1.745882
120 ppm c	20	1019.148	50.95738	7.605148

ANOVA

ce of Varic	*SS*	*df*	*MS*	*F*	*P-value*	*F crit*
Between (	0.829006	1	0.829006	0.125871	0.725984	4.279344
Within Gr	151.4813	23	6.586145			
Total	152.3103	24				

Anova: Single Factor

0.1% fCNT

SUMMARY

Groups	*Count*	*Sum*	*Average*	*Variance*
ML-14-426	5	232.7696	46.55393	2.753442
120 ppm c	20	1019.148	50.95738	7.605148

ANOVA

ce of Varic	*SS*	*df*	*MS*	*F*	*P-value*	*F crit*
Between (	77.56154	1	77.56154	11.47127	0.002538	4.279344
Within Gr	155.5116	23	6.761373			
Total	233.0731	24				

Anova: Single Factor

0.15% fCNT

SUMMARY

Groups	*Count*	*Sum*	*Average*	*Variance*
ML-14-426	5	275.5281	55.10563	0.000158
120 ppm c	20	1019.148	50.95738	7.605148

ANOVA

ce of Varic	*SS*	*df*	*MS*	*F*	*P-value*	*F crit*
Between (	68.83181	1	68.83181	10.95605	0.003056	4.279344
Within Gr	144.4984	23	6.282541			
Total	213.3303	24				

Appendix D

Table 28. Density measurements of Run #1 120 ppm 45° wear samples

120 ppm	090913-B1-S1		090913-B1-B3		090913-B1-S5		090913 -B2-S1	
Measurement	thickness	Diameter	thickness	Diameter	thickness	Diameter	thickness	Diameter
1	2.4	37.19	2.63	37.29	2.38	37.71	2.29	37.37
2	2.43	37.22	2.66	37.36	2.31	37.44	2.26	37.57
3	2.34	37.51	2.53	37.13	2.34	37.52	2.25	37.51
4	2.36	37.3	2.62	37.14	2.35	37.18	2.28	37.45
5	2.34	37.57	2.64	37.44	2.35	37.44	2.35	37.56
Average	2.374	37.358	2.616	37.272	2.346	37.458	2.286	37.492
Std. Dev.	0.036	0.154	0.045	0.122	0.022	0.170	0.035	0.074
	Volume	2600.86	Volume	2852.81	Volume	2583.97	Volume	2522.45

Table 29. Density measurements for Run #2 120 ppm 45° wear samples

120 ppm	020413-B2-S3		090913-B1-S4		020413-B1-S4		090913-B2-S4	
Measurement	thickness	Diameter	thickness	Diameter	thickness	Diameter	thickness	Diameter
1	2.33	37.33	2.41	37.47	2.25	37.75	2.65	37.99
2	2.31	37.08	2.27	37.61	2.22	37.57	2.53	37.94
3	2.48	37.55	2.38	37.79	2.33	37.67	2.5	37.97
4	2.29	37.48	2.37	37.61	2.21	37.8	2.61	37.91
5	2.44	37.47	2.38	37.69	2.39	37.45	2.57	37.94
Average	2.37	37.382	2.362	37.634	2.28	37.648	2.572	37.95
Std. Dev.	0.076	0.167	0.048	0.105	0.069	0.126	0.054	0.028
	Volume	2599.82	Volume	2626.09	Volume	2536.81	Volume	2907.80

Table 30. Density Measurements for Run #1 30 ppm 45° wear samples

30 ppm	090913-B2-S6		151113-B1-S3		090913-B1-S2		151113-B1-S5	
Measurement	thickness	Diameter	thickness	Diameter	thickness	Diameter	thickness	Diameter
1	2.43	36.55	2.28	37.35	2.5	37.71	2.43	37.41
2	2.45	36.06	2.27	37.24	2.48	37.73	2.41	37.42
3	2.41	36.33	2.34	37.07	2.32	37.76	2.35	37.05
4	2.35	36.96	2.19	37.14	2.44	37.76	2.44	37.58
5	2.44	36.18	2.34	36.99	2.5	37.7	2.14	36.7
Average	2.416	36.416	2.284	37.158	2.448	37.732	2.354	37.232
Std. Dev.	0.036	0.317	0.055	0.126	0.068	0.025	0.111	0.318
	Volume	2515.08	Volume	2475.54	Volume	2735.90	Volume	2561.59

Table 31. Density Measurements for Run #2 30 ppm 45° wear samples

30 ppm	090913-B2-S2		151113-B1-S2		151113-B1-S1		151113-B1-S4	
Measurement	thickness	Diameter	thickness	Diameter	thickness	Diameter	thickness	Diameter
1	2.48	37.62	2.44	37.29	2.53	37.95	2.38	37.39
2	2.48	37.14	2.44	37.42	2.49	37.87	2.25	37.37
3	2.44	37.45	2.37	37.59	2.5	37.66	2.38	37.34
4	2.41	37.44	2.46	37.1	2.44	37.54	2.38	37.41
5	2.49	37.73	2.32	37.2	2.47	37.84	2.31	37.49
Average	2.46	37.476	2.406	37.32	2.486	37.772	2.34	37.4
Std. Dev.	0.030	0.200	0.053	0.171	0.030	0.150	0.053	0.051
	Volume	2712.13	Volume	2630.56	Volume	2784.27	Volume	2569.38

Table 32. Density Measurements for Run #1 120 ppm 22° wear samples

120 ppm	151113-B1-S6		151113-B2-S2		151113-B2-S4		151113-B2-S6	
Measurement	thickness	Diameter	thickness	Diameter	thickness	Diameter	thickness	Diameter
1	2.47	37.75	2.44	37.84	2.46	37.37	2.49	37.78
2	2.35	37.96	2.31	37.85	2.49	37.56	2.45	37.91
3	2.27	37.5	2.45	37.78	2.46	37.48	2.43	37.77
4	2.2	37.83	2.28	37.23	2.52	37.43	2.44	37.85
5	2.61	37.98	2.45	37.7	2.31	37.51	2.44	37.75
Average	2.38	37.804	2.386	37.68	2.448	37.47	2.45	37.812
Std. Dev.	0.146	0.174	0.075	0.231	0.072	0.065	0.021	0.059
	Volume	2670.07	Volume	2659.27	Volume	2698.04	Volume	2749.76

Table 33. Density Measurements for Run #2 120 ppm 22° wear samples

120 ppm	200214-B1-S2		200214-B1-S4		200214-B1-S6		200214-B2-S2	
Measurement	thickness	Diameter	thickness	Diameter	thickness	Diameter	thickness	Diameter
1	2.3	37.24	2.3	37.53	2.21	36.94	2.36	37.69
2	2.21	37.34	2.29	37.24	2.28	37.34	2.35	37.79
3	2.29	37.34	2.33	37.37	2.23	37.26	2.28	37.61
4	2.26	37.45	2.17	37.53	2.38	36.92	2.27	37.66
5	2.27	37.55	2.31	37.46	2.27	37.18	2.33	37.1
Average	2.266	37.384	2.28	37.426	2.274	37.128	2.318	37.57
Std. Dev.	0.031	0.106	0.057	0.110	0.059	0.170	0.037	0.242
	Volume	2486.00	Volume	2506.98	Volume	2460.73	Volume	2568.42

Table 34. Density measurements for Run #1 30 ppm 22° wear samples

30 ppm	151113-B2-S1		151113-B2-S3		151113-B2-S5		200214-B1-S1	
Measurement	thickness	Diameter	thickness	Diameter	thickness	Diameter	thickness	Diameter
1	2.52	37.81	2.25	37.83	2.43	37.72	2.25	37.9
2	2.41	37.76	2.27	37.81	2.43	37.67	2.03	37.72
3	2.35	37.8	2.29	37.73	2.42	37.7	2.21	37.72
4	2.49	37.94	2.29	37.82	2.43	37.75	2.08	37.78
5	2.44	37.71	2.21	37.88	2.33	37.67	2.28	37.81
Average	2.442	37.804	2.262	37.814	2.408	37.702	2.17	37.786
Std. Dev.	0.060	0.077	0.030	0.048	0.039	0.031	0.098	0.067
	Volume	2739.62	Volume	2539.03	Volume	2686.92	Volume	2432.15

Table 35. Density Measurements for Run #2 30 ppm 22° wear samples

30 ppm	200214-B1-S3		200214-B1-S5		200214-B2-S1		200214-B2-S3	
Measurement	thickness	Diameter	thickness	Diameter	thickness	Diameter	thickness	Diameter
1	2.29	37.79	2.31	37.94	2.59	37.7	2.15	37.75
2	2.22	37.71	2.31	37.87	2.48	37.69	2.15	37.74
3	2.32	37.72	2.3	37.75	2.46	37.72	2.12	37.76
4	2.17	37.84	2.27	37.84	2.42	37.61	2.04	37.73
5	2.25	37.64	2.33	37.81	2.54	37.99	2.13	37.75
Average	2.25	37.74	2.304	37.842	2.498	37.742	2.118	37.746
Std. Dev.	0.053	0.069	0.020	0.063	0.060	0.130	0.041	0.010
	Volume	2515.68	Volume	2590.00	Volume	2793.26	Volume	2368.85